

**SLOVAK UNIVERSITY OF TECHNOLOGY IN BRATISLAVA
FACULTY OF CHEMICAL AND FOOD TECHNOLOGY**

Reference number: FCHPT-10881-67132



**MATHEMATICAL MODELING AND OPTIMAL OPERATION OF
MEMBRANE PROCESSES
DOCTORAL THESIS**

Bratislava, 2019

Ing. Ayush Sharma

SLOVAK UNIVERSITY OF TECHNOLOGY IN BRATISLAVA
FACULTY OF CHEMICAL AND FOOD TECHNOLOGY



MATHEMATICAL MODELING AND OPTIMAL OPERATION OF
MEMBRANE PROCESSES

DOCTORAL THESIS

FCHPT-10881-67132

Study program: Process Control

Study field number: 2621

Study field: 5.2.14 Automation

Workplace: Department of Information Engineering and Process Control

Supervisor: prof. Ing. Miroslav Fikar, DrSc.

Bratislava, 2019

Ing. Ayush Sharma



DOCTORAL THESIS TOPIC

Author of thesis: Ing. Ayush Sharma
Study programme: Process Control
Study field: 5.2.14. Automation
Registration number: FCHPT-10881-67132
Student's ID: 67132

Thesis supervisor: prof. Ing. Miroslav Fikar, DrSc.

Title of the thesis: **MATHEMATICAL MODELING AND
OPTIMAL OPERATION OF MEMBRANE PROCESSES**

Date of entry: 02. 09. 2014
Date of submission: 01. 06. 2019

Ing. Ayush Sharma
Solver

prof. Ing. Miroslav Fikar, DrSc.
Head of department

prof. Ing. Miroslav Fikar, DrSc.
Study programme supervisor

Acknowledgements

Firstly I would like to express my sincere gratitude to my honorable supervisor Prof. Miroslav Fikar for his help, patience and guidance during my study and research. Secondly I would like to thank Dr. Martin Jelemenský for the co-operation regarding research, publications, and other official deeds. I would also like to thank Dr. Radoslav Paulen for providing insights into the field of my study and for his precious comments while researching and publishing the research. Special gratitude goes to the entire staff of Institute of Information Engineering, Automation and Mathematics for helping me to overcome all obstructions professionally and socially. At last, thanks goes to my family for supporting me during my studies, and actually for the support throughout life.

Ayush Sharma
Bratislava, 2019

Abstract

The objective of this thesis is to operate membrane processes optimally in theory followed by in experiments. The research work comprises mathematical modeling, simulation, optimization, and implementation of optimal operation of batch membrane diafiltration processes.

The purpose of membrane separation is to increase the concentration of the product (macro-solute) and decrease the concentration of impurities (micro-solute). A combination of semi-permeable membrane and diluant addition (diafiltration), is used to serve the purpose.

The optimal operation implemented in this research is model based, and hence the modeling of membrane processes forms the first part of this work. Modeling of different configurations of membrane processes has been done, with some new model derivations to help the research field. The batch open-loop and closed-loop diafiltration configurations are studied. The modeling section also includes dynamically fitting the existing models to the experimental data, to obtain the optimal parameter values.

The modeling is followed by the simulation and implementation of optimal operation. Implementation involves performing the optimal operation on a laboratory scale membrane separation plant. The aim of optimization is to find analytically the addition rate of solvent (diluant) into the feed tank in order to reach the final concentrations whilst minimizing costs.

The objectives to be minimized are processing time, or diluant consumption, or both for batch open-loop diafiltration processes. Pontryagin's minimum principle is utilized to attain the analytical solution for optimal operation. The optimal operation derivation is verified experimentally on a plant using nanofiltration form of membrane separation. Case studies are implemented showing the optimal operation and its comparison with the current or traditional industrial strategies of membrane separation.

In case of batch closed-loop diafiltration processes the objectives to be minimized are time, or diluant consumption, or power, or a combination of them. The numerical methods of orthogonal collocations, and control vector parameterization are applied to obtain the optimal operation strategies. Case studies are studied in simulation. The inferences are established regarding the advantages and disadvantages of batch closed-loop over open-loop configuration.

Keywords

Membrane separation, Modeling, Optimal operation, Nanofiltration, Diafiltration, Pontryagin's minimum principle, Batch implementation.

Abstrakt

Cieľom tejto dizertačnej práce je návrh optimálneho riadenia membránových procesov a jeho overenie v laboratórnych podmienkach. Výskum pozostáva z matematického modelovania, simulácie, optimalizácie a implementácie optimálneho riadenia pre membránové diafiltračné procesy.

Zmyslom filtrovania za pomoci membrán je zvýšenie koncentrácie produktu (makrozložky) a zníženie koncentrácie nečistôt (mikrozložky). To je dosiahnuté použitím polopriepustných membrán a za pomoci rozpúšťadla (diafiltrácia).

Optimálne riadenie implementované v tejto práci je založené na modelovaní a modelovanie membránových procesov tvorí prvú časť tejto práce. Súčasťou je modelovanie rozličných konfigurácií membránových procesov s následným odvodením nových modelov za účelom posunutia oblasti výskumu danej problematiky. Taktiež študujeme vlastnosti diafiltračných konfigurácií so zatvoreným (closed-loop) a otvoreným obehom (open-loop) pre spracovanie v dávkach. Práca obsahuje aj dynamické párovanie existujúcich modelov s dátami získanými z experimentov za účelom získania optimálnych hodnôt parametrov.

Modelovanie je nasledované simuláciou a implementáciou optimálneho riadenia. Implementácia zahŕňa vykonanie optimálnych operácií riadenia v laboratórnych podmienkach na zariadení vykonávajúcom membránovú filtráciu. Cieľom optimalizácie je analyticky nájsť mieru pridávania rozpúšťadla do vstupnej nádrže za cieľom dosiahnutia finálnej koncentrácie pri čo najmenších prevádzkových nákladoch.

Cieľom je minimalizovať procesný čas, rozpúšťadlo, alebo kombináciu týchto veličín pre diafiltračné procesy s otvoreným obehom pre spracovanie v dávkach. Využívame Pontrjaginov princíp minima za účelom dosiahnutia analytického riešenia pre optimálne riadenie. Výsledné odvodené optimálne riadenie je následne overené experimentom na zariadení s použitím nanofiltračnej formy membránovej filtrácie. Prípadové štúdie sú implementované, ukazujú optimálne riadenie a jeho porovnanie so súčasnými a tradičnými priemyselnými postupmi membránovej filtrácie.

V prípade vsádzkovej diafiltrácie so zatvoreným obehom je cieľom minimalizovať čas spracovania, spotrebu rozpúšťadla, výkonu alebo kombinácie týchto veličín. Použitím numerických metód ortogonálnej kolokácie a parametrizácie vektora riadenia získavame optimálne prevádzkové stratégie. Taktiež študujeme simulačné prípadové štúdie. Zistenia sú zhodnotené na záver v porovnaní výhod a nevýhod konfigurácií so zatvoreným a otvoreným obehom pre vsádzkové procesy.

Kľúčové slová

Membránová separácia, modelovanie, optimálne riadenie, nanofiltrácia, diafiltrácia, Pontrjaginov princíp minima, vsádzkové procesy.

Contents

| | | |
|----------|--|-----------|
| 1 | Introduction | 19 |
| I | Theoretical Background | 23 |
| 2 | Membrane Process | 25 |
| 2.1 | Membrane Separation – Processing Modes | 26 |
| 2.1.1 | Batch Separation | 26 |
| 2.1.2 | Continuous Separation | 26 |
| 2.1.3 | Diafiltration | 26 |
| 2.1.4 | Feed & Bleed | 27 |
| 2.2 | Membrane Separation – Plant Configurations | 27 |
| 2.2.1 | Batch Plant – Open-loop Configuration | 29 |
| 2.2.2 | Batch with Partial Recirculation Plant – Closed-loop Configuration | 29 |
| 2.2.3 | Series Membrane Assembly Units | 30 |
| 2.2.4 | Parallel Membrane Assembly Units | 31 |
| 2.3 | Membrane Types | 31 |
| 2.3.1 | Microfiltration | 31 |
| 2.3.2 | Ultrafiltration | 33 |
| 2.3.3 | Nanofiltration | 33 |
| 2.3.4 | Reverse Osmosis | 33 |
| 2.4 | Nanodiafiltration | 34 |
| 2.5 | Membrane Material | 34 |
| 2.5.1 | Organic Membranes | 34 |
| 2.5.2 | Inorganic Membranes | 34 |
| 3 | Optimal Control Theory | 35 |
| 3.1 | Optimization Problem | 35 |
| 3.2 | Optimization Problem – Solution | 36 |
| 3.3 | Pontryagin’s Minimum Principle | 36 |

| | | |
|-----------|---|-----------|
| 3.4 | Control Vector Parameterization | 38 |
| 3.4.1 | Finite Differences Method | 40 |
| 3.4.2 | The Sensitivity Method | 40 |
| 3.4.3 | Adjoint Method | 41 |
| 3.5 | Orthogonal Collocation | 41 |
| II | Thesis Contributions | 45 |
| 4 | Open-Loop Batch Diafiltration | 47 |
| 4.1 | Mathematical Modeling | 47 |
| 4.1.1 | Modeling Assumptions | 47 |
| 4.1.2 | Model Derivation | 48 |
| 4.1.3 | Model | 49 |
| 4.1.4 | Diluant Input Modes | 50 |
| 4.2 | Laboratory Membrane Plant | 51 |
| 4.2.1 | Communication and Operation | 53 |
| 4.2.2 | Pressure (TMP) Control | 56 |
| 4.2.3 | Temperature Control | 56 |
| 4.2.4 | Diluant Addition | 57 |
| 4.3 | Experimental Modeling | 60 |
| 4.3.1 | Problem Definition | 61 |
| 4.3.2 | Problem Solution | 61 |
| 4.3.3 | Results | 62 |
| 4.4 | Optimal Control | 65 |
| 4.4.1 | Problem Formulation | 65 |
| 4.4.2 | Problem Solution | 65 |
| 4.5 | Optimal Control – Case Studies | 67 |
| 4.5.1 | Case Study 1 | 68 |
| 4.5.2 | Case Study 2 | 71 |
| 4.5.3 | Case Study 3 | 73 |
| 5 | Closed-Loop Batch Diafiltration | 77 |
| 5.1 | Mathematical Modeling | 77 |
| 5.1.1 | Modeling Assumptions | 77 |
| 5.1.2 | Model Derivation | 78 |
| 5.1.3 | Complete Model | 80 |
| 5.1.4 | Model Simplifications | 81 |
| 5.1.5 | Alternate Configuration Model – Input to the Loop | 82 |
| 5.1.6 | Effect of Loop Parameters | 82 |
| 5.2 | Optimal Control | 83 |
| 5.2.1 | Problem Formulation | 83 |

| | | |
|----------|--|------------|
| 5.2.2 | Problem Solution | 84 |
| 5.3 | Optimal Control – Case Studies | 84 |
| 5.3.1 | Limiting Flux Model | 84 |
| 5.3.2 | Separation of Lactose and Proteins | 88 |
| 5.3.3 | Separation of Albumin and Ethanol | 91 |
| 6 | Conclusions | 95 |
| | Bibliography | 97 |
| | Author’s Publications | 105 |
| | Curriculum Vitae | 107 |
| | Resumé (in Slovak) | 111 |

List of Figures

| | | |
|------|---|----|
| 2.1 | Classification of membrane processes, based on flow to the membrane. | 25 |
| 2.2 | Multi-stage continuous filtration. | 27 |
| 2.3 | Schematic representation of a batch diafiltration process. | 28 |
| 2.4 | Multi-stage continuous diafiltration. | 28 |
| 2.5 | Feed and bleed operation mode. | 29 |
| 2.6 | Batch membrane filtration with complete (open-loop) and partial recirculation (closed-loop) of retentate. | 30 |
| 2.7 | Multi-membrane assembly connections. | 31 |
| 2.8 | Classification of membranes. | 32 |
| 3.1 | Continuous control trajectory. | 38 |
| 3.2 | Discretized control trajectories. | 39 |
| 3.3 | Distribution of time intervals and collocation points for state and control variables for $K_x = K_u = 2$ | 42 |
| 4.1 | Batch DF process flow scheme | 48 |
| 4.2 | P&I diagram of the laboratory nanodiafiltration process. | 52 |
| 4.3 | Industrial communication and control devices connected to membrane plant. | 54 |
| 4.4 | Human Machine Interface (HMI) designed using WinCC flexible environment, to run and control the membrane plant. | 55 |
| 4.5 | Control of transmembrane pressure. | 57 |
| 4.6 | Control of temperature. | 58 |
| 4.7 | Level control in the feed tank by using a diluant. | 59 |
| 4.8 | Control of feed tank level. | 60 |
| 4.9 | Permeate flow rate measurements vs simulated estimated models. | 63 |
| 4.10 | Comparison of lactose concentration: measured vs simulated data based on estimated models. | 64 |
| 4.11 | Comparison of NaCl concentration: measured and simulated data based on estimated models. | 64 |
| 4.12 | Concentration diagram for case studies along with the singular curve ($S = 0$). | 68 |

| | | |
|------|---|----|
| 4.13 | Case study 1: Permeate flow-rate measurements of traditional and optimal strategies. | 69 |
| 4.14 | Case study 1: Concentration measurements of lactose and NaCl for traditional and optimal strategies. | 70 |
| 4.15 | Case study 2: Permeate flow-rate measurements of traditional and optimal strategies. | 72 |
| 4.16 | Case study 2: Concentration measurements of lactose and NaCl for traditional and optimal strategies. | 72 |
| 4.17 | Concentration measurements of lactose and NaCl for traditional and optimal strategies, along with the initial and final conditions. | 75 |
| 4.18 | Permeate flow rate measurements of traditional and optimal strategies. | 75 |
| 5.1 | Batch diafiltration with partial recirculation process flow scheme | 79 |
| 5.2 | Evolution of component (c_1 and c_2) total concentrations for different scenarios. | 86 |
| 5.3 | Optimal values of control α for different scenarios. | 86 |
| 5.4 | Optimal values of control s for different scenarios. | 86 |
| 5.5 | Pareto front diagram to depict the relation between optimized results, when moving from minimum time to minimum power. | 88 |
| 5.6 | Separation of lactose from proteins: total concentration diagram. | 90 |
| 5.7 | Separation of lactose from proteins: optimal values of control α | 90 |
| 5.8 | Separation of lactose from proteins: optimal values of control s | 90 |
| 5.9 | Separation of albumin and ethanol: total concentration diagram. | 93 |
| 5.10 | Separation of albumin and ethanol: optimal values of control α | 93 |
| 5.11 | Separation of albumin and ethanol: optimal values of control s | 93 |

List of Tables

| | | |
|-----|--|----|
| 2.1 | Typically applied pressures and pore sizes for different types of pressure-driven membrane processes. | 32 |
| 4.1 | Parameters of the models. | 62 |
| 4.2 | Experimental results: comparison of total processing time and diluant consumption for different scenarios in case study 1. | 70 |
| 4.3 | Simulation results: comparison of total processing time and diluant consumption for different scenarios in case study 1. | 71 |
| 4.4 | Experimental comparison of total processing time and diluant consumption for different scenarios in case study 2. | 73 |
| 4.5 | Comparison of time taken by traditional and optimal strategies. | 76 |
| 5.1 | Comparison of total processing time, volume needed to be pumped, and diluant consumption for different scenarios. | 87 |
| 5.2 | Separation of lactose from proteins: comparison of individual cost functions for different scenarios. | 91 |
| 5.3 | Separation of albumin and ethanol: comparison of individual cost functions for different scenarios. | 92 |

List of Abbreviations

| | |
|-----|---------------------------------|
| C | Concentration (mode) |
| CVD | Constant-Volume Diafiltration |
| DVD | Dynamic-Volume Diafiltration |
| VVD | Variable-Volume Diafiltration |
| DF | Diafiltration |
| D | Dilution (mode) |
| MF | Microfiltration |
| NF | Nanofiltration |
| NLP | Non Linear Programming |
| RO | Reverse Osmosis |
| RP | Recirculation Pump |
| TMP | Transmembrane Pressure |
| UF | Ultrafiltration |
| CVP | Control Vector Parameterization |
| OC | Orthogonal Collocation |
| ODE | Ordinary Differential Equation |
| AE | Algebraic Equation |

Chapter 1

Introduction

Most of the products that we require in our modern lives exist, or are manufactured in combination with other products or unwanted impurities. The objective of separation is to get these product/s purified from these impurities or byproducts. Separation is used throughout our life, in order to separate eatables from non-eatables, drinkable from non-drinkables, etc. We can even do it through our senses, for example visually. In current era, most of the manual actions and works have been replaced by machines. It applies to the separation process too. Separation is done industrially at large scale now. Chemical, petrochemical, food, biotechnology, and agriculture industries use separation techniques intensively. The other use of separation in most industries is to clean the effluent water for reuse. The separation can be achieved using techniques like solvent based extraction, distillation, supercritical fluid extraction, sedimentation aided with coagulants and flocculants, etc. The other technique that is widely admired, accepted, and used in industries for separation is membrane filtration.

Membrane separation process as described in Cheryan (1998) and Zeman (1996) is the separation of two or more different molecules from a solution, or from each other in a solution, using semi-permeable membranes. These membranes are specific filters, designed in order to pass certain molecules, and retain others, based on their size, charge, and ionic properties. Membranes have found numerous applications in water purification (Mallevalle et al., 1996), desalination, TOC (total organic carbon) minimization, juice clarification, product separation and purification (Crespo et al., 1994). The various driving forces for separation in membrane processes are concentration gradient, pressure, and electric potential. The governing principle of separation is based on the molecular size differences of the solutes which pass through the perm-selective membrane with different rates. The process is usually designed to increase the concentration of the valuable product/s, and to decrease the concentration of impurities.

The advantages of membrane aided separation over other techniques are:

1. Compared to distillation, membrane processes do not require high temperatures for separation. Hence, they prevent denaturation of valuable bio-products, like anti-bodies, vitamins, and other heat-labile products.
2. The solvent based extraction of product/s adds up the cost of solvent, compared to membrane

filtration. It also requires an additional step to remove this used solvent from the extracted product.

3. Membrane based processes do not require chemicals (coagulants, flocculants) for separation. It is much faster and gives higher product purity when compared to these chemical counterparts.

Once the process has been industrialized, the next demand is to automate the process and to control it. The first priority is to operate in a way that the required range of product purity is obtained. The next operational priority is to minimize the production/processing/separation costs to accomplish the first priority. Hence, modeling, control, and optimization is performed to achieve the required concentration of product/s, with assurance of cost minimization and minimum manual efforts. There are various methods in theory to design the control strategy to achieve these objectives of product quality and costs. These methods can design the control and automation strategy based on the prior knowledge of the process, i.e. the process model, input, output and state boundaries. The other way to control can be based on statistical data, intensive knowledge and experience, or trial and error method, i.e. try different inputs and study the results. This thesis uses the process knowledge (model, constraints) based derivation of optimal control strategy (both analytical and numerical).

The designing of automation and control strategy is followed by validation. Validation establishes that the control strategy developed meets our desired objectives or not. This validation can be simulation based, i.e. we apply the control strategy to a model and then simulate the model to observe and study the results, or it can be experimental. We present the results of both, i.e. simulation based and experimental validation.

We study automation, modeling, optimization, and control of membrane aided separation processes. Two diafiltration (DF) membrane separation types are considered:

1. batch diafiltration (batch open-loop DF),
2. batch diafiltration with partial recirculation (batch closed-loop DF).

DF is a technique where membrane separation is combined with external addition of a diluant (e.g. pure water), to reduce impurities. These processes are considered operating under constant trans-membrane pressure (TMP) and temperature.

The optimal operation of batch DF process is achieved by controlling the addition of diluant into the system in order to attain the desired separation and final required concentrations, whilst minimizing processing costs.

The batch open-loop DF optimization problem is a non-linear dynamic optimization problem. As it is a control-affine problem, Pontryagin's minimum principle (Pontryagin et al., 1962) will be utilized to obtain the optimal operation strategies analytically. In literature, several case studies are solved analytically and numerically in Paulen and Fikar (2016) to optimally operate membrane separation process using diluant rate as the input. These case studies show the comparison between the traditional approaches towards membrane operation, and the optimal membrane operation approaches. The existing models of separation are used in this book (Paulen and Fikar, 2016) from literature. The study is completely in simulation and presents no experimental results. In this thesis batch open-loop DF will be studied in laboratory conditions, and the separation rate will be dynamically modeled based

on experimental data (Sharma et al., 2017a, 2018). Further, this experimental model will be used to find the optimal strategy to minimize the processing time, or diluant consumption, or a weighted combination of both. The optimal strategies will be firstly shown in simulation. After simulation, selected case studies will be implemented on a membrane separation plant, and verified experimentally. The traditional industrial strategy will also be performed on the plant to achieve the same objectives, and to compare with the implemented optimal strategies.

In case of batch closed-loop DF there are two manipulated variables: diluant addition rate and recirculation ratio. This process can aim at operation with the objective to minimize time, or to minimize the power required to achieve the separation, or to minimize the diluant addition or multi-objective. This is again a non-linear dynamic optimization problem, but is found to be not affine w.r.t. control inputs. Hence, only theoretical and simulation studies will be presented for this process in thesis.

Thesis Contributions

The aim of this thesis is to study mathematical modeling and optimal control of batch diafiltration processes in theory and in laboratory practice. The optimal control is studied using methods of dynamic optimization and provides improvements compared to traditional operations. The main contributions of this thesis can be summarized as follows:

- Study of batch closed-loop DF processes: mathematical modeling, numerical optimization, and case studies together with comparison to batch open-loop DF (Sharma et al., 2015, 2017b).
- Implementation and verification of optimal operation strategy in laboratory conditions for batch open-loop DF processes, comparison of the proposed optimal strategies with the traditional ones (Sharma et al., 2018, 2019).

Some partial results were obtained for parameter estimation problems for open-loop diafiltration using experimental data (Sharma et al., 2016a, 2017a, 2018).

Additionally, I also contributed as a team member to results in optimal control of membrane processes subject to fouling (Jelemenský, 2016, Jelemenský et al., 2015a,b, 2016).

The thesis is presented here in two parts. The first part comprises the theory on membrane separation processes (Chapter 2) and optimal control (Chapter 3). Both analytical and numerical methods are presented, along with benefits and drawbacks of each technique.

The second part includes thesis contributions: new developments in modeling and optimal control of membrane processes.

Chapter 4 will present the batch open-loop DF processes. The process modeling is going to be discussed. The membrane plant used will be described after the modeling section. This will cover the experimental procedures to obtain the results along with the details of the hardware (plant) and its automation, visualization, and basic control. The parameter estimation problem will be solved next to obtain models based on experimental results. The second part of the chapter will deal with the optimal control of open-loop batch DF. This will include problem definition (objective function) for optimizing the process based on the process model, constraints, and desired objectives. This will be

followed by the solution to this optimal control problem. Simulation of case studies will be presented further, to study the effects of optimal strategies. Finally, the results of optimal operation of batch open-loop DF process is going to be shown in experimental conditions, together with the discussion on these results.

Chapter 5 will present the batch closed-loop DF processes. It will cover mathematical derivation of model equations for batch DF with partial recirculation. Alternative model derivations and model simplifications will be also presented. Next, the optimal control problem to minimize the processing costs is going to be defined and solved using numerical techniques. Simulation case studies will be presented to demonstrate the optimal strategies.

Part I

Theoretical Background

Chapter 2

Membrane Process

In this chapter, basic idea, types and forms of membranes and membrane separation techniques are discussed. Generally, membrane separation is passing the solution to be separated through a semi-permeable membrane. The solution consists of solutes to be separated. The membrane can allow complete passage, partial passage, or no passage at all to a solute, depending on its molecular size and mass. The stream that passes through the membrane is called **permeate**, while the membrane rejected stream is **retentate**.

On the basis of flow of feed to the membrane, the membrane separation processes can be classified as dead-end (Fig. 2.1(a)): where the flow of feed is perpendicular to the membrane surface, and cross-flow filtration (Fig. 2.1(b)): where the flow is parallel to the membrane surface. All the liquid that is introduced in dead-end mode passes through the membrane. Hence, there is no retentate stream in dead-end mode (Li and Li, 2015). On the contrary, flow is tangential rather than direct into the filtration media for cross-flow mode. Cross-flow mode utilizes a high fluid circulation rate tangential to the membrane to minimize the accumulation of particles at the membrane surface (Li, 1972).

The significant advantages of cross-flow filtration over dead-end are:

- fouling is minimized,

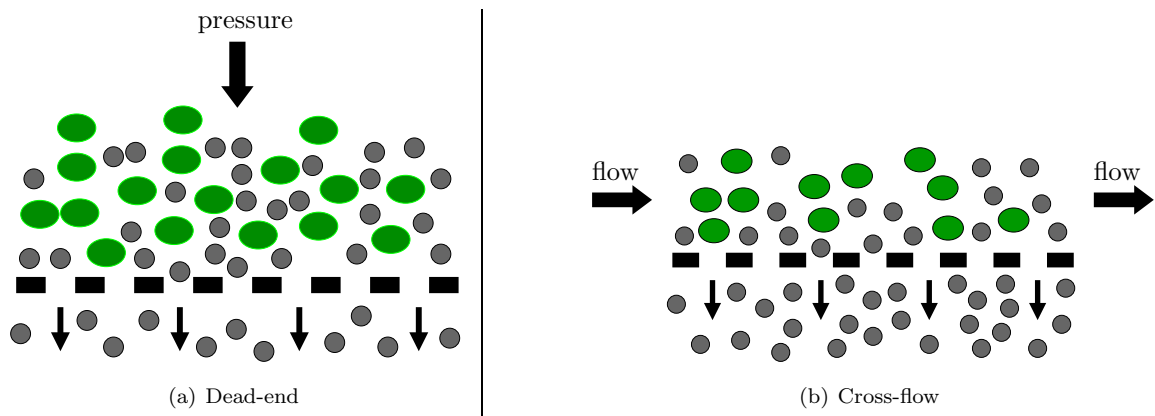


Figure 2.1: Classification of membrane processes, based on flow to the membrane.

- fouling minimization results in longer membrane life,
- higher permeate flow rates, as the pores are not directly clogged by the solutes,
- due to quick formation of solid particle layer over the membrane, dead-end mode cannot be used for continuous processing and is only used to process batches, while the cross-flow mode is ideal for both batch and continuous processing.

Next, we discuss other types of membrane separation processes based on various criteria.

2.1 Membrane Separation – Processing Modes

This section classifies membrane processes based on their mode of operation. This translates to differences in membrane plant designs, w.r.t. inflows and outflows of the system.

2.1.1 Batch Separation

In batch processing mode the feed is added to the tank initially, and no further inclusion of feed solution is permitted until the final objective is attained, and process is stopped. This mode is used mostly when only concentrating the product is the objective. One of the many current applications of batch separation includes; purification and fractionation of wastewater coming from olive oil industries (Cassano et al., 2013).

2.1.2 Continuous Separation

Unlike batch mode where the feed is only added initially, in continuous mode the feed is added continuously into the feed tank. One of the classes of continuous separation is multi-stage continuous processing (Fig. 2.2). As presented in Ramaswamy et al. (2013), this plant comprises several feed and bleed modules in series. Two classes of pumps are required for each module: a feed pump and a re-pressurizing pump (R-pump). This mode helps in achieving higher flux when compared to classical continuous or feed and bleed mode. A minimum of 3 modules is usually applied, and most common industrial range is 6-7.

2.1.3 Diafiltration

Diafiltration can be used for separation of two or more solutes from one another (e.g. separation of a salt/s from protein/s or sugar/s or both, separation of sugar/s from protein/s, or indeed separation of one protein/sugar from another protein/sugar), and especially for reducing the concentration of micro-solute (impurity), by the addition of a diluant. Hence, it can be used for concentrating product or reducing impurity, or both. The membrane used should allow easy passage of the solute desired in the permeate while substantially retaining the other solute. A set-up used for batch diafiltration is shown in Fig. 2.3.

The batch membrane diafiltration plant studied in this thesis consists of the following crucial parts (Fig. 2.3):

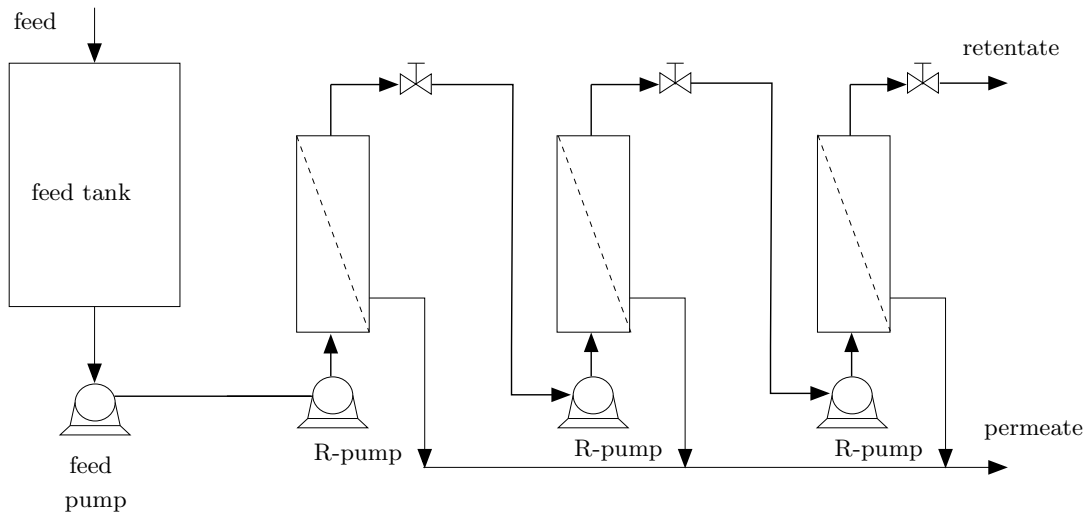


Figure 2.2: Multi-stage continuous filtration.

- feed tank – it is the source for the feed solution, and as it is a batch process no feed is added during the run,
- feed pump (P1) – it is the pump that forces the solution from feed tank towards the membrane,
- membrane (M) – it is the source for the separation of solutes (product and impurity),
- diluant pump (P3) – it is needed to force the diluant into the tank at controlled rate.

Diafiltration can also be carried out in a continuous fashion using the set-up shown in Fig. 2.4. Its simplest configuration is known as single-pass diafiltration. Continuous diafiltration, on the contrary to batch diafiltration, realizes a steady-state separation in which the product (i.e., the final retentate) is not concentrated in the feed vessel as filtration progresses, but is continuously withdrawn from the system during the entire course of filtration.

2.1.4 Feed & Bleed

Feed and bleed mode can be operated as a single loop system (one membrane module), or multi-loop system (multiple modules). In feed and bleed, the retentate is partially bled off and a part stays in the circulation loop. Nothing returns to feed tank in feed and bleed mode. They are generally operated in continuous manner, with fresh feed being pumped into the loop to balance the retentate bleed and permeation. In feed and bleed mode membrane always encounters the highest concentration and this results in lowest flux. Multi-loop feed and bleed design is the most common configuration in food processing applications. The scheme of this mode is shown in Fig. 2.5.

2.2 Membrane Separation – Plant Configurations

This classification is based on the structure of the plant and its hardware setup.

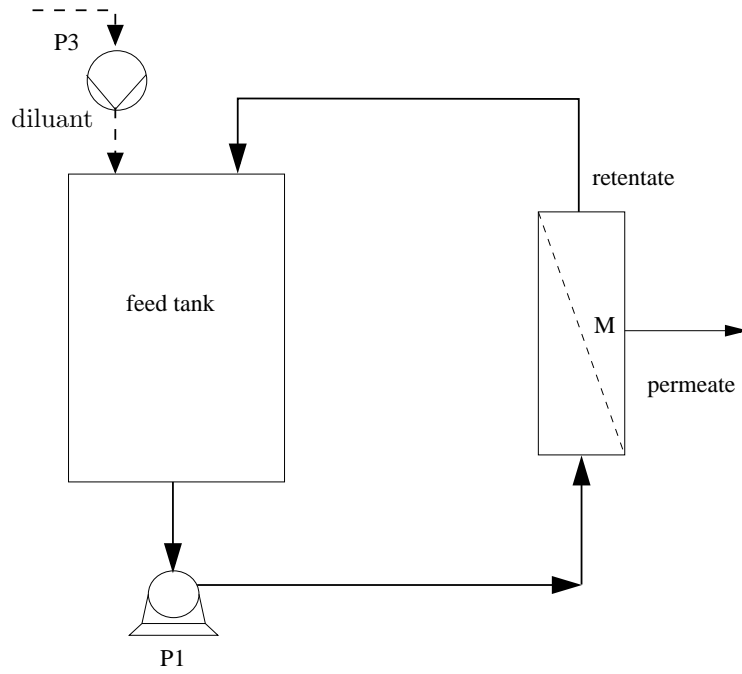


Figure 2.3: Schematic representation of a batch diafiltration process.

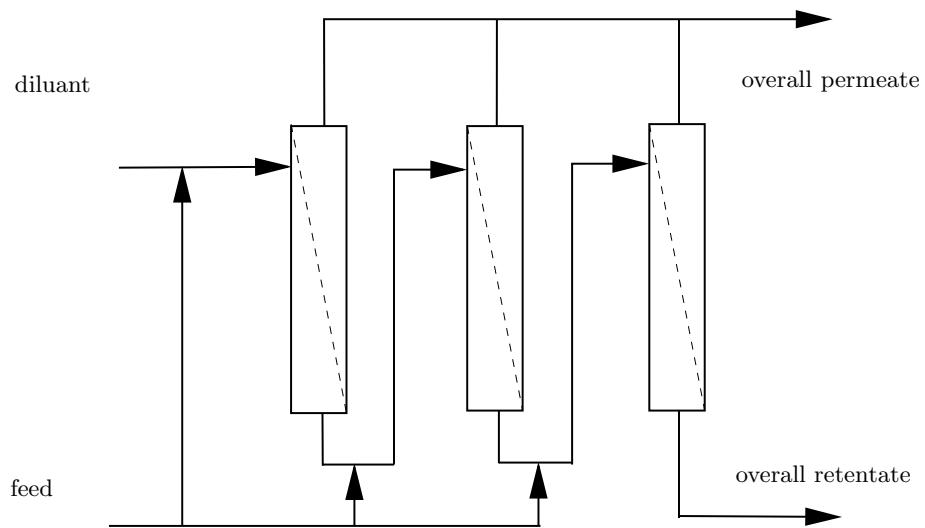


Figure 2.4: Multi-stage continuous diafiltration.

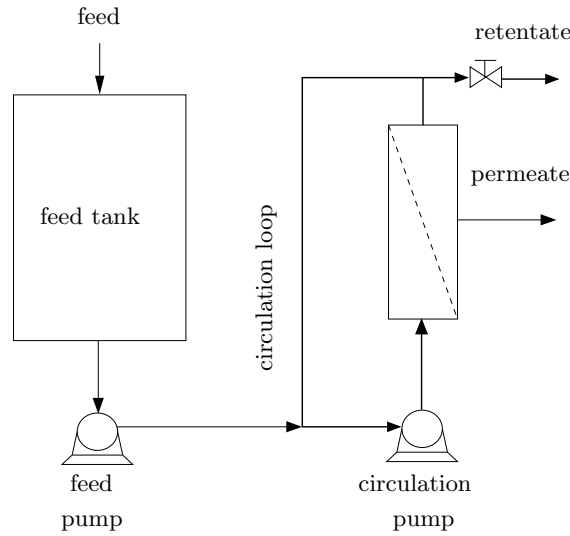


Figure 2.5: Feed and bleed operation mode.

2.2.1 Batch Plant – Open-loop Configuration

As shown in Fig 2.6(a), a batch membrane separation unit generally consists of a feed tank containing solution with the solutes to be separated, a semi-permeable membrane for performing the separation, and a feed pump to push the feed towards the membrane at desired pressure. Through the membrane the feed gets separated in two streams: retentate stream, i.e. the concentrated stream with macro-solute/s, which returns back to the feed tank, and the permeate stream comprising of micro-solute/s or just solvent, that leaves the system. In this configuration, the retentate is completely recycled back to the feed tank and hence it is also known as open loop batch (Fig 2.6(a)). A batch concentration process is usually operated at constant transmembrane pressure. Due to the continuous increase of solute concentration in the feed, the permeate flux declines with time.

2.2.2 Batch with Partial Recirculation Plant – Closed-loop Configuration

As in batch plant, this configuration too has a feed tank, a semi-permeable membrane, and a feed pump. Besides these, closed-loop configuration additionally has a recirculation loop, and a recirculation pump (Fig. 2.6(b)).

In this configuration, the feed goes to the membrane from tank and the retentate returns back to the tank but some portion of the retentate flow can be directed back through a recirculation pipe (Fig. 2.6(b)) and pump to the membrane. The retentate splitting ratio could range between 0 and 1. This system or membrane operation according to Todaro and Vogel (2014), Mallevalle et al. (1996), is also called *Batch closed loop* operation. The process in a way is also similar to fed-batch with recirculating loop operating mode given in Foley (2011), and feed and bleed operating mode given in Todaro and Vogel (2014), as there is a feed going in. It can be still categorized inside semi-batch or batch as it is not the feed itself but is a diluant; which is not continuous; and is fed at discrete intermittent times to attain optimal operation. Closed loop batch or topped-off batch as mentioned in Cheryan (1998) is used when permeate is the required product, for e.g., fruit juice clarification and

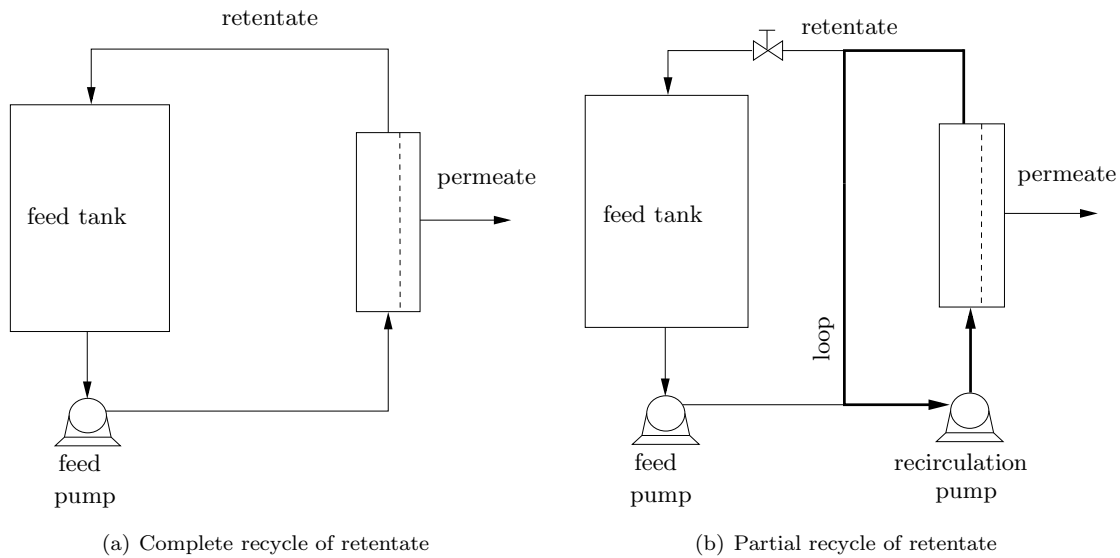


Figure 2.6: Batch membrane filtration with complete (open-loop) and partial recirculation (closed-loop) of retentate.

microfiltration of whey. The batch closed-loop operation has following advantages over traditional batch (open-loop) operating mode:

1. This configuration provides a controlled and defined flow rate, irrespective of the degree of fouling and changes in feed composition (Rapaport, 2006).
2. The pipe diameter can be smaller than in conventional batch (Cheryan, 1998, Rapaport, 2006).
3. The feed tank size can also be smaller for the closed-loop setup as part of the solution volume is permanently inside the loop. This reduces problems of foaming Cheryan (1998), Tamime (2012). Temperature and quality of sensitive retentate products can be maintained which can be difficult in open-loop batch (AWWA, 2005).
4. For large systems with remote tankage this setup can save quite a lot of large piping and with a small pressurizing feed pump, a large amount of energy by keeping the loop pressure high (Dow Water & Process Solutions, Jornitz and Meltzer, 2007, Rapaport, 2006).
5. In membrane bioreactors, partial recycle of retentate resulted in higher nutrient uptake, which helped producing a higher biomass concentration (Bilad et al., 2014).

2.2.3 Series Membrane Assembly Units

In this setup, as one membrane is not enough for achieving the separation goals; many membranes are connected in series, and the output of one is the input for the next membrane. In desalination, the series connection of reverse osmosis membranes is applied extensively. In practice there are 6 to 7 membrane modules in series. The saline or seawater passes through the first module. About 90% of it

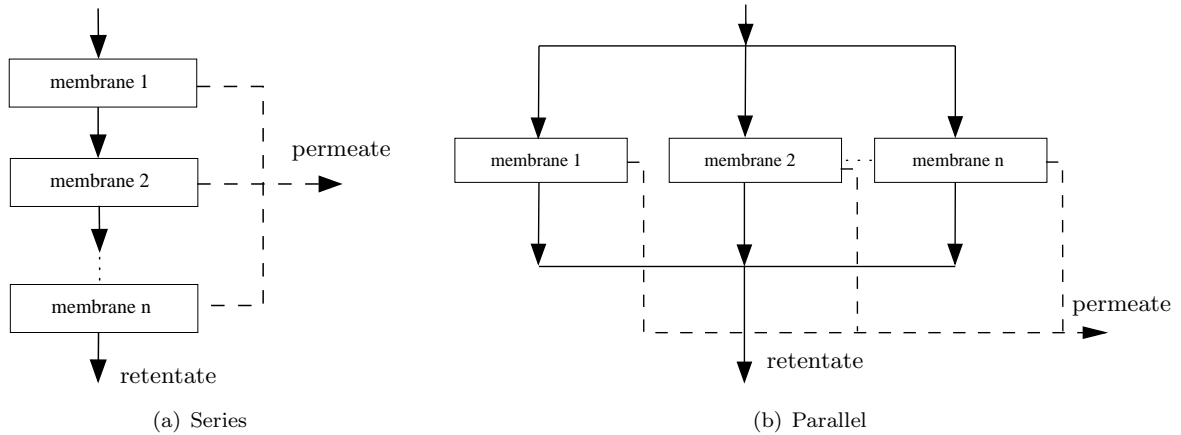


Figure 2.7: Multi-membrane assembly connections.

is rejected and it enters the second membrane module as a concentrated feed. The separation occurs in the second module and again the concentrated retentate stream passes on to the next module, and so on. The pressure difference and the flow rate is the maximum through the first membrane, and it reduces at each next membrane, and hence minimum at the last membrane module. The schematic representation can be studied from Fig. 2.7(a). The clean water recovery is at maximum in the first membrane module, and at minimum in the last one connected in series.

2.2.4 Parallel Membrane Assembly Units

In this setup, many semi-permeable membranes are connected in parallel. In this connection of membrane modules, the same feed goes to all membranes at any time instance during the processing (Fig. 2.7(b)). The retentates recombine and are recycled back to the feed reservoir, while the permeates may recombine and leave the system, or leave the system individually. If series and parallel connections are compared (Yu et al., 2015); parallel connection is inferior to series connection in separation quality and performance, but parallel is preferred when higher separation capacities and lower flow resistance is needed. Demmer and Nussbaumer (1999) published a work concluding that modules connected in parallel increase the flux, but on the sacrifice of performance. A similar comparison of parallel and series connections of membranes for membrane distillation was done by Khalifa et al. (2017). Again, parallel connection was found better than series in case of permeate flux. The combination of parallel and series connections is preferred and considered optimal.

2.3 Membrane Types

The pressure based membrane processes can be divided according to membrane pore size into microfiltration (MF), ultrafiltration (UF), nanofiltration (NF), and reverse osmosis (RO). A brief description of these membrane types is given in Fig. 2.8 and in Table 2.1.

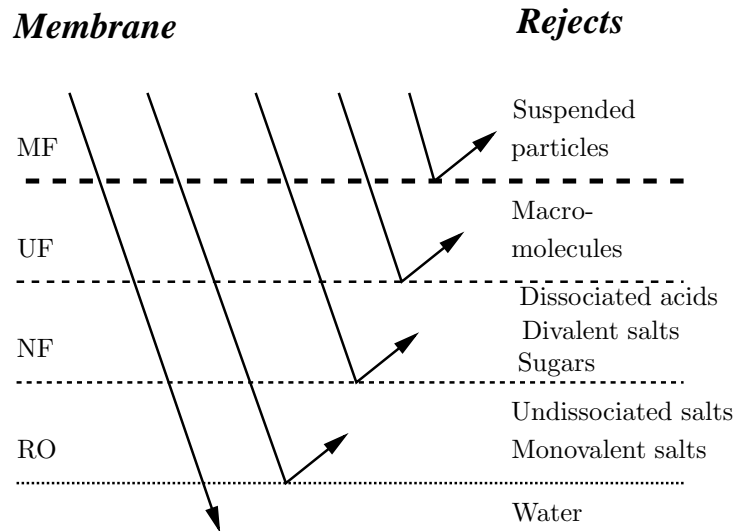


Figure 2.8: Membrane types w.r.t. pore size and filterable/retained components.

Table 2.1: Typically applied pressures and pore sizes for different types of pressure-driven membrane processes.

| | Applied pressure [bar] | Pore size [μm] | MWCO [dalton] |
|-----------------|------------------------|-----------------------------|------------------------------------|
| Microfiltration | 0.2 – 3.5 | 10 – 0.05 | $\geq 3 \times 10^5$ |
| Ultrafiltration | 1 – 10 | 0.05 – 0.002 | 5×10^3 to 5×10^6 |
| Nanofiltration | 5 – 40 | 0.002 – 0.001 | 200 to 400 |
| Reverse Osmosis | 10 – 100 | < 0.001 | ≤ 100 |

2.3.1 Microfiltration

Microfiltration (MF) membranes are characterized by pore size of $10 - 0.05 \mu\text{m}$. The pressure required is minimum for microfiltration, i.e. $0.2 - 3.5 \text{ bar}$. Microfiltration is usually used as pre-treatment for other separation processes, and is used in combination with ultrafiltration and reverse osmosis. The most prominent use of microfiltration membranes pertains to the treatment of potable water. In biological fluids, it is mostly used for removing micro-organisms. In milk processing it is again used for removing the pathogenic micro-organisms, but unlike pasteurization it does not denature the proteins because of high temperature. Khemakhem et al. (2009) suggested new microfiltration membranes that support extreme temperatures and are applied in cuttlefish effluent treatment. Another common application of microfiltration is separating oil-water emulsions (Cui et al., 2008).

2.3.2 Ultrafiltration

Ultrafiltration (UF) membranes have pore size of $0.05 - 0.002 \mu\text{m}$. The pressure required for ultrafiltration ranges between $1 - 10 \text{ bar}$. Ultrafiltration is frequently used in chemical, pharmaceutical, and beverage industries. The most common application of ultrafiltration is purification and concentration of proteins. The most important medical application of ultrafiltration is blood dialysis. Ultrafiltration is used extensively in the dairy industry; particularly in the processing of cheese whey (Verasztó et al., 2013) to obtain whey protein concentrate (WPC), and lactose-rich permeate. The general applications of UF can be studied from Jönsson and Trägårdh (1990). One of the recent advances in UF includes developing membranes such that fouling is minimized and performance is enhanced (Abdel-Karim et al., 2018). The recent discovered application of UF includes waste-water extraction/filtration of nutrients specific to micro-algae growth (Sandefur et al., 2016).

2.3.3 Nanofiltration

Nanofiltration (NF) membrane having pore size smaller than microfilter and ultrafilter is basically used for partial demineralization of liquids. The membrane pore size between 0.5 and 2 nm and operating pressures between 5 and 40 bar . NF is used to achieve a separation between sugars, other organic molecules and multivalent salts on one hand, and monovalent salts and water on the other. NF membranes have a slightly charged surface. As the dimensions of the pores is slightly larger than the size of ions, charge interaction plays a dominant role in separation. This effect can be used to separate ions with different valences. Mohammad et al. (2015) outlines the current developments in the field of NF along with its future prospects.

2.3.4 Reverse Osmosis

The reverse osmosis (RO) membrane has the smallest pores of all membranes. Because of the small pore size only water can pass through. This is the reason why RO membranes are mainly used for water treatment. Therefore, all species like viruses, proteins, and others are retained and pure water is obtained from separation. RO membranes are also often used in households where they serve for cleaning water which is obtained from rain or from polluted piping. Further, RO technology has found

also its use in cosmetic, pharmaceutical, medical, and semiconductor production. Main applications of RO membranes are desalination of seawater and purification of liquids where the water is unwanted impurity (Lee et al., 2011). The typical characteristics of these membranes are summarized in Table 2.1 (MWCO = molecular weight cut-off).

2.4 Nanodiafiltration

In combination with nanofiltration, diafiltration is applied in this thesis for the experimental validations. This combination of NF and DF, i.e. nanodiafiltration, is abbreviated as NDF (Chandrapala et al., 2016). NDF applications include water softening, wastewater treatment, vegetable oil processing, beverage, dairy (Chen et al., 2017), juice and sugar industry (Conidi et al., 2017, Salehi, 2014). In production of lactose from cheese whey, NDF concentrates lactose molecules while passing and reducing salts (Das et al., 2016, Yin et al., 2011). NDF is also used for removal of lactic acid from acid dairy whey, for better crystallization of lactose (Chandrapala et al., 2016). This concentrated lactose is a commonly used material in the pharmaceutical industry as a carrier of drugs, e.g., in inhalations for asthma patients (Boerefijn et al., 1998). Besides pharmaceutical industry, in food and beverage industry lactose is emerging widely as a source for epilactose, galacto-oligosaccharides (Cohen et al., 2017, Verasztó et al., 2013), lactitol, lactobionic acid, and other important derivatives (Gutiérrez et al., 2012).

2.5 Membrane Material

The material that the membrane is made of, also effects the separation. It can decide the chemical charge, thermal, and other properties of membrane. Membrane material should be chosen based on the separation requirements, such as temperature needed during separation, cleaning agents used before and after use, charge of ions (polarity), etc.

2.5.1 Organic Membranes

These can comprise natural organic polymers, or synthetic organic polymers, or both. The examples of natural polymers include rubber, wool and cellulose, while the synthetic polymers include polytetrafluoroethylene (PTFE), polyamide-imide (PAI), and polyvinylidenedifluoride (PVDF).

Cellulose acetate membrane is used for all types of membrane separations, i.e. MF, UF, NF, and RO. The synthetic organic membranes are mostly used for MF and UF, but polyimide membrane is applied to all 4 membrane types.

2.5.2 Inorganic Membranes

Inorganic membranes are made of materials such as ceramic, carbon, silica, zeolite, various oxides (alumina, titania, zirconia) and metals such as palladium, silver and their alloys. Inorganic membranes can be porous or dense (non-porous). The well known application of inorganic membranes is in the field of gas separation (hydrogen from gas mixture).

The inorganic membranes are more expensive than the organic membranes, but they can provide higher temperature stability, resistance to solvents, resistance to chemicals. Hence, they are preferred when membrane needs to be sterilized after each use, or cleaned by strong chemicals.

In addition, research advancements have been achieved in developing *hybrid membranes*, which comprise both inorganic and organic components. *Bipolar membranes* with charge specificity have also been developed. So, a cation exchange and an anion exchange membrane are laminated together to make this bipolar membrane. These membranes are currently used in treating concentrated salt solutions.

Chapter 3

Optimal Control Theory

In this section, the theory regarding the optimization of membrane separation process is described. Dynamic optimization results in optimal state and control trajectories to attain certain objective. The thesis deals with constrained non-linear dynamic optimization problem. The membrane separation system studied exhibits non-linear dynamics.

In Section 3.1, the constrained dynamic optimization problem is defined, along with a general discussion on solving such a problem. Section 3.3 deals with analytical method of finding optimal control while the next two sections after that, i.e. 3.4 and 3.5 are dedicated to numerical techniques of solving such an approximation of this problem.

3.1 Optimization Problem

The dynamic optimization (optimal control) problem comprises of an objective functional, the model representing the process, and may have constraints over states and control inputs. This problem in general can be defined as

$$\min_{\mathbf{u}(t)} \mathcal{J} = G(t_f, \mathbf{x}(t_f)) + \int_{t_0}^{t_f} F(\tau, \mathbf{x}(\tau), \mathbf{u}(\tau)) d\tau \quad (3.1a)$$

s.t.

$$\dot{\mathbf{x}}(t) = \mathbf{f}(t, \mathbf{x}(t), \mathbf{u}(t)), \quad \mathbf{x}(t_0) = \mathbf{x}_0, \quad \mathbf{x}(t_f) = \mathbf{x}_f, \quad (3.1b)$$

$$\mathbf{u}_{\min} < \mathbf{u}(t) < \mathbf{u}_{\max}, \quad (3.1c)$$

where $\mathbf{x}(t) \in \mathbb{R}^{n_x}$ is the state vector and $\mathbf{u}(t) \in \mathbb{R}^{n_u}$ is the control vector, respectively. Variables n_x , n_u denote the dimensions of the state and control vectors, respectively. The problem defined above aims at minimization of a scalar objective functional comprising of G (evaluated at the final time t_f) and F (evaluated over a period of time $[t_0, t_f]$), subject to system state differential equations, initial, terminal conditions, and constraint over the control vector.

The objective functional stated above (3.1a) is called the Bolza form. If the objective functional

is only defined at the final time then it is the Mayer form, i.e.

$$\min_{\mathbf{u}(t)} \mathcal{J} = G(t_f, \mathbf{x}(t_f)). \quad (3.2)$$

Similarly, if the objective functional is evaluated over the entire time interval then it is known as the Lagrange form, i.e.

$$\min_{\mathbf{u}(t)} \mathcal{J} = \int_{t_0}^{t_f} F(\tau, \mathbf{x}(\tau), \mathbf{u}(\tau)) d\tau. \quad (3.3)$$

The three forms defined above are interconvertible as stated in Bellman (1963).

3.2 Optimization Problem – Solution

In this thesis, the optimization is achieved using *optimal control theory* approaches studied from Hull (2003), and Bryson, Jr. and Ho (1975).

In general, the techniques to solve the optimization control problem can be classified into direct and indirect methods. In the former approach, the optimal control problem is firstly discretized, and then solved. The basic idea of direct optimization methods is to discretize the control problem, and then apply nonlinear programming (NLP) techniques to the resulting finite-dimensional optimization problem. In the latter one (indirect method), discretization is not required, but a prior knowledge of the solution structure is required. In case the cost function is of non-differentiable nature, the direct methods of dynamic optimization are used.

Another classification includes analytical methods and numerical methods to solve optimal control problems. Analytical methods include dynamic programming, variational calculus and Pontryagin's minimum principle. While, the numerical methods can be based on:

- discretization of control, e.g. control vector parameterization (CVP) method (Balsa-Canto et al., 2001, Goh and Teo, 1988), and control vector iteration (CVI) method,
- and on complete discretization, i.e. both states and control trajectories are parameterized e.g. orthogonal collocation (OC) (Biegler, 2007).

The analytical method of Pontryagin's minimum principle, and numerical methods of CVP and OC are approached and discussed further.

3.3 Pontryagin's Minimum Principle

This dynamic optimization method is classified into the indirect approaches. This is an analytical way of finding the solution to our problem, and leads to a global solution. This requires the cost function to be of differentiable nature. This principle as formulated in Pontryagin et al. (1962) is an extension of calculus of variations.

Pontryagin's Minimum Principle (PMP) finds the optimal control strategy while satisfying the so called necessary conditions of optimality (NCO) (Bryson, Jr. and Ho, 1975, Hull, 2003). These

necessary conditions of optimality are based on the Hamiltonian function. This Hamiltonian function using (3.1) can be defined as:

$$H(t, \mathbf{x}, \mathbf{u}, \boldsymbol{\lambda}) = F(t, \mathbf{x}, \mathbf{u}) + \boldsymbol{\lambda}^T \mathbf{f}(t, \mathbf{x}, \mathbf{u}), \quad (3.4)$$

where $\boldsymbol{\lambda} \in \mathbb{R}^{n_x}$ is the vector of adjoint variables.

The Pontryagin's minimum principle states that in order to find the optimal control, the Hamiltonian function must be minimized, i.e.

$$H(t, \mathbf{x}, \mathbf{u}^*, \boldsymbol{\lambda}) \leq H(t, \mathbf{x}, \mathbf{u}, \boldsymbol{\lambda}), \quad (3.5)$$

where \mathbf{u}^* stands for optimal control, subject to NCO

$$\dot{\boldsymbol{\lambda}}^T = -\frac{\partial H}{\partial \mathbf{x}}, \quad \boldsymbol{\lambda}_f^T = \frac{\partial G}{\partial \mathbf{x}_f}, \quad (3.6)$$

$$\dot{\mathbf{x}}^T = \frac{\partial H}{\partial \boldsymbol{\lambda}}, \quad \mathbf{x}(t_0) = \mathbf{x}_0. \quad (3.7)$$

The derivation to these conditions can be studied in detail from Hull (2003).

This principle holds true for both autonomous (implicit function of time) or non-autonomous systems (explicit function of time). In this thesis, the states and objective functions both are assumed not to be explicit functions of time, hence we consider autonomous situation. The Hamiltonian can then be rewritten as:

$$H(\mathbf{x}, \mathbf{u}, \boldsymbol{\lambda}) = F(\mathbf{x}, \mathbf{u}) + \boldsymbol{\lambda}^T \mathbf{f}(\mathbf{x}, \mathbf{u}), \quad (3.8)$$

and for autonomous systems if the final time is free, the following condition holds as well

$$H(\mathbf{x}, \mathbf{u}, \boldsymbol{\lambda}) = 0, \quad \forall t \in [t_0, t_f]. \quad (3.9)$$

We will further assume that the system and cost function are affine in control. The control affine optimal control problem can be stated as

$$\min_{\mathbf{u}(t)} \mathcal{J} = \int_{t_0}^{t_f} F_0(\mathbf{x}) + F_u(\mathbf{x}) \mathbf{u} \, d\tau \quad (3.10a)$$

s.t.

$$(3.6), (3.7), (3.1c), \quad (3.10b)$$

$$\dot{\mathbf{x}}(t) = \mathbf{f}_0(\mathbf{x}) + \mathbf{f}_u(\mathbf{x}) \mathbf{u}. \quad (3.10c)$$

The Hamiltonian for such a problem is:

$$H(\mathbf{x}, \mathbf{u}, \boldsymbol{\lambda}) = F_0(\mathbf{x}) + F_u(\mathbf{x}) \mathbf{u} + \boldsymbol{\lambda}^T (\mathbf{f}_0(\mathbf{x}) + \mathbf{f}_u(\mathbf{x}) \mathbf{u}), \quad (3.11)$$

This Hamiltonian is thus also affine in control

$$H(\mathbf{x}, \mathbf{u}, \boldsymbol{\lambda}) = H_0(\mathbf{x}, \boldsymbol{\lambda}) + H_u(\mathbf{x}, \boldsymbol{\lambda}) \mathbf{u}, \quad (3.12)$$

If the control variable is bounded; as in (3.1c), then it minimizes the Hamiltonian if it lies on its boundaries, in the form of bang-bang control. If H_u is positive, then the minimum of H is achieved using \mathbf{u}_{\min} , if negative; using \mathbf{u}_{\max} . The special case is the singular case when

$$H_u = 0, \quad \mathbf{u}_s, \quad (3.13)$$

where $\mathbf{u}_s \in [\mathbf{u}_{\min}, \mathbf{u}_{\max}]$ is the singular control, and needs to be derived. The necessary conditions of optimality form a two point boundary value problem (TPBVP), which in general is very difficult to solve.

The next sections deal with the direct approaches of solving optimization problems. In direct approach, an approximation of the original dynamic optimization problem is done.

3.4 Control Vector Parameterization

Control vector parameterization (CVP) is an example of direct numerical methods for solving dynamic optimal control problems. CVP involves repeated solutions of differential equations. It is also known as direct sequential method. It is an approximation (discretization) of continuous control trajectory over finite time intervals. The approximation can be done using piecewise constants, piecewise linear functions, or any other parameterized functions, over time intervals.

Consider Fig. 3.1 representing a continuous trajectory of control. This original control profile

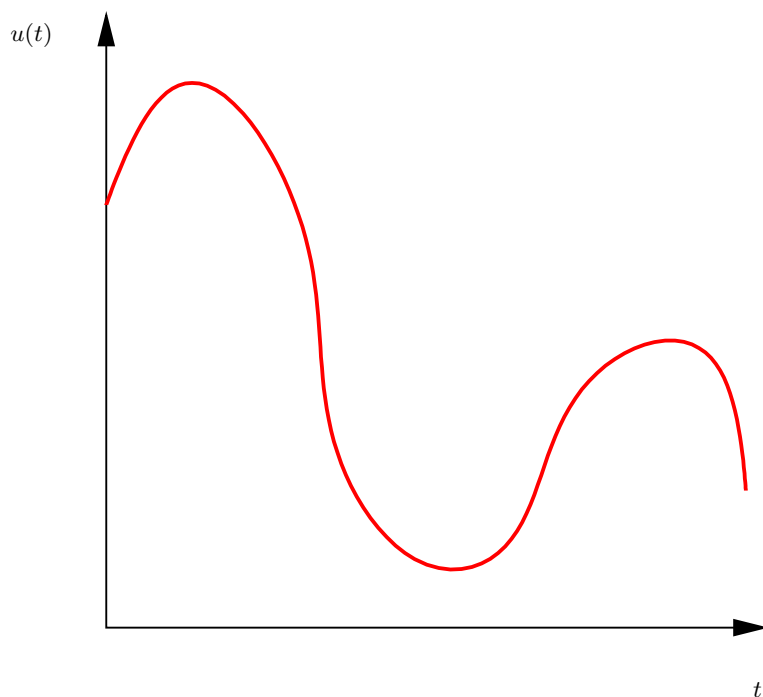


Figure 3.1: Continuous control trajectory.

can be discretized by for e.g. approximated constants (Fig. 3.2(a)), or linear functions (Fig. 3.2(b)), over time intervals. In Fig. 3.2(a), $u_1 \dots u_3$, represents constant control inputs, while in Fig. 3.2(b) $u_1 \dots u_7$ represent linear functions. The original continuous trajectory from Fig. 3.1 is represented by black dashed line Fig. 3.2. So, the discretized piecewise-constant control can be expressed as

$$\mathbf{u}(t) = \mathbf{u}_i, \quad t_{i-1} \leq t < t_i \quad (3.14)$$

where \mathbf{u}_i represents the constant control value over the time interval Δt_i , as defined in Fig. 3.2(a). This length of time interval can be defined as $\Delta t_i = t_i - t_{i-1}$. If number of intervals, i.e. $N_I = 3$,

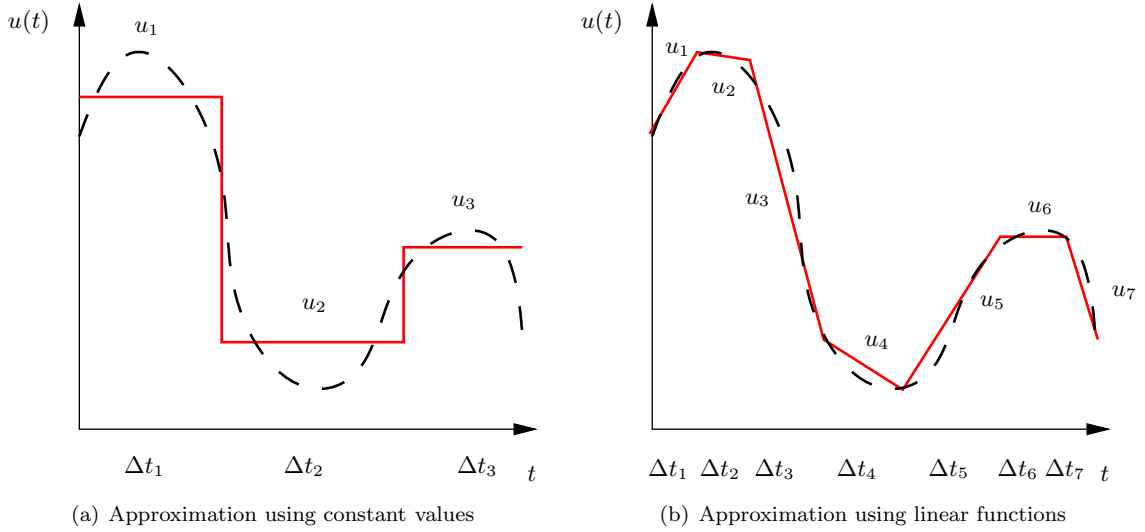


Figure 3.2: Discretized control trajectories.

it results in 6 degrees of freedom to our optimization problem (3 piecewise constant $\mathbf{u}_i + 3 \Delta t_i$). Similarly, the linear discretization can be expressed as

$$\mathbf{u}(t) = \mathbf{u}_{i-1} + \frac{\mathbf{u}_i - \mathbf{u}_{i-1}}{t_i - t_{i-1}} (t - t_{i-1}), \quad i = 1, \dots, N_I. \quad (3.15)$$

In thesis, approximation of control trajectory by constant values over time intervals is studied (3.14). The approximated piecewise-constant control can also be written as follows:

$$\mathbf{u}(t) = \sum_{i=1}^{N_I} \mathbf{u}_i \chi_{[t_{i-1}, t_i)}(t), \quad (3.16)$$

where

$$\chi_{[t_{i-1}, t_i)} := \begin{cases} 1, & \text{if } t \in [t_{i-1}, t_i), \\ 0, & \text{if } t \notin [t_{i-1}, t_i). \end{cases} \quad (3.17)$$

Hence, with the help of CVP we can transform the infinite dimensional problem of finding continuous trajectory of $\mathbf{u}(t)$, to a finite dimensional problem. This is done by using a set of parameters $\mathbf{y} \in \mathbb{R}^{n_y}$ ($n_y =$ number of optimized parameters) consisting of constant control inputs and corresponding time intervals, i.e.

$$\mathbf{y} = [\mathbf{u}_1, \dots, \mathbf{u}_{N_I}, \Delta t_1, \dots, \Delta t_{N_I}]. \quad (3.18)$$

The approximation problem defined above over the vector of optimized parameters \mathbf{y} is a NLP. In this problem, a finite set of variables needs to be found, such that the objective cost function is minimized. This problem can also be subjected to a set of constraints. In general, algorithms for NLP (sequential quadratic programming) use the cost and constraint gradients to generate search directions to improve optimization. In order to do this we need to compute the partial derivatives of cost function. There are three methods for finding the gradients according to Rosen and Luus (1991), i.e. :

- finite differences method,
- sensitivity method (variational method), and
- adjoint variables (costate) method.

These methods are described next.

3.4.1 Finite Differences Method

In this method of computing gradients, a minute variation/perturbation is given to each optimized variable (y_i) followed by evaluating the objective function (3.1), and it can be written as:

$$\nabla_{y_i} \mathcal{J} = \frac{\mathcal{J}(\mathbf{y}, y_i + \Delta y_i) - \mathcal{J}(\mathbf{y})}{\Delta y_i} \quad (3.19)$$

If the set of parameters to be optimized is large, this method of computing gradients requires to integrate large amount of functions. This method is less accurate when compared to adjoint and sensitivity methods for calculating gradients because of the choice of value of small change/variation given to the optimized variable, and due to the need of higher order gradients for non-linear systems. Finite differences method is easily implementable as no additional differential equations are to be evaluated, which will be added in the other two methods, presented further. This method is the default gradient calculator in *fmincon* (a nonlinear programming solver in *MATLAB*).

3.4.2 The Sensitivity Method

The method is based on so called sensitivities. These sensitivities are the partial derivatives of states with respect to decisive or optimized parameters \mathbf{y} . They are defined as:

$$\mathbf{s}_i = \frac{\partial \mathbf{x}}{\partial y_i}, \quad \mathbf{s}_i(0) = \mathbf{0}, \quad i = 1 \dots n_y \quad (3.20)$$

Now, the cost function and state equations are not explicit functions of \mathbf{y} , i.e. Δt_i and \mathbf{u}_i , and hence for $\dot{\mathbf{x}} = \mathbf{f}(t, \mathbf{x}, \mathbf{u})$, we need to define the partial derivative as:

$$\frac{\partial \dot{\mathbf{x}}}{\partial y_i} = \frac{\partial \mathbf{f}}{\partial \mathbf{x}} \frac{\partial \mathbf{x}}{\partial y_i} + \frac{\partial \mathbf{f}}{\partial \mathbf{u}} \frac{\partial \mathbf{u}}{\partial y_i}. \quad (3.21)$$

The sensitivity then can be formulated as:

$$\dot{\mathbf{s}}_i = \frac{\partial \mathbf{f}}{\partial \mathbf{x}} \mathbf{s}_i + \frac{\partial \mathbf{f}}{\partial \mathbf{u}} \frac{\partial \mathbf{u}}{\partial y_i}. \quad (3.22)$$

This generates a large set of differential equations, as each optimized parameter results in a set of differential equations, depending on number of states. This initial value sensitivity equation can be solved by forward integration, for e.g. *ode45* in *MATLAB*.

After defining the sensitivities, and using (3.1) and (3.22) the gradient of the objective function in general can be calculated as:

$$\frac{\partial \mathcal{J}}{\partial y_i} = \frac{\partial G}{\partial \mathbf{x}} \Big|_{t_f} \mathbf{s}_i + \int_{t_0}^{t_f} \frac{\partial F}{\partial \mathbf{x}} \mathbf{s}_i + \frac{\partial F}{\partial \mathbf{u}} \frac{\partial \mathbf{u}}{\partial y_i} dt. \quad (3.23)$$

Thus, to solve sensitivities and for computing gradients, we need to solve and integrate additional $n_x \times n_y$ differential equations. Hence, this method is not preferred when the set of optimized parameters is large, as integration is the most time consuming part of numerical optimization.

3.4.3 Adjoint Method

This method is suggested and applied when the set of optimized parameters is large. The Hamiltonian function H (3.4) is used in this method. The gradient of the objective function can be evaluated as given in (Paulen, 2010), i.e.

$$\begin{aligned}\frac{\partial \mathcal{J}}{\partial t_f} &= \frac{\partial G}{\partial t_f} + H(t_f), \\ \frac{\partial \mathcal{J}}{\partial t_i} &= \frac{\partial G}{\partial t_i} + H(t_i^-) - H(t_i^+), \\ \frac{\partial \mathcal{J}}{\partial \mathbf{u}_i} &= \mathcal{J}_{\mathbf{u}}(t_{i-1}) - \mathcal{J}_{\mathbf{u}}(t_i),\end{aligned}\tag{3.24}$$

where

$$\dot{\mathcal{J}}_{\mathbf{u}} = \frac{\partial H}{\partial \mathbf{u}}, \quad \mathcal{J}_{\mathbf{u}}(t_f) = \mathbf{0}.\tag{3.25}$$

The final gradients of objective function w.r.t. time intervals Δt_i can be written as:

$$\frac{\partial \mathcal{J}}{\partial \Delta t_i} = \sum_{i=1}^{N_I} \frac{\partial \mathcal{J}}{\partial t_i}, \quad i = 1 \dots N_I.\tag{3.26}$$

The solution is thus obtained by backward integration of costates initiating with the final conditions, from necessary conditions of optimality (3.6). This is to initiate the integrator. While forward integration of state equations is done with the initial state conditions.

The forward integration of the system is performed, and the solution is stored and then the backward integration of the adjoint system is done with the state approximation. This method is better than others when computing gradients for a system with large number of optimized parameters, but it leads to complexity in implementation, due to bi-directional integration.

3.5 Orthogonal Collocation

This method of numerical optimization transforms the original dynamic optimization problem (3.1) to a parametric optimization. Unlike CVP where only the control trajectory is parameterized, approximation of both state (\mathbf{x}) and control (\mathbf{u}) profiles is done in orthogonal collocations (OC).

Orthogonal polynomials replace the original trajectory of states and control for the approximation in this method (Lagrange polynomials). The approximation is made over collocation points, for both state and control. The roots of Legendre polynomials determine the distribution of these collocation points (Cuthrell and Biegler, 1987, Lauw-Bieng and Biegler, 1991, Čižniar, 2005).

Let us consider the system of ordinary differential equations (3.1b), with finite numbers of elements N_I in time $t \in [t_i, t_{i+1}]$. Then we approximate both states and control by polynomials $\hat{\mathbf{x}}$, and polynomials $\hat{\mathbf{u}}$, respectively. This approximation should be exact at the collocation points (Fig. 3.3).

The state and control variables approximated through Lagrange polynomials are defined as

$$\hat{\mathbf{x}}_i(t) = \sum_{k=0}^{K_x} \hat{\mathbf{x}}_{k,i} \phi_k(t) \quad \phi_k(t) = \prod_{r=0, r \neq k}^{K_x} \frac{t - t_{r,i}}{t_{k,i} - t_{r,i}}, \quad (3.27)$$

$$\hat{\mathbf{u}}_i(t) = \sum_{j=1}^{K_u} \hat{\mathbf{u}}_{j,i} \theta_j(t) \quad \theta_j(t) = \prod_{r=1, r \neq j}^{K_u} \frac{t - t_{r,i}}{t_{j,i} - t_{r,i}}, \quad (3.28)$$

$$\text{for } i = 1, \dots, N_I, \quad (3.29)$$

where K_x and K_u are the number of collocation points on states and control, respectively. Hence the vector of optimized parameters \mathbf{y} consists of parameters of approximated states ($\hat{\mathbf{x}}_{k,i}$), approximated controls ($\hat{\mathbf{u}}_{j,i}$), and time intervals (Δt_i), i.e.

$$\mathbf{y} = [\hat{\mathbf{x}}_{k,i}, \hat{\mathbf{u}}_{j,i}, \Delta t_i], \quad k = 0, \dots, K_x, \quad j = 1, \dots, K_u, \quad i = 1, \dots, N_I, \quad (3.30)$$

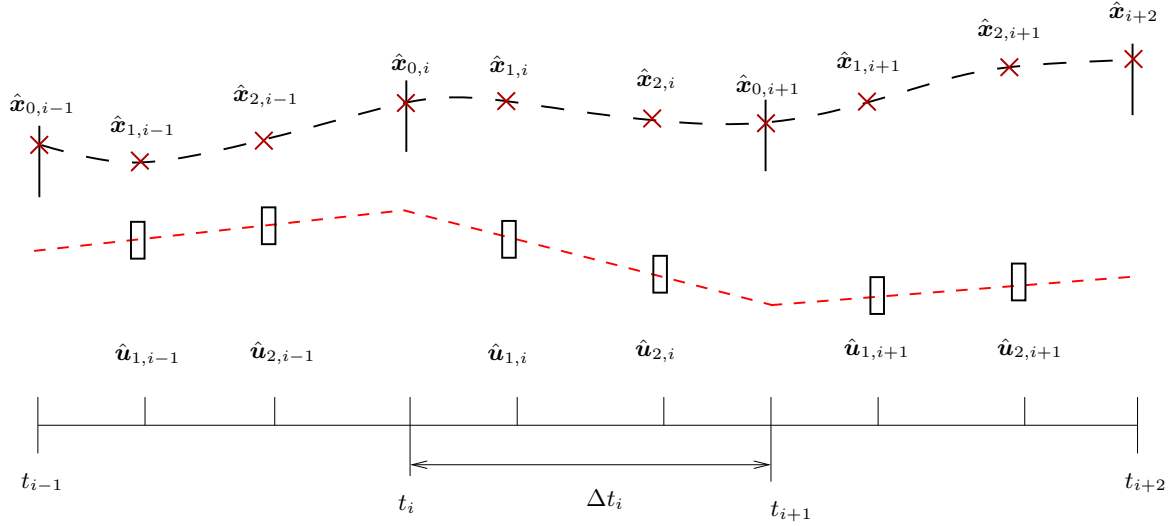


Figure 3.3: Distribution of time intervals and collocation points for state and control variables for $K_x = K_u = 2$

In Fig. 3.3 we can study an example of approximation points when $K_x = K_u = 2$, and $N_I = 3$. The collocation points on states are depicted using red cross. As $K_u = 2$, the control trajectory comes out to be a linear approximation in time. This control trajectory is represented in red dashed line.

So, the original state equations (3.1b) describing the system can be approximated over the collocation points as the following residual equation,

$$\sum \hat{\mathbf{x}}_{k,i} \dot{\phi}_k(\tau_k) - \Delta t_i \mathbf{f}(t_{k,i}, \hat{\mathbf{x}}_{k,i}, \hat{\mathbf{u}}_{j,i}) = \mathbf{0}, \quad k = 0, \dots, K_x, \quad j = 1, \dots, K_u, \quad i = 1, \dots, N_I, \quad (3.31)$$

where we consider each finite element normalized as $\tau \in [0, 1]$, i.e. the collocation points are placed between this range $[0, 1]$, at values according to roots of Legendre polynomials. Basic algebraic calculations are required for the implementation and solution of these stated residuals, and hence avoid

any kind of integration. The objective problem is transformed to:

$$\min_{\hat{\mathbf{x}}_{k,i}, \hat{\mathbf{u}}_{j,i}, \Delta t_i} \left\{ G(\hat{\mathbf{x}}_{t_f, N_I}) + \sum_{i=1}^{N_I} \int_{t_{i,0}}^{t_{i,f}} F(\hat{\mathbf{x}}_{k,i}, \hat{\mathbf{u}}_{j,i}, t) dt \right\}, \quad (3.32)$$

s.t.

$$\sum \hat{\mathbf{x}}_{k,i} \dot{\phi}_k(\tau_k) = \Delta t_i \mathbf{f}(t_{k,i}, \hat{\mathbf{x}}_{k,i}, \hat{\mathbf{u}}_{j,i}), \quad (3.33)$$

$$\hat{\mathbf{x}}_{0,1}(t_{1,0}) = \mathbf{x}_0, \quad \hat{\mathbf{x}}_{K_x, N_I}(t_{N_I, f}) = \mathbf{x}_f, \quad (3.34)$$

$$\hat{\mathbf{x}}_i(t_{i,0}) = \hat{\mathbf{x}}_{i-1}(t_{i-1, f}), \quad (3.35)$$

$$\hat{\mathbf{u}}_{j,i} \in [\hat{\mathbf{u}}_{\min}, \hat{\mathbf{u}}_{\max}], \quad (3.36)$$

where $k = 0, \dots, K_x$ i.e. for each state collocation point, $j = 1, \dots, K_u$ (for each control collocation point), $i = 1, \dots, N_I$ (for each time interval). The accuracy of approximation, and the speed of solving the optimization problem depends on the number of collocation points. Generally higher number of collocation points means higher precision, and longer solving time.

The OC method of numerical optimization is faster than CVP, as no integration needs to be performed. The accuracy is inferior to CVP as states are approximated, but significant differences are only found for large systems. For smaller systems with few states (as for batch DF in our research), the differences in results of optimization (costs, and optimized parameters) between CVP and OC are negligible.

There exist several software packages for implementing such numerical techniques of solving dynamic optimization problems in various programming environments. MATLAB packages such as OC based Dynopt (Čižniar et al., 2005) or CVP based DOTcvp (Hirmajer et al., 2008) and ACADO (Houska et al., 2011) are among those available freely. CasADi (Andersson, 2013) is a toolkit for nonlinear numerical optimization, depending on C++ library. It uses either collocation approach, or shooting based approach with the integration of ODE/DAE system. PROPT (Rutquist and Edvall, 2010) from TOMLAB is another toolbox that uses collocation methods for solving optimal control problems and is possible to be implemented using MATLAB. It is not for free but a free trial version can be used with MATLAB.

Finally, to summarize and compare the above explained numerical approaches. In general, OC produces a large sparse NLP formulation and is of infeasible type, where solution is obtained only if optimum is found. In CVP a large fraction of time and memory is spent in integrating the solution of differential equations, at each iteration. On the contrary, OC converts the differential equations to algebraic ones using polynomial functions, and hence is faster than CVP method. However, CVP method can exploit robustness and efficiency of modern ODE solvers. Some of these are capable to provide sensitivity information used for evaluation of a more accurate gradient information (Hirmajer and Fikar, 2006).

Part II

Thesis Contributions

Chapter 4

Open-Loop Batch Diafiltration

This chapter is dedicated towards the research contributions of this thesis, in the field of open-loop diafiltration. This chapter includes firstly the process mathematical modeling, then followed by the detailed description about the membrane plant utilized, and its basic control. Next part is the experimental modeling via parameter estimation. Then the optimal control formulation and results of laboratory experiments conclude this chapter. The research work published in Sharma et al. (2017a), Sharma et al. (2018), Sharma et al. (2016b) and Sharma et al. (2019) by the author is the source for this chapter.

The basic description of open-loop DF plant was presented in subsection 2.1.3. The detailed diagrammatic view with process variables is presented here in Fig. 4.1 to better understand the modeling part. The diluant inflow rate q_{in} is the external input. This flow rate can be defined in relation to permeate flow rate q_p ; variable α is the ratio between inflow of diluant to the feed tank, and permeate outflow, i.e. $\alpha = q_{in}/q_p$. This dimensionless variable α represents the process input.

4.1 Mathematical Modeling

In this chapter, the mathematical modeling of batch open-loop diafiltration membrane processes is presented. This model has been adapted from literature (Kovács et al., 2009b). The model is described by ordinary differential equations, representing the concentrations, and the feed tank volume, i.e. the states.

4.1.1 Modeling Assumptions

To derive the model, we will assume the following:

- The process operates at controlled constant transmembrane pressure i.e.

$$\Delta P = \frac{P_f + P_r}{2} - P_p, \quad (4.1)$$

is constant, where P_f , P_r , and P_p are the membrane inlet, retentate (outlet), and permeate side pressure, respectively.

- Density of the processed solution is assumed as constant.
- The ability of the membrane to reject a particular component is defined by a rejection coefficient R_i as

$$R_i(c_1, \dots, c, m) = 1 - \frac{c_{p,i}}{c_i}, \quad i = 1, \dots, m. \quad (4.2)$$

where m is the number of components and $c_i, c_{p,i}$, are the concentrations of i th component entering the membrane, and in the permeate, respectively.

Rejection coefficients are dimensionless numbers that represent the membrane's rejection towards a solute and can take values from the interval $[0, 1]$. This coefficient in general varies during the process and is a function of concentrations of the solutes, temperature and pressure. As the plant operates under constant pressure and temperature conditions, the rejection coefficients can be modeled as functions of concentrations.

This coefficient could be defined by models such as Donnan steric partitioning model (Cuartas-Uribe et al., 2007, Schaep et al., 1999) as a function of permeate flux for uncharged solutes, or by Kedem-Spiegler model (Spiegler and Kedem, 1966) as a function of q_p and ΔP . We assume in this study ΔP being constant. Therefore, for simplicity, this coefficient can be assumed to be either a constant or a function of the concentrations, and can be determined experimentally as given in Kovács et al. (2009a).

These assumptions can be easily maintained in practice, and are important in order to maintain the product quality.

4.1.2 Model Derivation

In this section, the derivation of the ODE's from the mass balance is presented. These ODE's describe the dynamics of concentration of solutes, irrespective of number of components (m). The rate of change of total volume in the system (refer Fig. 4.1) can be represented as:

$$\frac{dV}{dt} = \alpha q_p - q_p, \quad (4.3)$$

where V is the volume of the solution inside (refer Fig. 4.1) the feed tank, and is changing according to the rate of diluant into the tank (αq_p) and rate of permeate leaving the system (q_p). The permeate flow q_p can be determined experimentally as a function of concentrations of components c_i entering the membrane

$$q_p(A, c_1, \dots, c_m) = AJ(c_1, \dots, c_m), \quad (4.4)$$

where A represents the effective membrane area. $J(\cdot)$ stands for the permeate flux subject to unit membrane area and is also a function of concentrations (c_i). This permeation model q_p is non-linear, in all the cases studied in this thesis.

The concentration change for a component i during the processing (refer Fig. 4.1) can be obtained from the mass balance as:

$$\frac{d(c_i V)}{dt} = -c_{p,i} q_p, \quad (4.5)$$

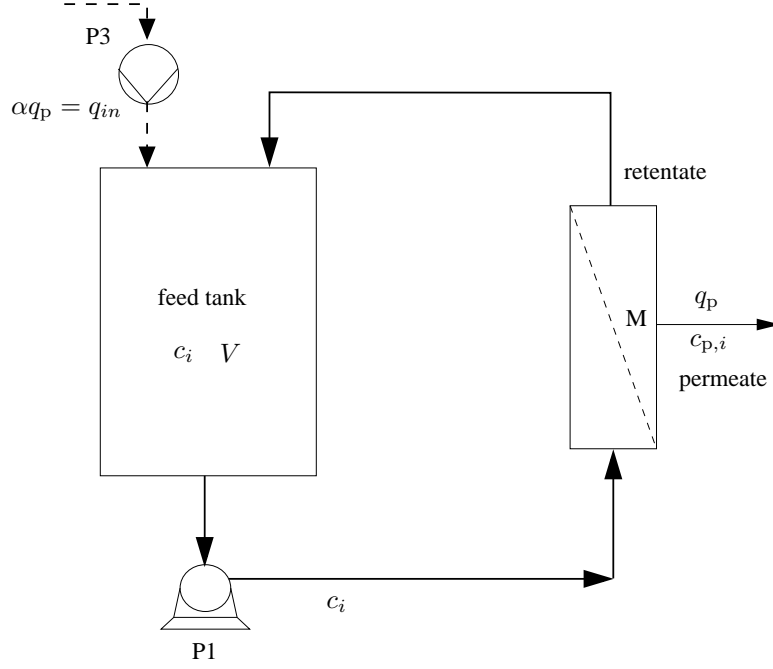


Figure 4.1: Batch DF process flow scheme

The solute leaves the system in the permeate flow with the concentration $c_{p,i}$. The ability of the membrane to reject a particular component can be taken from (4.2) as

$$R_i = 1 - \frac{c_{p,i}}{c_i}. \quad (4.6)$$

The use of (4.6) to replace $c_{p,i}$, leads the derivation from mass balance (4.5) to,

$$\frac{dc_i}{dt}V + c_i \frac{dV}{dt} = -(1 - R_i)c_i q_p, \quad (4.7)$$

which can be rewritten using (4.3) to

$$\frac{dc_i}{dt} = -c_i \frac{\alpha q_p}{V} + R_i c_i \frac{q_p}{V}. \quad (4.8)$$

4.1.3 Model

The final model for batch DF comprises tank dynamics, and the dynamics of component's concentrations. The ODE for tank volume with initial and final conditions can be rewritten using (4.3) as:

$$\dot{V} = (\alpha - 1)q_p, \quad V(0) = V_0, \quad V(t_f) = V_{t_f}. \quad (4.9)$$

The mass balance for the concentration dynamics for each solute with initial and final conditions can be given as

$$\dot{c}_i = \frac{c_i q_p}{V} (R_i - \alpha), \quad c_i(0) = c_{i,0}, \quad c_i(t_f) = c_{i,f}, \quad i = 1, 2, \dots, m. \quad (4.10)$$

In general, there are m (component concentrations c_i) + 1 (tank volume) equations, with m being the number of components. The number of unknown variables on the other hand is $m + 1$ (concentrations, volume) + 1 (α), and hence the degree of freedom is 1. This mathematical model helps

connecting the diluant addition rate, i.e. α , to the concentration of solutes, and to the volume of the feed tank.

Furthermore, two component/solute solution has been used for all experimental batch open-loop work. The solutes used are lactose (c_1) and NaCl (c_2). The experiments in this thesis are for concentrating lactose and reducing NaCl's concentration, using NDF.

The NDF model for the two component solution using the general model derived above, can be described by the following three differential equations

$$\frac{dc_1}{dt} = \frac{c_1 q_p}{V} (R_1 - \alpha), \quad c_1(0) = c_{1,0}, \quad (4.11a)$$

$$\frac{dc_2}{dt} = \frac{c_2 q_p}{V} (R_2 - \alpha), \quad c_2(0) = c_{2,0}, \quad (4.11b)$$

$$\frac{dV}{dt} = (\alpha - 1)q_p, \quad V(0) = V_0, \quad (4.11c)$$

where the constants R_1, R_2 are rejection coefficients of lactose and NaCl respectively.

It was observed during our preliminary experiments that the rejections for both lactose and NaCl stay around constant values. $R_i = 0$ implies that the i th solute passes through the membrane without any resistance. This is the case for the used membrane as it does not resist to a free passage of NaCl, hence $R_2 = 0$. On the contrary, $R_i = 1$ means that the membrane blocks the solute completely and its concentration in the permeate is zero, which is the property of membrane regarding rejection of lactose. Because of $R_1 = 1$ (at any time, mass of lactose stays constant),

$$c_1 V = c_{1,0} V_0 \quad \Rightarrow \quad c_1 = \frac{c_{1,0} V_0}{V}. \quad (4.12)$$

Eq. (4.12) can be used to eliminate volume from the model (4.11). This transforms the general model from three to two differential equations, i.e.

$$\frac{dc_1}{dt} = c_1^2 \frac{q_p}{c_{1,0} V_0} (1 - \alpha), \quad c_1(0) = c_{1,0}, \quad (4.13a)$$

$$\frac{dc_2}{dt} = -c_1 c_2 \frac{q_p}{c_{1,0} V_0} \alpha, \quad c_2(0) = c_{2,0}. \quad (4.13b)$$

4.1.4 Diluant Input Modes

The dilution rate or input ($\alpha \geq 0$) as discussed, is the dynamic degree of freedom for the NDF process. The classical operation of batch NDF or DF mostly uses piece-wise constant α using three simple modes (Foley, 2006, Jaffrin and Charrier, 1994):

- No diluant input ($\alpha = 0$), i.e. concentration mode (C): in this mode, the volume decreases (4.11c), and the mass of lactose is constant. As a result, the concentration of lactose increases (4.11a), while the concentration of NaCl stays constant (4.11b).
- The diluant inflow equals the outflow of permeate ($\alpha = 1$), i.e. constant volume diafiltration mode (CVD): lactose concentration remains constant (4.11a), as does the volume (4.11c), while NaCl concentration decreases in this mode due to dilution done by adding pure water as diluant (4.11b).

- Diluant flow-rate is less than the outflow of permeate ($0 < \alpha < 1$), i.e. variable volume diafiltration mode (VVD): volume decreases in this mode (4.11c), and hence lactose concentration increases (4.11a), while due to the dilution of solution, NaCl concentration decreases as well (4.11b).

In addition to these three modes, Lutz (2015), Paulen and Fikar (2016) have proposed two new basic modes:

- Dynamic volume diafiltration (DVD): this is similar to VVD mode as diluant flow-rate is less than the outflow of permeate, but unlike VVD α is not a constant but is varying with time ($0 < \alpha(t) < 1$).
- Pure dilution mode (D): in this mode a certain amount of diluant is instantaneously added to the solution. This can be represented by $\alpha = \infty$. Lactose and NaCl concentrations decrease proportionally in pure dilution mode. Due to the nature of this step, it can be done without the plant/process running (no energy used), and takes negligible amount of time.

Combination of different modes results in different costs and time to achieve certain concentration of product and impurities (Paulen et al., 2013).

4.2 Laboratory Membrane Plant

The modeling, optimal control problem and its solution, for batch open-loop DF were discussed previously in this chapter. Next step is to implement this theory in practice, i.e. to prove it experimentally. This section describes the membrane plant utilized to achieve these experimental objectives. The plant has also been used in education process (Sharma et al., 2016b).

The laboratory membrane separation plant used for performing nanodiafiltration experiments in this research work is shown in Fig. 4.2. This multi-membrane plant provides possibilities to use with or without diafiltration;

1. ultrafiltration or,
2. nanofiltration or,
3. reverse osmosis.

This choice of filtration is made by manually opening and closing the respective valves on the plant (NDF in this research work).

NFW-1812F nanofilter membrane manufactured by Synder Filtration, USA, with a cut-off range 300–500Da, and a membrane area of $A = 0.465 \text{ m}^2$ was used to perform the experiments.

The following steps describe the procedure of experiments.

1. The initial feed volume is added to the feed tank comprising the initial concentrations of solutes/components ($c_{1,0}$ for lactose and $c_{2,0}$ for NaCl) to be separated.

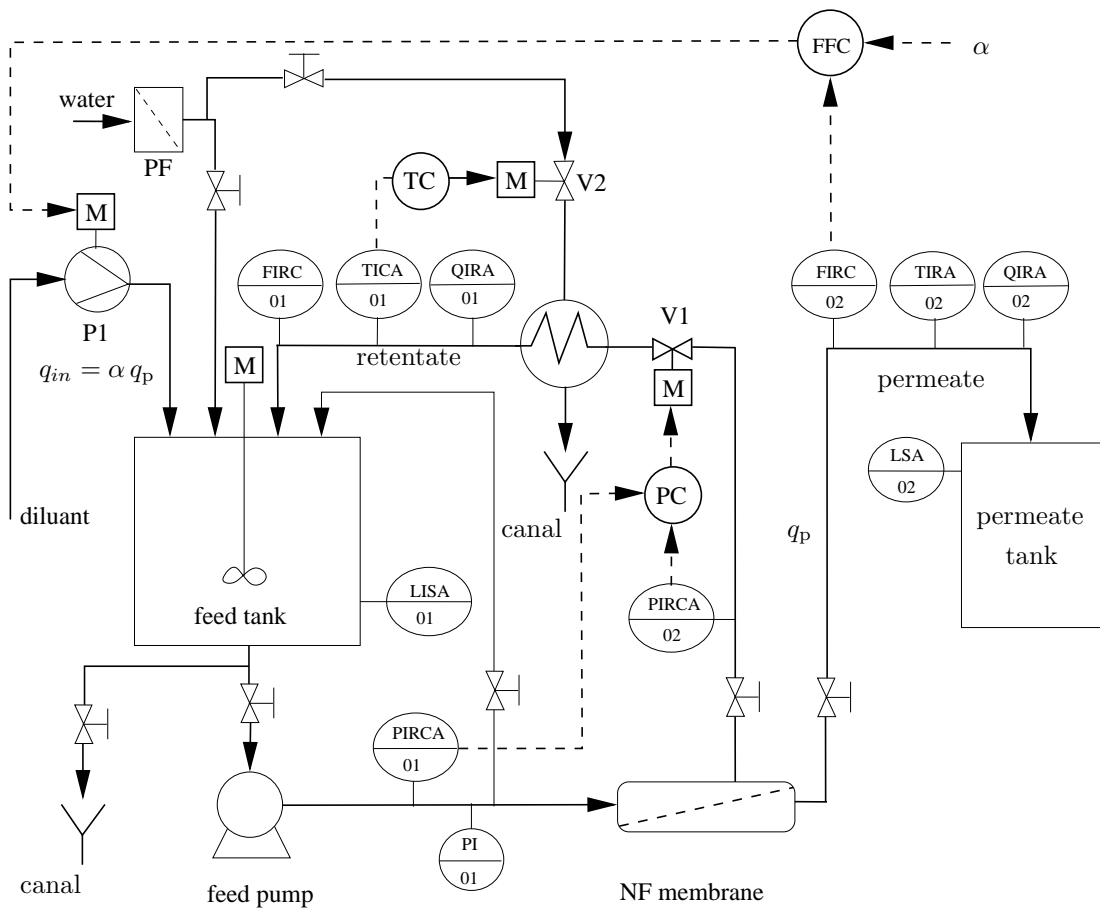


Figure 4.2: P&I diagram of the laboratory nanodiafiltration process.

2. At a fixed pumping power, resulting in certain pressure, the feed is pushed towards the membrane in cross-flow mode. The operation is started in the total recirculation mode, i.e. both the permeate and the retentate return to the feed tank. The concentrations and volume hence stay constant. This is done to stabilize:

- The transmembrane pressure (TMP) (4.1), where the membrane inlet pressure is measured using sensor PIRCA01, and retentate pressure using PIRCA02,
- The temperature of the solution,
- The hydrodynamic conditions, and to eliminate the initial fouling (Sharma et al., 2016a, 2017a).

As soon as all the physical parameters settle around or exhibit constant desired values, the experiment is started by letting the permeate leave the system towards permeate tank.

The measurements of all physical variables can be seen online for any given sampling time. These values can be stored for later calculations, or for online calculations while the experiments are running. HMI designed using WinCC environment (CITATION), and Simulink based HMI are used for this data visualization, storage, etc.

The permeate flow-rate is measured using sensor FT02 (see Fig. 4.2). The concentration of NaCl (c_2 [kg/m³]) in the retentate is inferred from the conductivity measurements (sensor QT01), as the contribution of lactose to conductivity of the solution is negligible. The calibration curve obtained is represented by using the experimentally obtained linear model

$$c_2 = 0.0007 \times QT [\mu S/cm] - 0.6949, \quad (4.14)$$

where QT represents the actual retentate conductivity.

The experiments done for this solution of lactose and NaCl (Sharma et al., 2016a, 2017a, 2018) show that the retentate comprises lactose and NaCl, while the permeate contains NaCl only.

Lactose concentration (c_1 [kg m⁻³]) at each sampling instance is calculated from the known initial mass, and the actual volume/level in the feed tank (LISA01). This is due the properties of the used membrane (Synder, 2014), that is designed to completely retain lactose in the system. Hence, the mass of lactose in the system, at any time during the experiment stays constant. Consequently, the concentration of lactose at any time is given by (4.12).

4.2.1 Communication and Operation

Various techniques have been implemented on the plant, for efficient communication between the sensors and the computer. The detailed description of techniques for this communication via signal transfer between various sensors and operator (PC) is presented here.

In Fig. 4.3 we can see the overall communication setup of the laboratory membrane process. This communication is done in two ways, i.e. by using programmable logic controller (PLC), and industrial network router (INR). The PLC is responsible for obtaining the basic data and for the control tasks. This is because PLC is connected directly to the sensors and actuators of the membrane plant. The PLC is also connected to the industrial Ethernet network, which is used as the main communication

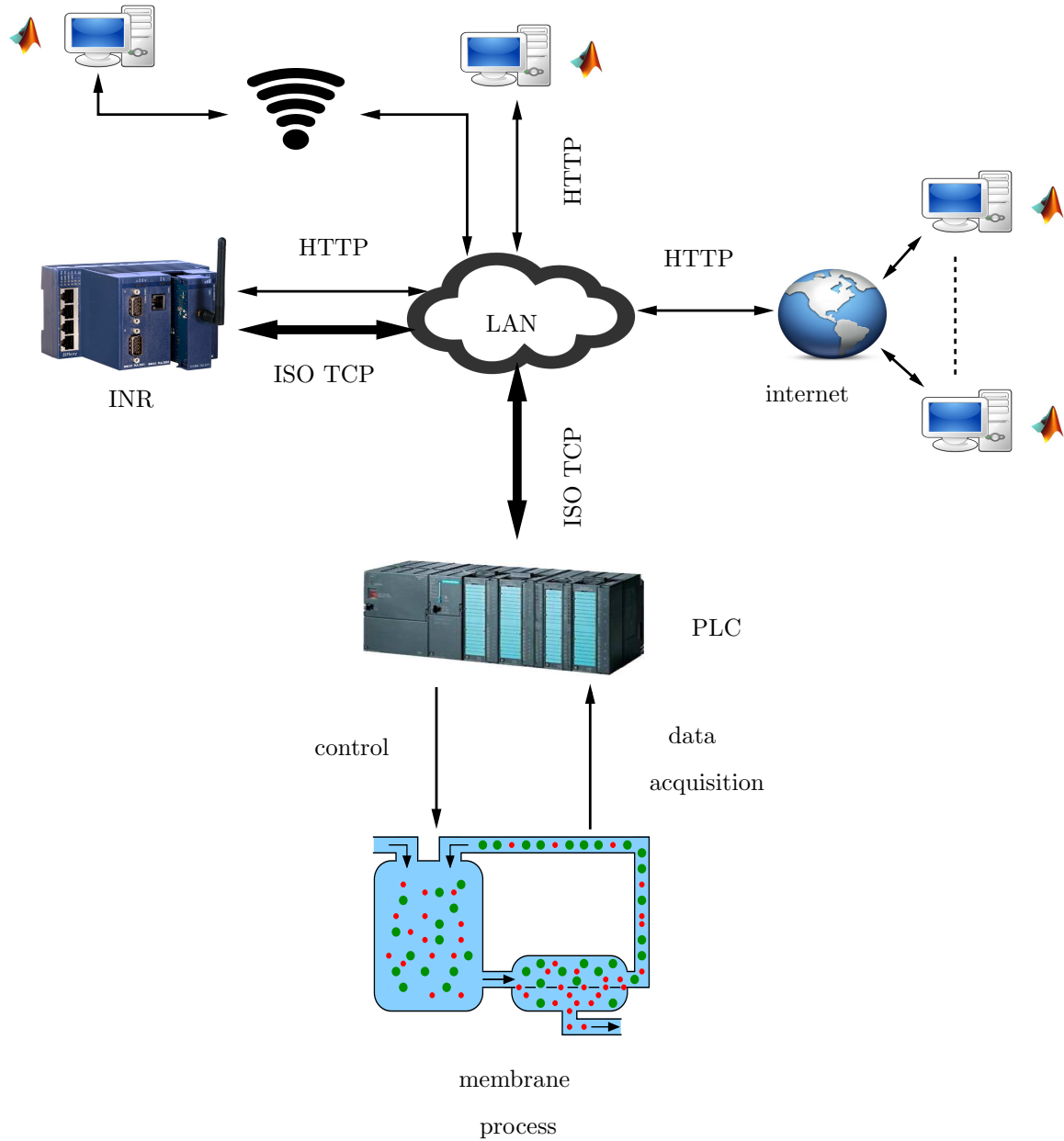


Figure 4.3: Industrial communication and control devices connected to membrane plant.

network within the laboratory, where the plant and all supplementary control devices are located. The second industrial device that extends the network usage of membrane plant is the industrial network router eWON Flexy 203 (eWON, 2014), that can be described as a coupler for the industrial controllers. The objectives of this INR are:

- industrial protocol translation;
- direct access to PLC program variables (read/update);
- data acquisition from PLC;
- server-side script runtime environment;
- data and event logging;
- process security and alarms;
- FTP and web server.

As this industrial router is not dependent on the used protocols, it allows universal communication with most of the industrially used equipments. The other important feature of INR is that it allows to access the internal program variables of PLC, through common HTTP, and hence allows to extend the plant's control system by various control environments that are capable of HTTP communication. These are e.g. web-based applications and visualizations, MATLAB, Python programs, etc. Since the used industrial network is connected to wide area network, this allows the users to connect to INR from different locations, either to use direct connection through (local PC or WiFi), or indirectly from a remote location through the Internet.

This aids in remote setup and functioning of laboratory. Operators do not need to install the appropriate software (MATLAB/Simulink, WinCC) on their computers and will communicate with the process through the Internet, where the visualization scheme is a part of a Web page.

MATLAB/Simulink and WinCC based visualizations are developed and used for operating the plant. From the visualization environment, the signals of physical variables (temperature, pressure, valve opening, etc.) are firstly sent to INR, and finally through PLC these signals are actuated on to the hardware.

A good visualization scheme is very important for controlling the process (Fig. 4.4). The visualization is not only for effective reading of data from the sensors, but it also allows to control the individual parts of the process (e.g. pumps, valves, agitator). The visualization developed in this work, allows the operator to directly implement the process constraints for the pump, valve, feed level etc. Trends, alarms, and shut-down rules have also been implemented for safety purposes.

These processes are highly influenced by operating parameters, such as temperature and pressure. The automation and control of these parameters is described next.

4.2.2 Pressure (TMP) Control

Pressure must be maintained between specific ranges, due to following reasons:

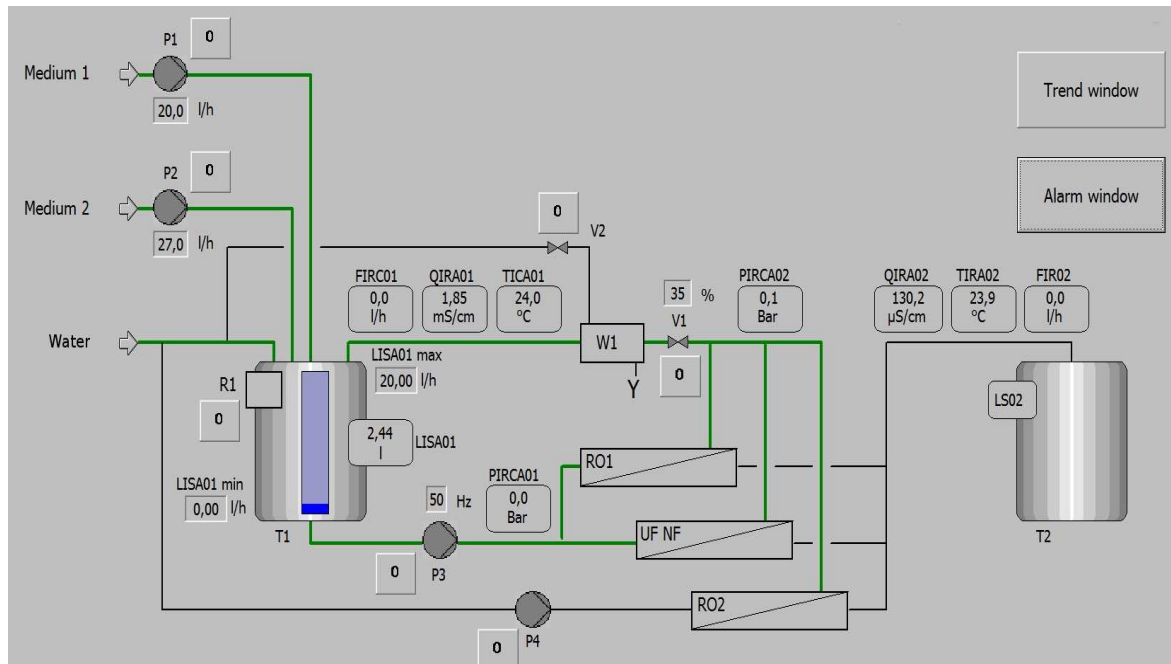


Figure 4.4: Human Machine Interface (HMI) designed using WinCC flexible environment, to run and control the membrane plant.

- the theory applied in this thesis is based on the assumption of constant pressure,
- pressure fluctuations result in oscillating measurements of other quantities, for e.g. flow rates,
- uncontrolled pressure changes will most likely lead to hardware damage,

and hence the identification and control of the pressure is a necessity. The pressure could be changed by two actuators, i.e., the feed pump and the retentate side valve (V1). This valve can be opened in the range 0–100%. To protect the feed pump, its rotational speed is kept constant, while the retentate valve is used for TMP control.

The TMP control is achieved using a pressure controller (PC). A proportional controller is implemented to perform this regulation. TMP (4.1) is calculated based on the inlet and outlet pressure of the membrane and is computed in the controller part. The controller actuates the corresponding opening of the valve V1 based on the current measurement based calculated TMP, and reference TMP. Fig. 4.5 shows an example where the desired TMP, i.e. 24 bar (dashed red line) and the measured TMP (solid blue line) are compared. The designed controller was sufficiently good to maintain TMP at desired value, with an acceptable error margin of 0-5 % from set point, and despite of changing concentration (increase in lactose from 80 to 450[kg/m³]).

4.2.3 Temperature Control

The temperature of the solution (retentate, permeate) increases as the experiment progresses. The high pressure pump on the membrane inlet generates heat and is one of the reasons for this increase in temperature. The other reason for heat generation is due to the fluid dynamics resulting in molecular

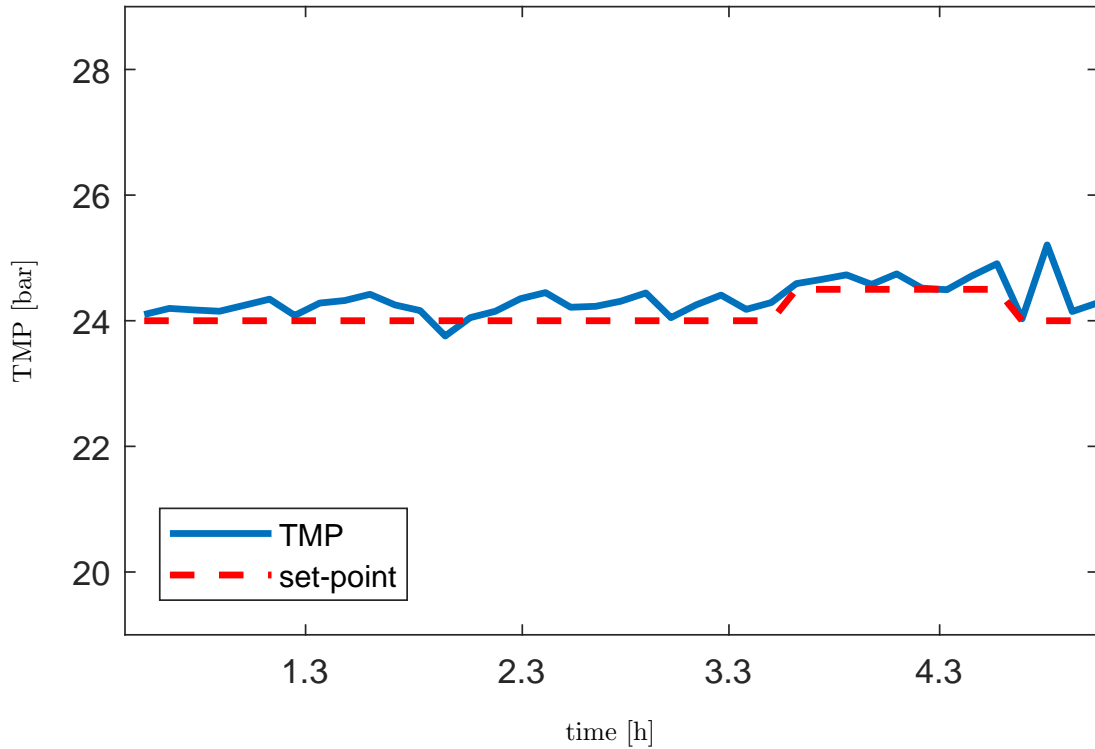


Figure 4.5: Control of transmembrane pressure.

frictional heat, and viscous heat. Therefore, the temperature needs to be controlled and maintained in a safe zone.

As shown in Fig. 4.2, the plant is equipped with a heat exchanger in order to cool the retentate returning to the feed tank. The plant has temperature sensors on both retentate and permeate sides.

The temperature of the solution is maintained at a constant value using the heat exchanger with cooling water and a temperature controller (TC). Fig. 4.6 shows an example where the controller is trying to maintain the retentate temperature (solid blue line) near the referenced or desired set-point (dashed red line).

The designed controller was sufficiently good to maintain the temperature within limits, but it can be observed that there exist oscillations. Due to imperfection of the employed valve, the temperature cannot be held constant and has an average deviation of ± 0.6 °C. This causes minor fluctuations in measurements of other process variables in experiments.

4.2.4 Diluant Addition

The experiments in this thesis include diafiltration (NDF). This diluant (reverse osmosis water) addition for NDF is done using additional pumps. Diluant addition at a controlled rate is extremely important for this research. Hence, flow ratio controller (FFC in Fig. 4.2) has been implemented to pour diluant into the feed tank precisely based on calculations. This calculation can be based on the measurement of volume inside feed tank (level control), or the amount of permeate leaving the system

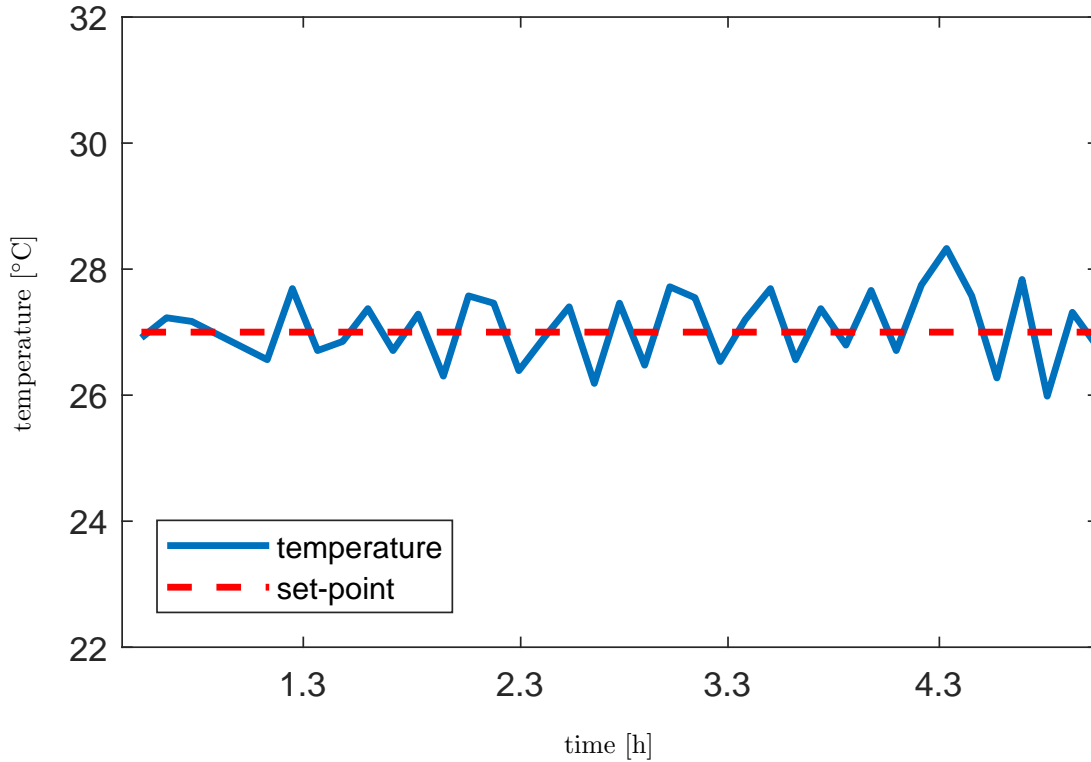


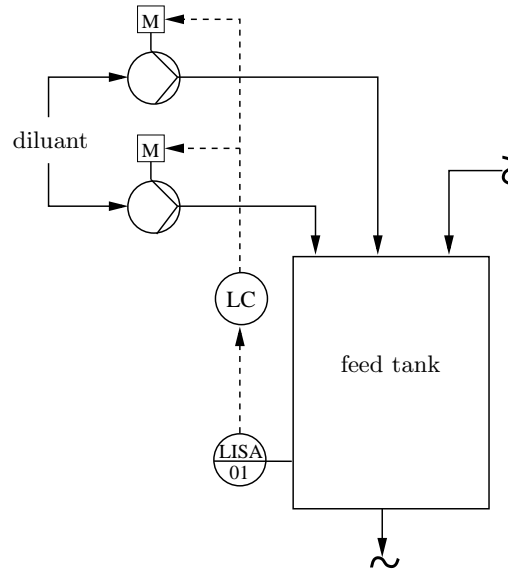
Figure 4.6: Control of temperature.

per unit time (permeate flow rate based control).

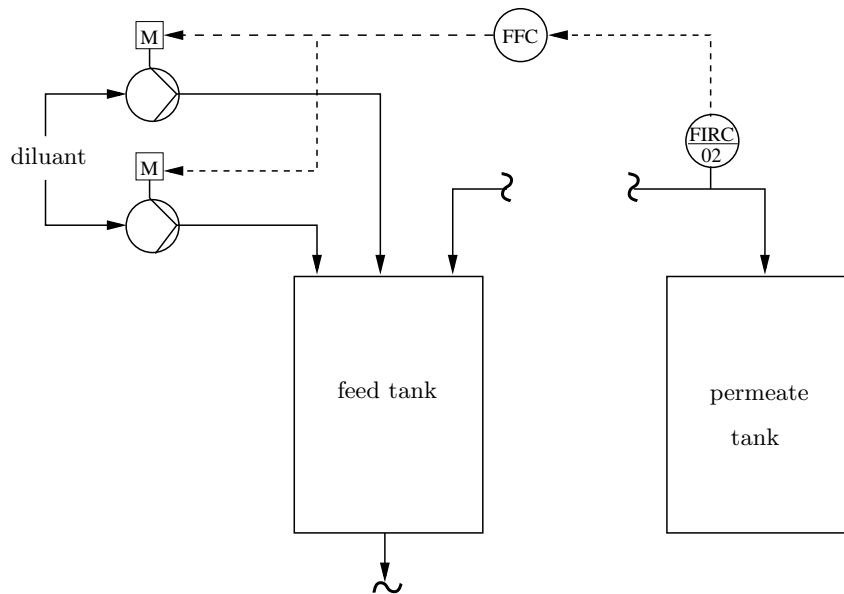
The level/volume measurement sensor (LISA01) of the feed tank is constrained in the range 0.003–0.032 m³ (3–32 L). The controller directly manipulates inlet flows to the tank as shown in Fig. 4.7(a) using the level transmitter as sensor.

The diluant addition can also be changed indirectly by manipulating the ratio between the diluant inflow and permeate flow (Fig. 4.7(b)), i.e. α . In this case, the permeate flow sensor (FIRC02) is used to indirectly account the decrease in system volume, and accordingly the pumps adjust the flow rate of diluant.

In Fig. 4.8, an example is presented for controlling the level inside the feed tank. The objective is to maintain the level of tank at a constant value of 0.00324 m³ (3.24 L), using permeate flow rate based control. This is done by putting $\alpha = 1$ (inflow = outflow) in the visualization scheme. Based on the permeate flow rate measurement fluctuations (FIRC02), we can observe the corresponding minor fluctuations in measured feed volume. An average deviation of 0.00005 m³ (50 mL) has been measured during the experiments.



(a) Direct feed tank level control with the aid of level transmitter.



(b) Indirect level control in the feed tank using ratio of diluant and permeate flows (permeate flow transmitter)

Figure 4.7: Level control in the feed tank by using a diluant.

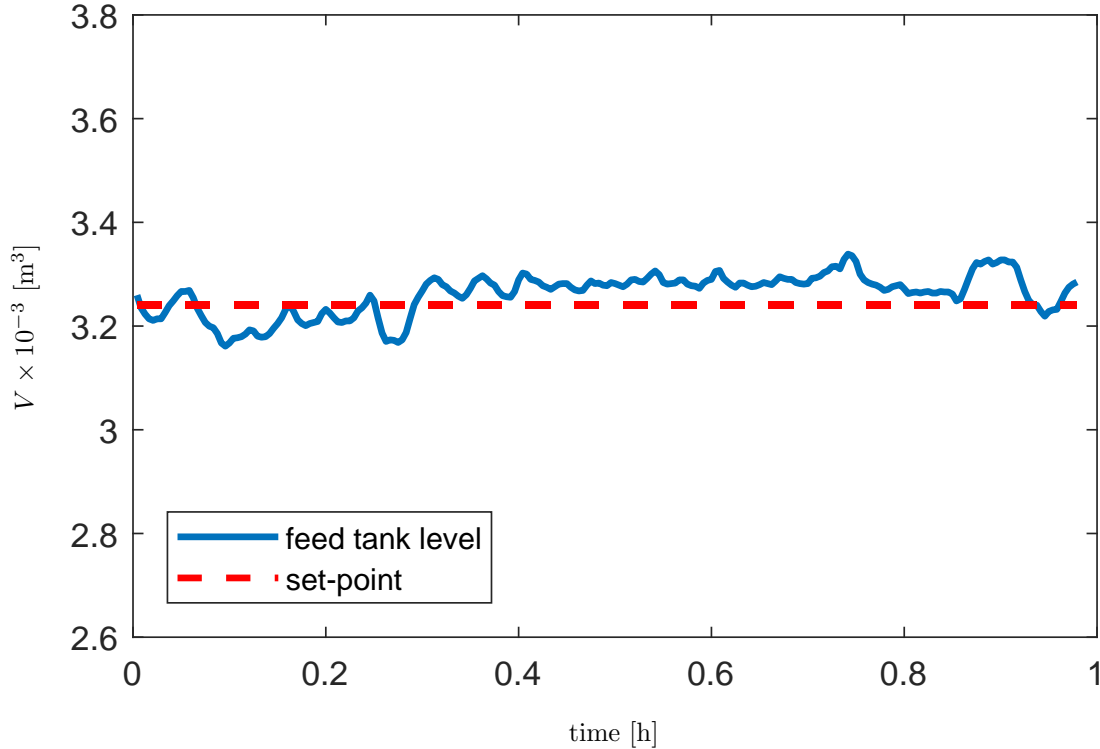


Figure 4.8: Control of feed tank level.

4.3 Experimental Modeling

The permeate flow rate (q_p) present in the model equations is generally a function of concentration, pressure and temperature for a given membrane. In this thesis, the batch membrane operation is done by maintaining constant pressure and temperature. Therefore, the permeate flow rate is only a function of concentrations. This relation needs to be identified and parameterized experimentally in order to develop the further research on this process. This experimental modeling work has been published in Sharma et al. (2016a, 2017a, 2018).

Two different models were fitted with the permeate flow rate data i.e., a function of lactose and NaCl concentration:

- Limiting flux (LF) model: This model has been taken from Balannec et al. (2005), Blatt et al. (1970), Tang and Leckie (2007). The model defines the permeate flow rate as a function of time-varying lactose (macro-solute) concentration and the parameters, i.e. mass transfer coefficient ($\gamma_1 \text{ mh}^{-1}$) and limiting concentration of lactose ($\gamma_2 \text{ mh}^{-1}$).

$$q_p = k A \ln \left(\frac{c_{\text{lim}}}{c_1} \right) = A (\gamma_1 + \gamma_2 \ln(c_1)), \quad (4.15)$$

This model is used as the dependence of permeate flow on NaCl concentration is quite low. This can be inferred from studying the CVD part of experiment (Fig. 4.9), where the NaCl is decreasing, but the magnitude of change in q_p is very small.

Two such models have been fitted. Firstly, by taking the complete experimental data (both C and CVD modes), i.e. LF₁. Secondly, as this model is only a function of c_1 , and c_1 is not varying

a lot during the second part of experiment (CVD mode in Fig. 4.10), hence a model was fitted using only the data from the first part of experiment, i.e. LF₂.

- Generalized limiting flux (GLF) model: Based on the preliminary experiments, a form of the model of q_p used in this work is defined as generalized limiting flux model (GLF), (Rajagopalan and Cheryan, 1991)

$$q_p = A(\gamma_1 + \gamma_2 \ln(c_1) + \gamma_3 \ln(c_2)), \quad (4.16)$$

It incorporates concentrations of both solutes and can be reduced to the limiting flux model with $\gamma_3 \text{mh}^{-1} = 0$.

The optimal parameter estimation problem to fit the flow rate data to the permeate flow rate model and the concentration data to state values can be formulated as:

4.3.1 Problem Definition

$$\min_{\gamma_1, \gamma_2, \gamma_3} \sum_{i=1}^N \left(\frac{(q_p(t_i) - q_{p,m}(t_i))^2}{\delta_{q_p}} + \sum_{j=1}^2 \frac{(c_j(t_i) - c_{j,m}(t_i))^2}{\delta_{c_j}} \right) \quad (4.17a)$$

s.t.

$$\dot{c}_1 = c_1^2 \frac{q_p}{c_{1,0} V_0} (1 - \alpha), \quad (4.17b)$$

$$\dot{c}_2 = -c_1 c_2 \frac{q_p}{c_{1,0} V_0} \alpha, \quad (4.17c)$$

$$c_1(0) = c_{1,0}, \quad c_2(0) = c_{2,0}, \quad (4.17d)$$

$$q_p = (4.16) \text{ or } (4.15), \quad (4.17e)$$

where $q_{p,m}(t_i)$, $c_{1,m}(t_i)$, and $c_{2,m}(t_i)$ represent measured permeate flow-rates and concentrations of the solutes at measurement times (t_i). The number of observations or data points is represented by N . In the model equations volume V has been replaced using (4.12). The weighting of each term in the objective function is represented by coefficients δ_{q_p} , δ_{c_1} , δ_{c_2} , which are set to experimentally observed variances of the corresponding measurements.

Note, that in contrast to other standard least-squares approaches that would fit the permeate flow-rate (4.16) or (4.15) against the measurements of concentrations, the employed estimation procedure incorporates the mass balance equations (4.17b)–(4.17d), which serves the purpose of data reconciliation against the errors in concentration measurements. Such approach results in consistent and more precise parameter estimates.

4.3.2 Problem Solution

Based on our experimental results it is clear that at constant temperature and TMP; NF permeation rate depends on concentrations of both lactose and NaCl, i.e. $q_p = q_p(c_1, c_2)$. The membrane fouling occurs only for a short initial period and stabilizes quickly. The lactose molecules being larger in size have significantly larger effect on the permeate flow when compared to NaCl molecules. Data

Table 4.1: Parameters of the models.

| model | GLF | LF ₁ | LF ₂ |
|------------|--------|-----------------|-----------------|
| γ_1 | 3.0 | 2.8 | 3.4 |
| γ_2 | 1109.9 | 1246.7 | 723.7 |
| γ_3 | 0.1 | - | - |

from an NDF experiment that concentrated lactose from 40 kg/m³ to 120 kg/m³, (C mode) and that reduced NaCl from 3.35 kg/m³ to 1 kg/m³ (CVD mode) was used to perform the fitting of models from literature of such kind. The experiment was done in total recirculation mode (permeate returns to feed tank, volume and concentrations remain constant) until fouling got constant, and then permeate was allowed to leave the system. 56 data points of flow rate were used to perform model fitting. The sample time was 0.025 h.

The above non-linear least-squares problem was implemented and solved using MATLAB, and the states were integrated using an ode45 solver.

4.3.3 Results

The resulting parameters are given in Table 4.1 and the permeate flow rates and concentrations in Figs. 4.9–4.11. It can be observed that the GLF model fits the data better than the LF models, especially in the second part of the experiment with $\alpha = 1$. This is expected as the GLF model can accommodate the variations in the concentration $c_2(t)$. The value of sum of squared errors was at the minimum for GLF model, increased slightly for LF₁ model, and was maximum for LF₂ model. The comparison of the estimation between LF₁ and LF₂ models shows that for C mode the LF₂ model fits the data better, but when simulated for CVD mode the results were worst. It concretes that even though LF model is solely a function of c_1 , still data for both C and CVD modes are required for fitting the complete NDF data. The measured and the simulated concentrations were satisfactorily corresponding to each other, for all fitted models (Fig 4.10, 4.11).

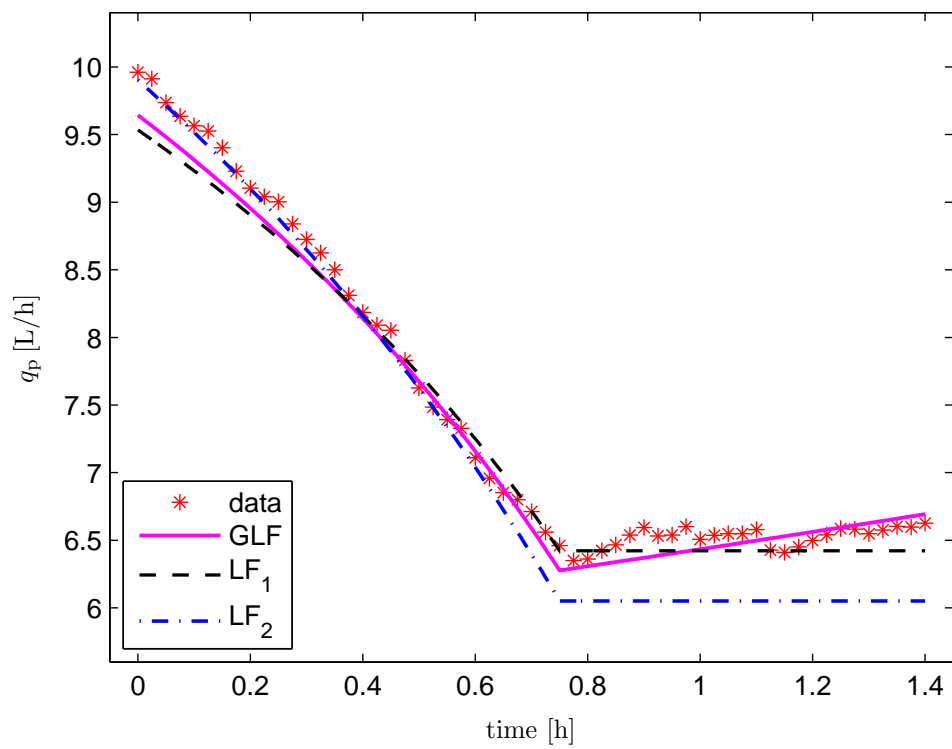


Figure 4.9: Permeate flow rate measurements vs simulated estimated models.

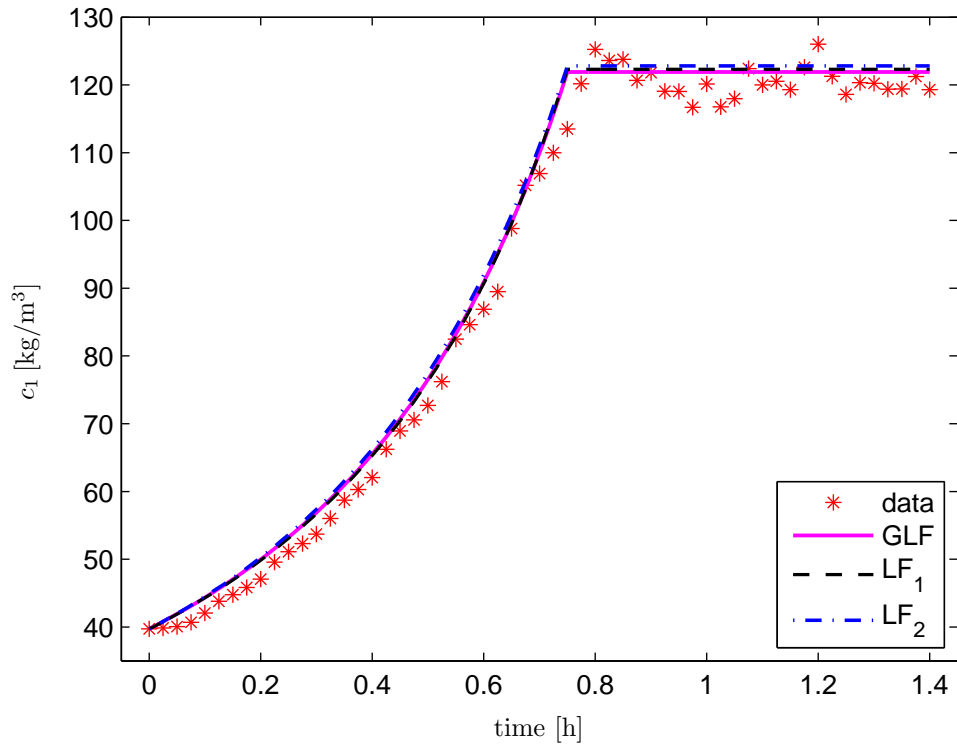


Figure 4.10: Comparison of lactose concentration: measured vs simulated data based on estimated models.

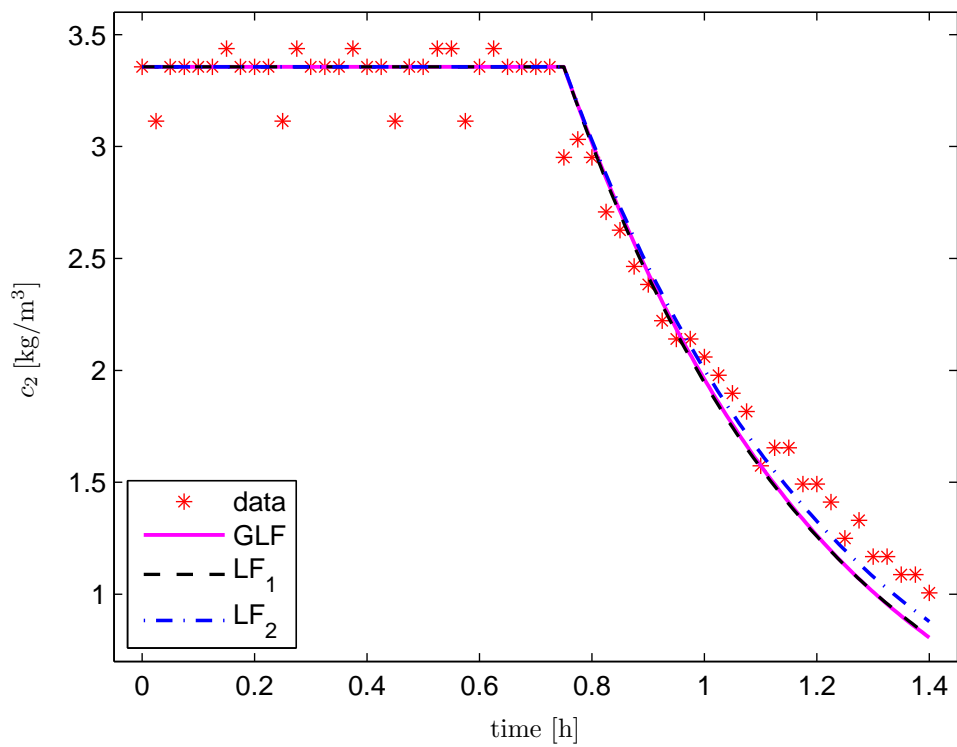


Figure 4.11: Comparison of NaCl concentration: measured and simulated data based on estimated models.

4.4 Optimal Control

The objective of the membrane process optimization is to find a time-dependent input function $\alpha(t)$, which results in the increase of lactose concentration from initial value $c_{1,0}$ to final value $c_{1,f}$ and in the simultaneous reduction of the salt concentration from $c_{2,0}$ to final value $c_{2,f}$, whilst minimizing the operating costs.

4.4.1 Problem Formulation

The operating costs can be minimized in various ways. The most common is minimization of the processing time

$$t_f^* = \min_{\alpha(t)} t_f = \min_{\alpha(t)} \int_0^{t_f} 1 dt, \quad (4.18)$$

where t_f denotes the time needed to bring the process from the given initial concentrations to desired final ones. Time minimization results in reduction of costs by decreasing the consumption of electric energy (mainly used for running the pumps) and labor costs.

Another generally used cost function deals with the overall diluant consumption. It is given as the total volume of the diluant addition to reach the desired concentrations i.e.

$$V_D^* = \min_{\alpha(t)} V_D = \min_{\alpha(t)} \int_0^{t_f} q_0 dt = \min_{\alpha(t)} \int_0^{t_f} \alpha q_p dt. \quad (4.19)$$

In order to incorporate both processing time (t_f) and diluant consumption (V_D), a weighted objective function can be defined. The resulting optimal control problem can be formulated as:

$$\mathcal{J}^* = \min_{\alpha} w_T t_f + w_D V_D, \quad (4.20a)$$

s.t.

$$\dot{c}_1 = c_1^2 \frac{q_p}{c_{1,0} V_0} (R_1 - \alpha), \quad c_1(0) = c_{1,0}, \quad (4.20b)$$

$$\dot{c}_2 = c_1 c_2 \frac{q_p}{c_{1,0} V_0} (R_2 - \alpha), \quad c_2(0) = c_{2,0}, \quad (4.20c)$$

$$c_1(t_f) = c_{1,f}, \quad c_2(t_f) = c_{2,f}, \quad (4.20d)$$

$$q_p = q_p(c_1, c_2). \quad (4.20e)$$

The non-negative weighting coefficients w_T, w_D represent the weight (or price) for a unit of processing time and diluant consumption, respectively. The process engineer can decide on the values of these coefficients based on the prevailing costs of respective quantities or based on known unit costs. One can opt for time ($w_D = 0 / \text{€m}^3$) or diluant ($w_T = 0 / \text{€h}$) minimization, or shift in-between these goals, by changing the values of these coefficients.

4.4.2 Problem Solution

The theoretical analysis of the optimal operation of batch membrane processes can be found in Paulen and Fikar (2016) and it is based on Pontryagin's minimum principle (Pontryagin et al., 1962).

The optimal diluant addition strategy consists of three successive operation modes, where the first and the last mode corresponds to operation with α being saturated on constraints (either concentration

or pure dilution mode). The second mode is characterized by the singular curve equation ($S = 0$) and diluant rate α , which are functions of both solute's concentrations (Paulen and Fikar, 2016)

$$S = w_T \left(q_p + \frac{\partial q_p}{\partial c_1} c_1 + \frac{\partial q_p}{\partial c_2} c_2 \right) + w_D q_p^2 = 0, \quad (4.21)$$

$$\alpha = \frac{\frac{\partial S}{\partial c_1} c_1}{\frac{\partial S}{\partial c_1} c_1 + \frac{\partial S}{\partial c_2} c_2}. \quad (4.22)$$

The middle mode for the lactose-salt system for the GLF model (4.16), using singular curve (4.21) and singular control equation (4.22) is given as

$$S(c_1, c_2) = A w_T (\gamma_1 + \gamma_2 + \gamma_3 + \gamma_2 \ln c_1 + \gamma_3 \ln c_2) + A^2 w_D (\gamma_1 + \gamma_2 \ln(c_1) + \gamma_3 \ln(c_2))^2 = 0, \quad (4.23)$$

$$\alpha = \frac{\gamma_2}{\gamma_2 + \gamma_3} = 0.914. \quad (4.24)$$

Hence, the optimal middle mode for this system with GLF model is VVD. The optimal concentration of macro-solute (lactose) to switch to the middle mode can be derived from (4.23) for the following three cases:

1. Multi-objective i.e. $w_T > 0$ and $w_D > 0$:

$$c_1^* = \exp \left(- \frac{\gamma_1 + \gamma_3 \ln(c_2) + \frac{w_T - \sqrt{w_T} \sqrt{(w_T + (\gamma_2 - \gamma_3) 4Aw_D)}}{2Aw_D}}{\gamma_2} \right), \quad (4.25)$$

2. Time-optimal i.e. $w_T > 0$ and $w_D = 0$:

$$c_1^* = \exp \left(- \frac{\gamma_1 + \gamma_2 + \gamma_3 + \gamma_3 \ln(c_2)}{\gamma_2} \right), \quad (4.26)$$

3. Diluant-optimal i.e. $w_T = 0$ and $w_D > 0$:

$$c_1^* = \exp \left(- \frac{\gamma_1 + \gamma_3 \ln(c_2)}{\gamma_2} \right). \quad (4.27)$$

The first and the third mode are either C ($\alpha = 0$) or D ($\alpha = \infty$) mode. This depends on initial and desired final concentrations w.r.t. to the singular curve (the sign of $S(c_{1,0}, c_{2,0})$ and $S(c_{1,f}, c_{2,f})$). In the first section one takes the mode that brings the concentrations of the solutes to the singular curve ($S(c_1, c_2) = 0$ or c_1^*). Hence, if the initial concentration of macro-solute is less than optimal switching concentration, then we need to use C mode to increase macro-solute's concentration to reach there. On the contrary, we need to reduce macro-solute's concentration using D mode if initial concentration of macro-solute is more than optimal switching concentration. These cases for initial mode are:

$$\alpha = \begin{cases} 0 \text{ (C mode)}, & \text{if } c_{1,0} < c_1^*, \\ \infty \text{ (D mode)}, & \text{if } c_{1,0} > c_1^*, \text{ and} \\ \alpha_s, & \text{if } c_{1,0} = c_1^*. \end{cases} \quad (4.28)$$

The third section starts at singular curve and chooses the mode that finishes at the desired final concentrations. That is, if the macro-solute is over-concentrated than its final concentration at the

end of second (singular) section, then D mode needs to be applied to dilute the solution and reach the final concentrations. On the contrary, if the macro-solute was not concentrated enough during the previous two modes, C mode needs to be applied again to reach the final concentrations.

Now, for the limiting flux model (4.15), using the same general singular curve (4.21) and singular control equation (4.22), the optimal switching condition and control can be given as

$$S(c_1, c_2) = w_T A k \left(\ln \frac{c_{\text{lim}}}{c_1} - 1 \right) + w_D A^2 k^2 \ln \left(\frac{c_{\text{lim}}}{c_1} \right)^2 = 0, \quad (4.29)$$

$$\alpha = \frac{\frac{\partial S}{\partial c_1} c_1}{\frac{\partial S}{\partial c_1} c_1} = 1. \quad (4.30)$$

Therefore, the optimal middle control in case of limiting flux is CVD. Note: the optimality of CVD in minimum-time (time-optimal) case was previously found by Ng et al. (1976).

For limiting flux model, the optimal switching concentration of lactose to the middle mode can be found analytically for;

1. Multi-objective i.e. $w_T > 0$ and $w_D > 0$:

$$c_1 = c_{\text{lim}} \exp \left(\frac{w_T - \sqrt{w_T^2 + 4kAw_Tw_D}}{2Akw_D} \right), \quad (4.31)$$

2. Time-optimal i.e. $w_T > 0$ and $w_D = 0$:

$$c_1 = \frac{c_{\text{lim}}}{e}, \quad (4.32)$$

3. Diluant-optimal i.e. $w_T = 0$ and $w_D > 0$:

$$c_1 = c_{\text{lim}}. \quad (4.33)$$

The modes to be applied in first and third section depend on the initial and final conditions w.r.t. the singular curve.

The middle optimal control for both models is constant, but different. The singular curve is also different for the models, and this translates into changes in start and end points (concentrations) of the middle mode.

4.5 Optimal Control – Case Studies

The purpose of case studies is to demonstrate both in simulations and experimentally, the proposed optimal membrane separation strategy (section 4.4) using batch open-loop NDF, and its advantages to existing (traditional) industrial strategies. This work has been published in Sharma et al. (2019) and Sharma et al. (2018).

Lactose monohydrate ($M = 360.31 \text{ g/mol}$) is the purified and concentrated product while sodium chloride ($M = 58.44 \text{ g/mol}$) is the impurity to be removed. Reverse osmosis water is used as a solvent to prepare solutions, and also as the diluant for DF.

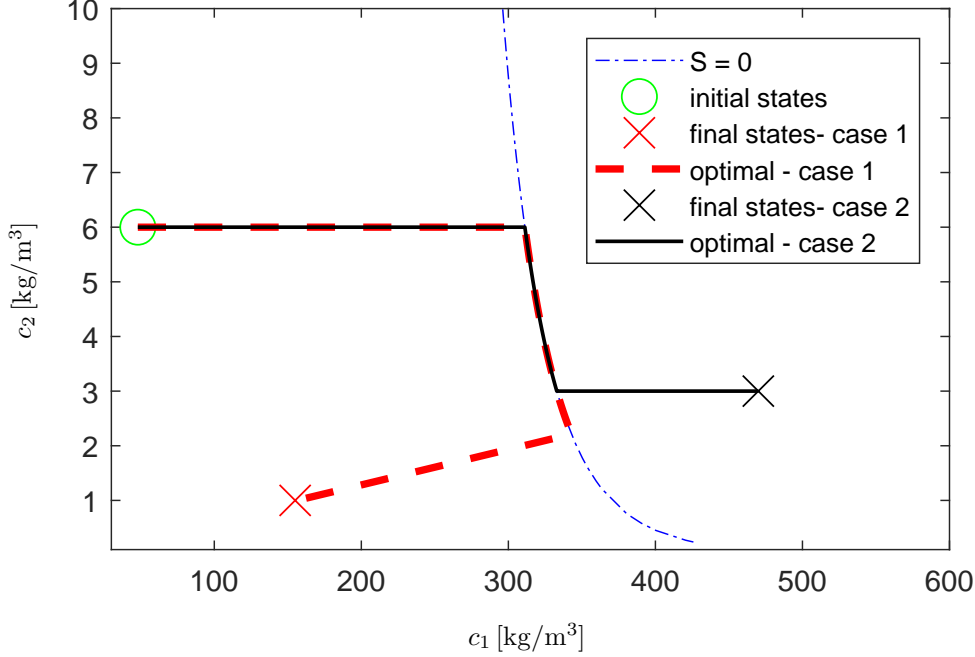


Figure 4.12: Concentration diagram for case studies along with the singular curve ($S = 0$).

For the first two case studies (case study 1 and 2), the process initial conditions are as follows: the volume of the solution $V_0 = 0.032 \text{ m}^3$, the lactose concentration $c_{1,0} = 48 \text{ kg/m}^3$ and the salt concentration $c_{2,0} = 6 \text{ kg/m}^3$. The difference in case study 1 and 2 lies in the final concentrations. We will study two possible final concentration sets: $(c_{1,f}, c_{2,f}) = (155 \text{ kg/m}^3, 1 \text{ kg/m}^3)$ and $(c_{1,f}, c_{2,f}) = (470 \text{ kg/m}^3, 3 \text{ kg/m}^3)$. These initial and final points are shown in Fig. 4.12 together with the singular curve (4.23) for minimum time settings ($w_D = 0$). The final points are chosen so that they are positioned to the left and to the right of the singular curve, respectively.

As the initial point is located to the left of the singular curve, the optimal initial operation mode for both cases is the C mode. When the final point lies to the left of the singular curve, the optimal terminal (third) operation mode is the D mode. In the opposite case another C mode is used to finish the processing.

Case study 3 is different from case study 1 and 2 in both initial and final conditions. This case study is presented to confirm the optimality results with different sets of starting and desired concentrations of lactose and NaCl.

4.5.1 Case Study 1

Three strategies were experimentally tested:

Traditional two step strategy C-CVD: ($\alpha = \{0, 1\}$): pure NF using the C mode until lactose concentration increases to the desired final value ($c_1 = c_{1,f} = 155 \text{ kg/m}^3$) followed by the CVD mode to reduce NaCl concentration to the final value ($c_2 = c_{2,f} = 1 \text{ kg/m}^3$).

Time-optimal strategy C-VVD-D: ($\alpha = \{0, 0.914, \infty\}$), $w_D = 0$: The concentration mode is used to keep the salt concentration constant $c_2 = c_{2,0} = 6 \text{ kg/m}^3$ and to increase the lactose concen-

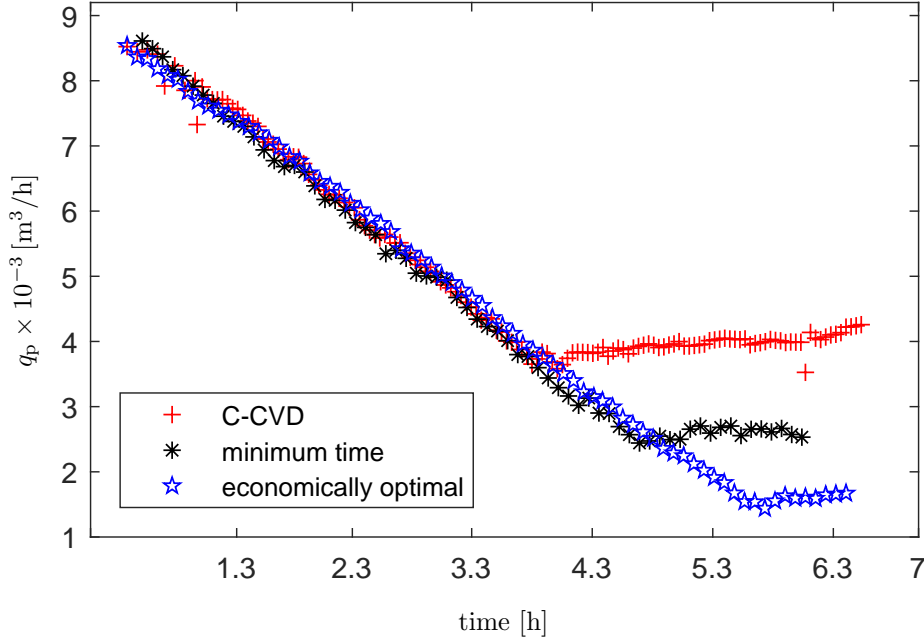


Figure 4.13: Case study 1: Permeate flow-rate measurements of traditional and optimal strategies.

tration to $c_1 = \exp(-(\gamma_1 + \gamma_2 + \gamma_3 + \gamma_3 \ln c_2)/\gamma_2) = 311.2 \text{ kg/m}^3$, which follows from (4.23). Then, the VVD mode is applied until the condition $c_1/c_2 = c_{1,f}/c_{2,f}$ is met. This ends the separation process and an appropriate amount of water is added to the solution.

Economically optimal strategy C-VVD-D: ($\alpha = \{0, 0.914, \infty\}$), $w_T = 1 \text{ €/h}$, $w_D = 0.2 \text{ €/m}^3$.

The only difference to the time-optimal strategy is the lactose concentration to be reached in the concentration mode. The singular curve (4.23) is shifted to the right in the concentration diagram and the VVD mode is applied when $c_1 = 438.2 \text{ kg/m}^3$. This switching concentration is found numerically using the values of w_T, w_D from (4.23).

The switching concentration of lactose is quite high in both of the optimal cases. The solubility of lactose at the given temperature is lower than that of our requirements (Yalkowsky et al., 2016). However, as lactose is totally retained by the membrane, so it does not effect significantly our optimal strategy and the process of separation. Moreover, due to high flow rate of retentate returning to the tank, the solution was continuously mixed/stirred, and lactose was not observed to be settled at the bottom or segregated in pipes. Hence, the only significant variable effected by lactose concentration is q_p , and that we have studied and modeled in this thesis.

Measurements from the conducted experiments are presented in the permeate flow-rate diagram (Fig. 4.13) and in the concentration diagram (Fig. 4.14). The permeate diagram shows that although the duration of the concentration mode is the shortest in the classical strategy, the subsequent CVD mode makes the final processing time the longest.

The concentration diagram (Fig. 4.14) shows initial and final points (green and red circles, respectively) as well as solid lines indicating dilution mode at the end of processing with optimal strategies.

Table 4.2 summarizes experimentally obtained values of final processing times and water consumption. Relative values $\Delta t_f, \Delta V_D$ take the maximum value in the column as 100% and show reduction

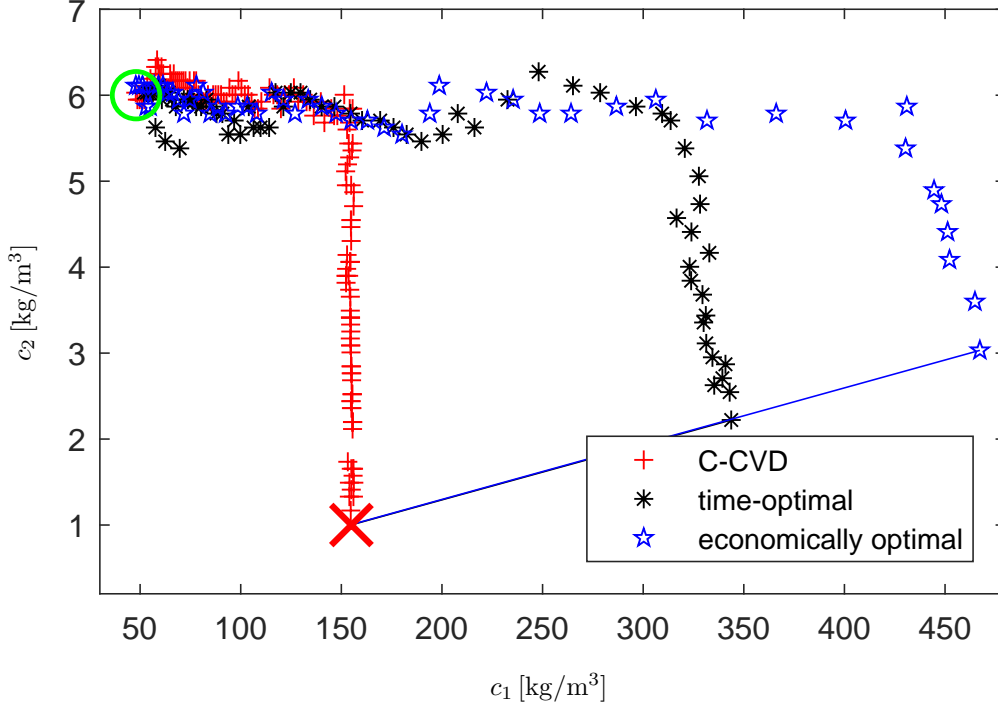


Figure 4.14: Case study 1: Concentration measurements of lactose and NaCl for traditional and optimal strategies.

Table 4.2: Experimental results: comparison of total processing time and diluant consumption for different scenarios in case study 1.

| Strategy | t_f [h] | Δt_f [%] | $V_D \times 10^{-3}$ [m ³] | ΔV_D [%] | Cost [€] |
|----------------------|-----------|------------------|--|------------------|----------|
| traditional (C-CVD) | 6.53 | 100.00 | 10.69 | 100.00 | 6.53 |
| time-optimal | 6.04 | 92.50 | 9.16 | 85.61 | 6.04 |
| economically optimal | 6.40 | 98.01 | 7.96 | 74.39 | 6.40 |

in other experiments (e.g. time-optimal takes only 92.5% of time required by C-CVD approach). The cost in the table is calculated by taking the price per unit of time and diluant volume from the economically optimal strategy ($w_T = 1 \text{ €/h}$, $w_D = 0.2 \text{ €/m}^3$).

We can notice that the traditional strategy is worse in both the indicators compared to the proposed optimal ones. These take 92-98% of the processing time and 74-86% of the diluant consumption. Although the economically optimal strategy is close to the traditional one in the terms of the processing times, its diluant usage is significantly lower.

It is interesting to compare these experimental results with simulations/predictions based on the model. Table 4.3 shows the same information as Table 4.2. We can clearly see that the permeate model parameters fitted are not perfect and some discrepancies can be observed. When the processing times are compared, the differences are between 5-10%. Diluant consumption shows larger differences indicating that the model parameter estimation might be improved.

Table 4.3: Simulation results: comparison of total processing time and diluant consumption for different scenarios in case study 1.

| Strategy | t_f [h] | Δt_f [%] | $V_D \times 10^{-3}$ [m ³] | ΔV_D [%] | Cost [€] |
|----------------------|-----------|------------------|--|------------------|----------|
| traditional (C-CVD) | 6.15 | 100.00 | 17.75 | 100.00 | 9.70 |
| time-optimal | 5.72 | 93.00 | 10.10 | 56.40 | 7.74 |
| economically optimal | 5.80 | 94.31 | 8.91 | 50.20 | 7.58 |

Overall, the C mode takes longer time in experiments than in simulations, whereas CVD/VVD takes shorter duration in experiments when compared to simulations. Note that economic difference between both optimal strategies is practically negligible, which is due to chosen unit prices.

It is worth noting that besides reducing processing time and diluant consumption, the optimal strategies can be applied with existing setup comparable to the industrial standard and without any new hardware. Also, no on-line optimization/calculations are required: the switching concentrations and control is found out prior to the start of an experiment.

Further improvement can be achieved by re-estimating the model parameters while performing the separation (online parameter estimation). This may result in implementation of a truly real-time optimal strategy, but at the expense of online optimization/calculations, and hardware/software modifications.

4.5.2 Case Study 2

Three strategies were implemented and compared:

Traditional two step strategy C-CVD: ($\alpha = \{0, 1\}$): pure NF using the C mode till lactose concentration increases to the desired final value ($c_1 = c_{1,f} = 470 \text{ kg/m}^3$) followed by the CVD mode to reduce NaCl concentration to the final value ($c_2 = c_{2,f} = 3 \text{ kg/m}^3$).

Traditional three step strategy C-CVD-C: ($\alpha = \{0, 1, 0\}$): using the limiting flux model (Ng et al., 1976), apply the concentration mode until lactose concentration increases to ($c_1 = c_{\text{lim}}/e = 458 \text{ kg/m}^3$) followed by the CVD mode to reduce NaCl concentration to the final value ($c_2 = c_{2,f} = 3 \text{ kg/m}^3$). The third step is again the C mode to concentrate lactose to its desired final concentration $c_1 = c_{1,f} = 470 \text{ kg/m}^3$.

Time-optimal strategy C-VVD-C: ($\alpha = \{0, 0.914, 0\}$), $w_D = 0$: The concentration mode is used to increase the lactose concentration to $c_1 = 311.2 \text{ kg/m}^3$ which follows from (4.23). Then, the VVD mode is applied until NaCl concentration equals to the final value ($c_2 = c_{2,f} = 3 \text{ kg/m}^3$). The third step is again the C mode to concentrate lactose to its final concentration $c_1 = c_{1,f} = 470 \text{ kg/m}^3$.

The experimental results are shown in Figs. 4.15, 4.16 and Table 4.2. The permeate flow-rate diagram, (Fig. 4.15) shows that all three strategies started at a similar initial flow rate due to the identical initial concentrations. The initial trajectory of flow rate during the C mode is the same for

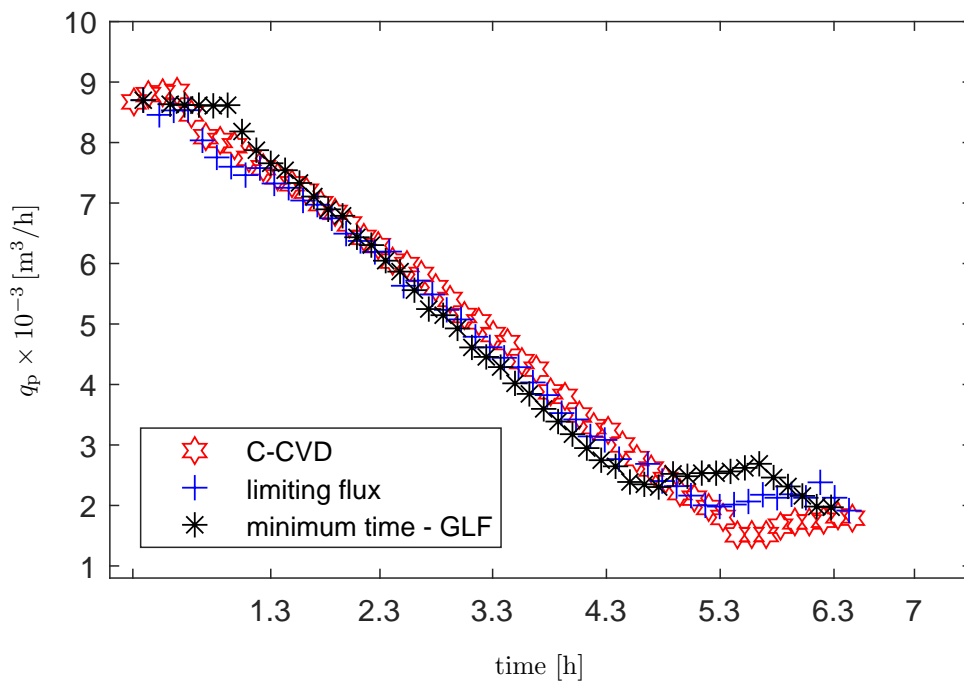


Figure 4.15: Case study 2: Permeate flow-rate measurements of traditional and optimal strategies.

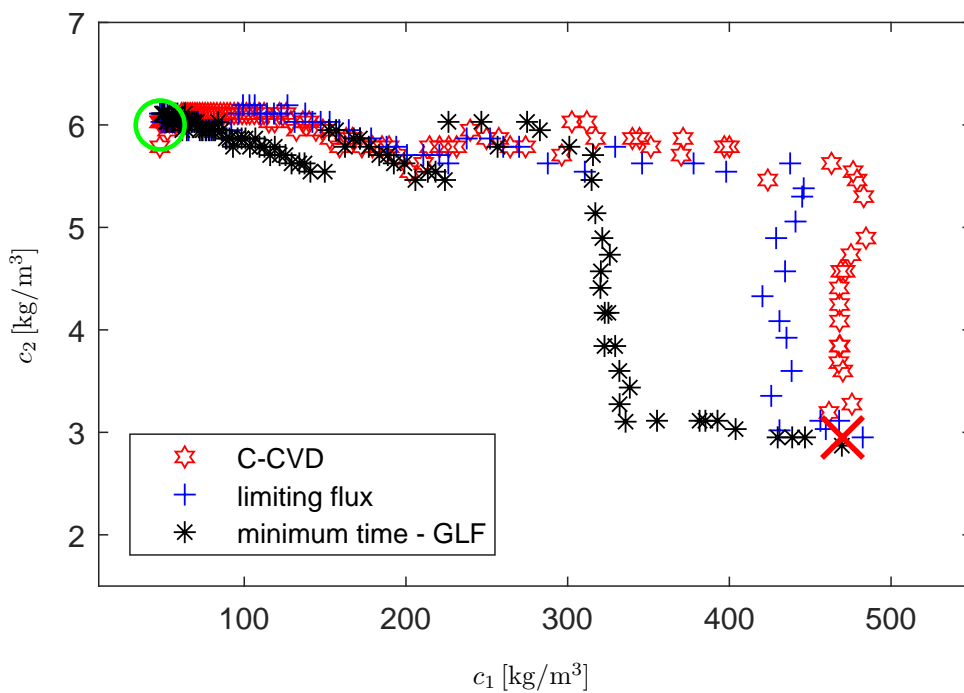


Figure 4.16: Case study 2: Concentration measurements of lactose and NaCl for traditional and optimal strategies.

Table 4.4: Experimental comparison of total processing time and diluant consumption for different scenarios in case study 2.

| Strategy | t_f [h] | Δt_f [%] | $V_D \times 10^{-3}$ [m ³] | ΔV_D [%] | Cost [€] |
|---------------------|-----------|------------------|--|------------------|----------|
| traditional (C-CVD) | 6.54 | 100 | 2.37 | 75.72 | 7.01 |
| limiting flux | 6.38 | 97.75 | 2.65 | 84.76 | 6.91 |
| time-optimal: GLF | 6.34 | 97.00 | 3.13 | 100.00 | 6.97 |

all three of them. The flow-rate trajectory is different in the later part due to difference in inputs for different strategies. The flow-rate in the three step strategies reduces, then stays around a constant value, and finally reduces again. On the other hand, for the C-CVD two step strategy, the flow-rate reduces while concentrating lactose and increases slightly while reducing NaCl. However, only negligible differences can be observed in the final processing times.

When comparing the concentration diagrams, both traditional strategies apply the CVD step at higher lactose concentration whereas the optimal strategy switches to the VVD mode earlier (Fig. 4.16). The initial and final concentrations are represented by same markers as in case study 1.

Table 4.4 presents experimental results for processing time and diluant consumption. As also observed from figures, time-optimal strategy does not bring much improvement and there is no reason to abandon classical strategies in this case. The simulation results are not shown here but they confirm these implications. Relative values Δt_f and ΔV_D compare time and diluant consumptions.

Simulation results for diluant minimization show consumption of only $V_D = 1.63 \times 10^{-3} \text{ m}^3$ i.e. 48% of diluant needed by the time optimal strategy. This strategy is C-VVD-D, and takes the longest to get to the final concentrations ($t_f = 7.2 \text{ h}$). The switching concentration to D mode for this strategy is very high (917 kg/m³) and unattainable on this plant, for the given initial conditions of concentrations and feed volume. Therefore, realistic practical approach to diluant consumption minimization would concentrate the solution as much as working conditions allow.

4.5.3 Case Study 3

The experiment objective was to drive the lactose concentration from 50 kg/m³ to 110 kg/m³, and to reduce the NaCl concentration from 5.3 kg/m³ to 1 kg/m³, using NDF. The initial volume of the solution was 0.021 m³. The three strategies were implemented, i.e.

Traditional two step strategy ($\alpha = \{0, 1\}$) : concentrate using C mode till lactose increases to final concentration ($c_1 = c_{1,f} = 110 \text{ kg/m}^3$), then using CVD mode reduce NaCl to reach the final objective ($c_2 = c_{2,f} = 1 \text{ kg/m}^3$).

Time-optimal for GLF model ($\alpha = \{0, \alpha_s, \infty\}$) :

1. Use C mode to drive from initial concentrations to reach singular surface ($S = 0$), i.e. concentrate till lactose concentration (c_1) is 332.7 kg/m³.

2. Stay on the singular surface using singular control α_s , till the condition $c_1/c_2 = c_{1,f}/c_{2,f}$ is met. The separation process ends with this step.
3. The final step is to get the final concentrations using D mode, and it practically takes negligible amount of time. This is represented by the continuous line to the final concentrations (red circle) in Fig. 4.17.

Time-optimal for LF₁ model($\alpha = \{0, \alpha_s, \infty\}$) :

1. Use C mode to drive from initial concentrations to reach singular surface ($S = 0$), i.e. concentrate till lactose concentration (c_1) is $\gamma_2/e = 458.6 \text{ kg/m}^3$.
2. Stay on the singular surface using singular control α_s , till the condition $c_1/c_2 = c_{1,f}/c_{2,f}$ is met.
3. The final step is to get the final concentrations using D mode, as in for GLF model (Fig. 4.17).

The volume measurement device on the plant is constrained by $0.003\text{-}0.032 \text{ m}^3$. As we use volume measurement to get the concentration of lactose (4.12), hence for the given initial volume of 0.021 m^3 , the maximum concentration of lactose is constrained to 340 kg/m^3 . The implementation of LF₁ strategy was thus compromised, and instead of concentrating lactose to 458.6 kg/m^3 , we concentrated to 340 kg/m^3 .

The results and comparison of the three strategies is quantified and represented in Figs. 4.17 and 4.18 and Table 4.5. Figure 4.14 shows evolution of concentrations $c_1(t)$ and $c_2(t)$, where the initial and final points are marked as green and red circle, respectively. The dilution mode, which is present for optimal strategies derived from GLF and LF₁ model, is represented by solid lines. It is clear that all three strategies were able to drive the solution to the desired concentrations of lactose and NaCl.

The permeate flow rate diagram (Fig. 4.18) shows that all strategies started at similar initial flow rate as the initial concentrations were identical. The trend of decrease in flow rate as the concentration of lactose increased is also same for all three of them. The reason behind the reduction of time with time-optimal strategy (Table 4.5) is the step when NaCl concentration is reduced. It can be observed in the flow rate figure that although due to over-concentrating lactose in optimal strategies the C mode takes longer time (t_1 in Table 4.5), as a result the time for CVD in case of LF₁ and VVD in case of GLF reduces (t_2 in Table 4.5). This reduction results in overall reduction of time (t_f in Table 4.5) as we stop the process after CVD/VVD, and do the instantaneous D mode to reach the desired concentrations. The optimal strategies took 87-90% of the time taken by traditional strategy (Δt_f in Table 4.5), which directly translates to cost percent in this case study.

The results of case study 3 also confirm that models fitted were good enough but were still not perfect, in context of time-optimal operation. As we can see from the equation for S (4.23), that during the VVD mode the permeate flow rate should be constant, i.e. $q_p = \gamma_1(\gamma_3 + 1)$. Now, if we look at the experimental values of q_p from Fig. 4.13, we observe that during the VVD mode for optimal GLF operation the permeate flow is varying. This may result from the differences in model parameters from one batch to another, and because the optimal switchings were done based on concentration and

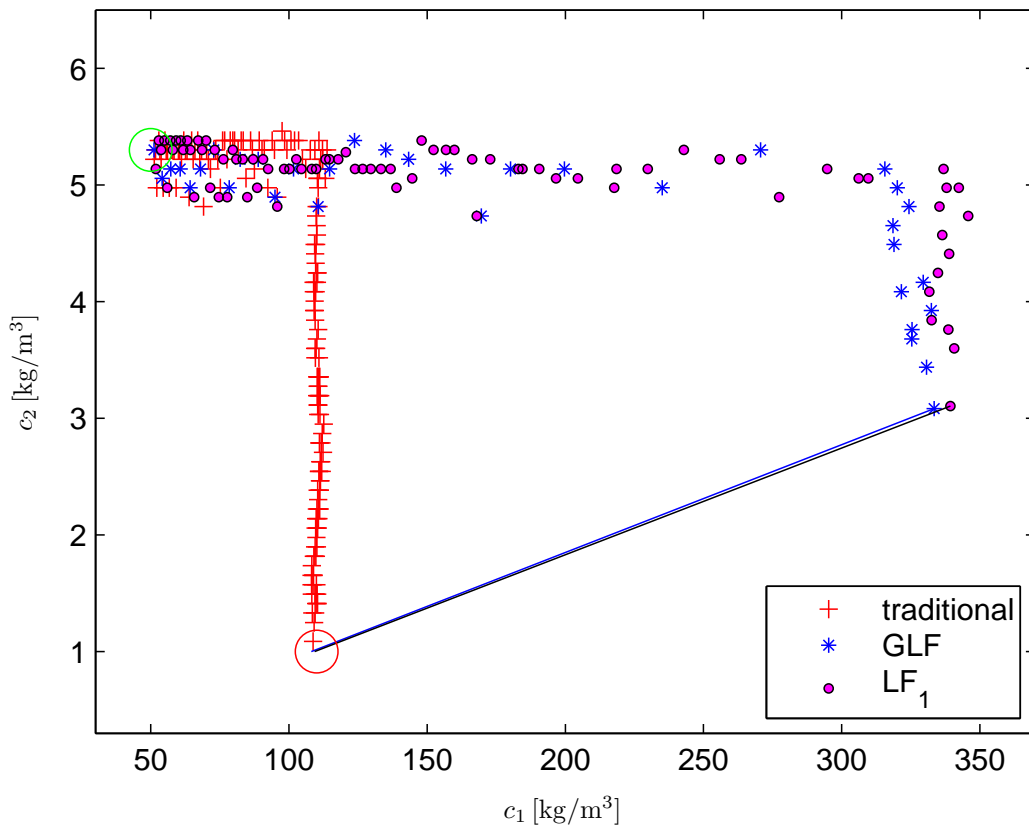


Figure 4.17: Concentration measurements of lactose and NaCl for traditional and optimal strategies, along with the initial and final conditions.

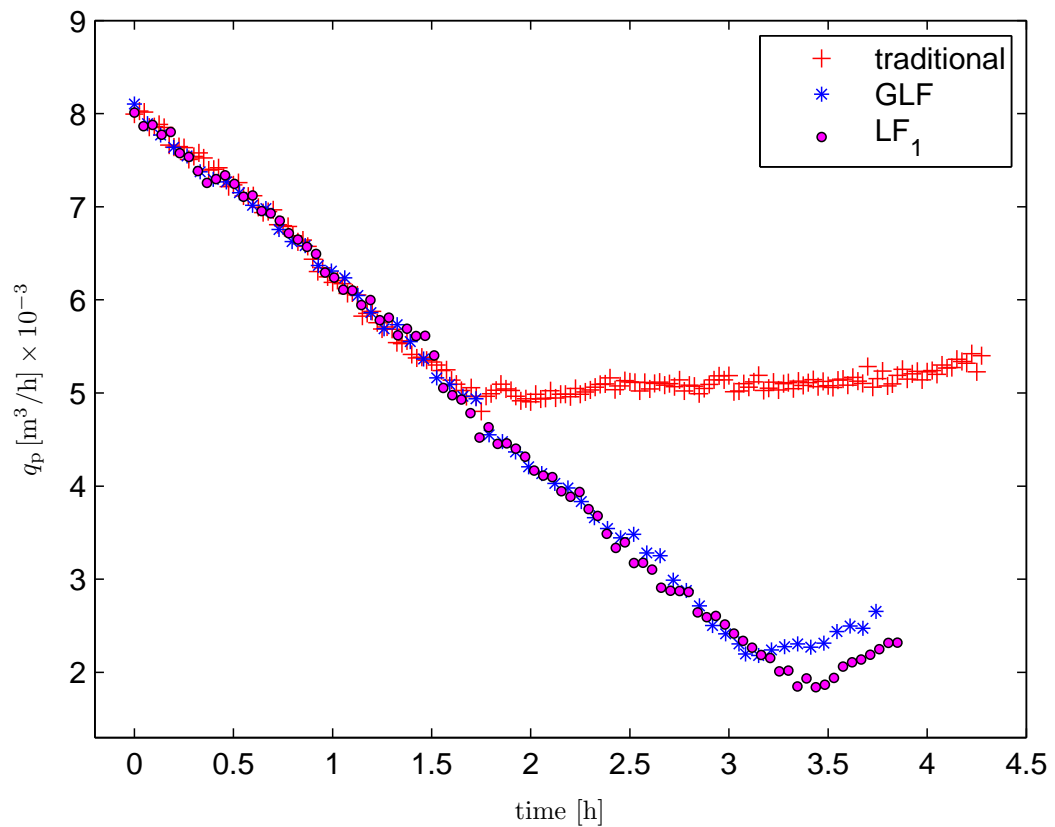


Figure 4.18: Permeate flow rate measurements of traditional and optimal strategies.

Table 4.5: Comparison of time taken by traditional and optimal strategies.

| Strategy | t_1 [h] | t_2 [h] | t_f [h] | Δt_f [%] |
|-----------------|-----------|-----------|-----------|------------------|
| traditional | 1.75 | 2.53 | 4.28 | 100 |
| GLF | 3.08 | 0.66 | 3.74 | 87 |
| LF ₁ | 3.35 | 0.50 | 3.85 | 90 |

not on q_p . As discussed in previous cases studies this could be avoided by estimating the model while performing the experiment (online parameter estimation).

In these 3 case studies, despite of the fact that experimental results were not identical to simulation/expected results, it was experimentally demonstrated and proved the optimal operation strategies resulted in economic benefits.

Chapter 5

Closed-Loop Batch Diafiltration

In this chapter, the mathematical modeling and optimal control of batch with partial recirculation of retentate mode of diafiltration, is presented. This thesis work has been published in Sharma et al. (2017b) and Sharma et al. (2015).

The batch process with recirculation possesses the units of an open-loop DF plant, as given at page 26. Besides these, the following additional parts are installed on batch closed-loop DF plant:

- recirculation loop – this loop aids in the partial recirculation of retentate,
- recirculation pump (P2) – the pump that forces the partially recycled retentate in the recirculation loop,
- recycle valve (V1) – the valve to split the retentate, and is representing as actuator for splitting or recirculation ratio. In this work it is denoted by s .

5.1 Mathematical Modeling

The section below describes the modeling for the closed-loop DF system, and the ODE's describing the dynamics of concentration of solutes.

5.1.1 Modeling Assumptions

To derive the model, we will assume the following in addition to the modeling assumptions made for deriving batch open-loop model (Section 4.1.1):

- The piping and construction of the plant is considered to be unaltered during the run and hence for closed-loop DF the loop volume V_L is constant. The flow rate inside the loop q_L is also constant (Fig. 5.1).
- The number of the components to be separated is two, thus there is a macro-solute and micro-solute. A generalization to the model with more components is straightforward and will not be considered here.

- The rejection coefficient R_i from (4.2) can be written for closed-loop batch DF as

$$R_i = 1 - \frac{c_{p,i}}{c_{L,i}}, \quad i = 1, 2. \quad (5.1)$$

where $c_{L,i}, c_{p,i}$, are the concentrations of i th component entering the membrane from loop and leaving the membrane as permeate, respectively.

- We assume for initial conditions of the process that the liquid of the volume V_0 and the component concentrations $c_{1,0}, c_{2,0}$ resides in the feed tank and in the piping.

5.1.2 Model Derivation

The batch closed-loop diafiltration configuration provides two dimensionless variables as manipulated inputs:

- diluant addition rate $\alpha \geq 0$
- partial recycle ratio $s \in [0, 1]$, i.e. the splitting factor for retentate recirculation. The flow of the retentate from the membrane q_r is thus distributed into two streams: one returning to the feed tank sq_r , while the other to the loop $(1 - s)q_r$ (Fig. 5.1).

The whole process model can be divided into two parts: *recirculation loop* and *feed tank*.

Modeling of Recirculation Loop with Membrane Module

As V_L is constant, the mass balance of the loop given under the assumption of constant density of the liquid in the loop can be written as

$$\frac{dV_L}{dt} = q_1 - q_p - sq_r = 0, \quad (5.2)$$

where q_1 is the flow rate out of the tank and towards the recirculation loop, and sq_r is the fraction of the retentate that returns to the tank.

The permeate flow rate q_p as in open-loop batch DF, is usually determined experimentally as a nonlinear function of concentrations of components entering the membrane ($c_{L,1}, c_{L,2}$), i.e.

$$q_p(c_{L,1}, c_{L,2}) = AJ(c_{L,1}, c_{L,2}), \quad (5.3)$$

where A and $J(\cdot)$ stand for the effective membrane area and permeate flux subject to unit membrane area.

As there is no accumulation of mass in the membrane module, the overall and component mass balance of the membrane module give

$$q_L = q_r + q_p, \quad (5.4)$$

$$q_L c_{L,i} = q_r c_{r,i} + q_p c_{p,i}, \quad (5.5)$$

where $c_{r,i}$ is the concentration of i th component in retentate.

The retentate flow q_r in (5.2) can be replaced using (5.4) to get

$$q_1 = q_p + s(q_L - q_p) = sq_L + q_p(1 - s). \quad (5.6)$$

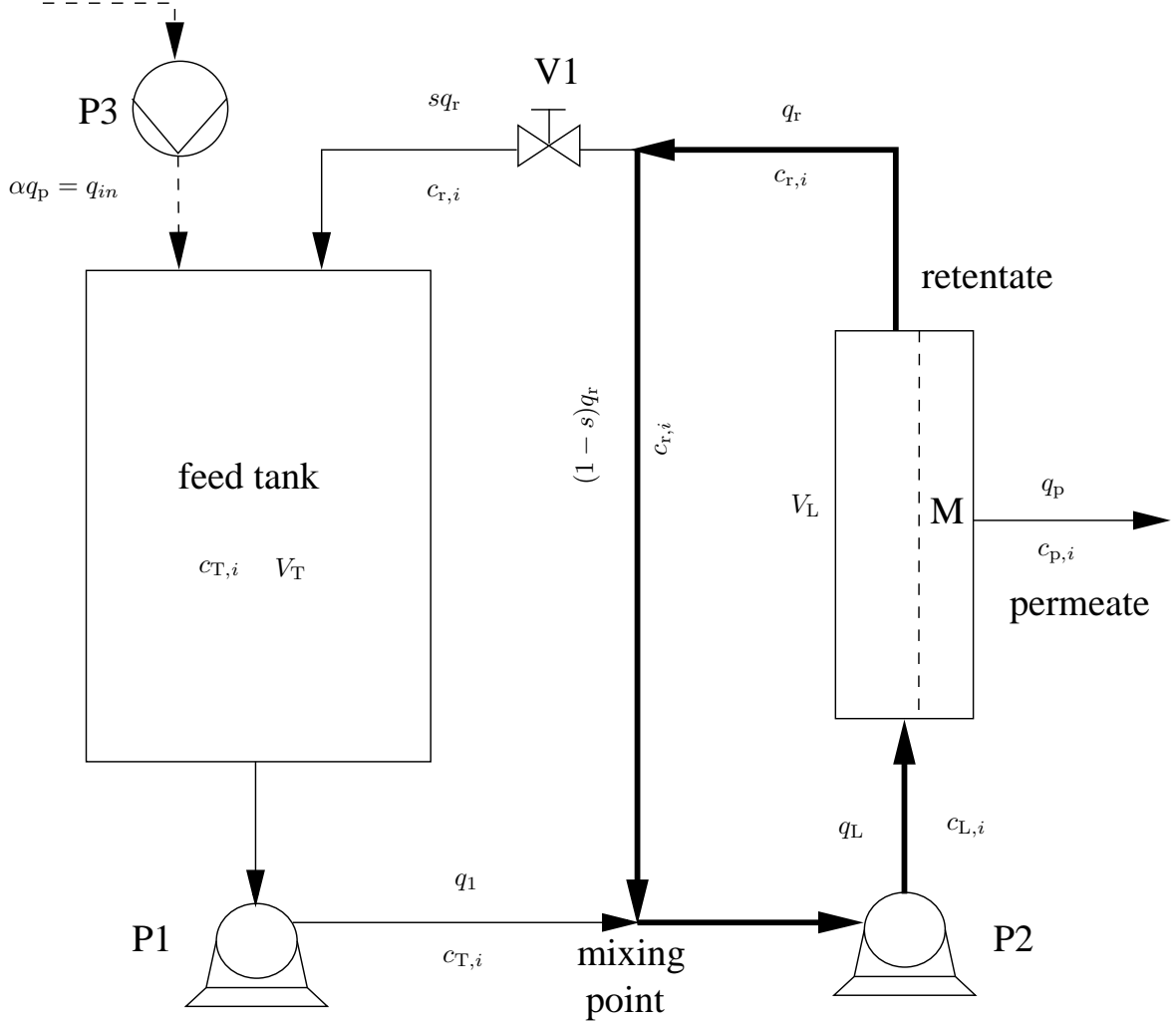


Figure 5.1: Batch diafiltration with partial recirculation process flow scheme

The change in concentration of a component inside the loop ($c_{L,i}$) can be derived from mass balance of a solute, i.e.

$$\frac{dc_{L,i}V_L}{dt} = c_{L,i}\frac{dV_L}{dt} + V_L\frac{dc_{L,i}}{dt} = q_1c_{T,i} - sq_r c_{r,i} - q_p c_{p,i}, \quad (5.7)$$

where $c_{T,i}$ is the concentration of i th component inside the feed tank.

The differential equation that describes the evolution of component concentration inside the loop can then be obtained by substituting $q_r c_{r,i}$ from (5.5) and $c_{p,i}$ from (4.2) into (5.7), and by using the assumption that V_L is constant, i.e.

$$\begin{aligned} V_L \frac{dc_{L,i}}{dt} &= q_1 c_{T,i} - s[q_L c_{L,i} - q_p c_{L,i}(1 - R_i)] - q_p c_{L,i}(1 - R_i) \\ &= q_1 c_{T,i} + c_{L,i}[-q_p + q_p R_i - q_L s + q_p s - q_p R_i s] \\ &= c_{T,i}[s q_L + q_p(1 - s)] + c_{L,i}[-q_p + q_p R_i - q_L s + q_p s - q_p R_i s], \quad i = 1, 2. \end{aligned} \quad (5.8)$$

Modeling of Feed Tank

The total mass balance in the feed tank gives

$$\frac{dV_T}{dt} = \alpha q_p + s q_r - q_1. \quad (5.9)$$

In the equation above, q_r is replaced using (5.4), and q_1 using (5.6) to yield

$$\frac{dV_T}{dt} = \alpha q_p + s(q_L - q_p) - s q_L - q_p(1 - s), \quad (5.10a)$$

$$= (\alpha - 1)q_p. \quad (5.10b)$$

This equation representing the change of volume is identical to the standard batch open-loop configuration and can also be obtained directly from the overall mass balance of the process.

The mass balance of a component in the feed tank yields

$$\frac{dc_{T,i}V_T}{dt} = c_{T,i}\frac{dV_T}{dt} + V_T\frac{dc_{T,i}}{dt} = s q_r c_{r,i} - q_1 c_{T,i}. \quad (5.11)$$

Substituting dV_T/dt from (5.10b), $q_r c_{r,i}$ from (5.5), and $c_{p,i}$ from using (4.2) gives

$$V_T\frac{dc_{T,i}}{dt} = s[q_L c_{L,i} - q_p c_{L,i}(1 - R_i)] - q_1 c_{T,i} - c_{T,i}[\alpha q_p - q_1 + s(q_L - q_p)]. \quad (5.12)$$

Finally, substituting for q_1 from (5.6) we get the final equation

$$V_T\frac{dc_{T,i}}{dt} = s c_{L,i}[q_L - q_p(1 - R_i)] - c_{T,i}[\alpha q_p + s(q_L - q_p)], \quad i = 1, 2. \quad (5.13)$$

5.1.3 Complete Model

The complete model can then be described by the following system of ordinary differential and algebraic equations:

$$\frac{dV_T}{dt} = (\alpha - 1)q_p, \quad V_T(0) = V_0 - V_L \quad (5.14a)$$

$$V_T\frac{dc_{T,1}}{dt} = c_{L,1}s(q_L - q_p + q_p R_1) - c_{T,1}[s(q_L - q_p) + \alpha q_p], \quad c_{T,1}(0) = c_{1,0}, \quad (5.14b)$$

$$V_T\frac{dc_{T,2}}{dt} = c_{L,2}s(q_L - q_p + q_p R_2) - c_{T,2}[s(q_L - q_p) + \alpha q_p], \quad c_{T,2}(0) = c_{2,0}, \quad (5.14c)$$

$$V_L\frac{dc_{L,1}}{dt} = c_{T,1}[s q_L + q_p(1 - s)] \\ + c_{L,1}[-q_L s - q_p - q_p R_1 s + q_p s + q_p R_1], \quad c_{L,1}(0) = c_{1,0}, \quad (5.14d)$$

$$V_L\frac{dc_{L,2}}{dt} = c_{T,2}[s q_L + q_p(1 - s)] \\ + c_{L,2}[-q_L s - q_p - q_p R_2 s + q_p s + q_p R_2], \quad c_{L,2}(0) = c_{2,0}. \quad (5.14e)$$

The total liquid volume is given by an algebraic equation as

$$V = V_T + V_L. \quad (5.14f)$$

Similarly, the total concentration of a component is influenced by its respective tank and loop concentrations, and can be written as

$$c_i = \frac{V_T c_{T,i} + V_L c_{L,i}}{V_T + V_L} \quad i = 1, 2. \quad (5.14g)$$

The model (5.14) thus comprises 5 differential and 3 algebraic equations. The model variables are the tank and total volumes (V_T, V), the tank, loop, and total concentrations ($c_{T,1}, c_{T,2}, c_{L,1}, c_{L,2}, c_1, c_2$). There are two degrees of freedom: diluant rate α and recirculation ratio s that serve as manipulated variables. The permeate flow q_p as well as the rejection coefficients R_1, R_2 are functions of loop concentrations defined by (5.3), (4.2). Note that this model is nonlinear and affine in manipulated variables.

5.1.4 Model Simplifications

We will discuss three possible model simplifications and abstractions here. The first two will have implications on optimal control and operation of the process.

In the first case, the complete model boils down to the classical batch diafiltration model (open-loop) if there is no recirculation and the whole retentate stream returns to the tank ($s = 1$). In that case, it follows from Fig. 5.1 that $q_1 = q_L, V = V_T, V_L = 0$, and $c_i = c_{T,i} = c_{L,i}$. The resulting model contains three differential equations

$$\frac{dV}{dt} = (\alpha - 1)q_p, \quad V(0) = V_0, \quad (5.15a)$$

$$V \frac{dc_1}{dt} = c_1 q_p (R_1 - \alpha), \quad c_1(0) = c_{1,0}, \quad (5.15b)$$

$$V \frac{dc_2}{dt} = c_2 q_p (R_2 - \alpha), \quad c_2(0) = c_{2,0}. \quad (5.15c)$$

In the second case, the whole recirculation loop with the membrane module can be thought of as an abstraction of a membrane with some different properties. Note that in this case the recirculation ratio s is an inner variable of the process and the abstraction will hide it. This means, that the closed-loop process shown in Fig. 2.6(b) can be replaced with the open-loop process shown in Fig. 2.6(a) with only one manipulated variable α .

The third case discusses a situation when V_T is significantly greater than V_L . This means that the recirculation loop has only a small influence on the overall process and its dynamics can be neglected. Therefore, the original system of 5 differential equations can be replaced by three differential and two algebraic equations

$$\frac{dV_T}{dt} = (\alpha - 1)q_p, \quad V_T(0) = V_0 - V_L, \quad (5.16a)$$

$$V_T \frac{dc_{T,1}}{dt} = c_{L,1}s(q_L - q_p + q_p R_1) - c_{T,1}[s(q_L - q_p) + \alpha q_p], \quad c_{T,1}(0) = c_{1,0}, \quad (5.16b)$$

$$V_T \frac{dc_{T,2}}{dt} = c_{L,2}s(q_L - q_p + q_p R_2) - c_{T,2}[s(q_L - q_p) + \alpha q_p], \quad c_{T,2}(0) = c_{2,0}, \quad (5.16c)$$

$$\begin{aligned} 0 &= c_{T,1}[s q_L + q_p(1 - s)] \\ &+ c_{L,1}[-q_L s - q_p - q_p R_1 s + q_p s + q_p R_1], \quad c_{L,1}(0) = c_{1,0}, \end{aligned} \quad (5.16d)$$

$$\begin{aligned} 0 &= c_{T,2}[s q_L + q_p(1 - s)] \\ &+ c_{L,2}[-q_L s - q_p - q_p R_2 s + q_p s + q_p R_2], \quad c_{L,2}(0) = c_{2,0}. \end{aligned} \quad (5.16e)$$

Clearly, the model can be rewritten with three differential equations only—the loop concentrations can be derived from the algebraic equations and substituted back to differential ones. However, that would break the model structure being affine in manipulated variables.

Simulations with the model (5.16) have confirmed that its behavior is close to the full model (5.14) if the assumptions are satisfied.

5.1.5 Alternate Configuration Model – Input to the Loop

An alternate closed-loop membrane process configuration often used in the industry introduces diluant directly to the loop instead of the tank. The aim is to rapidly decrease the macro-solute concentration and to slow down concentration-polarization effects on the membrane.

The derivation of the complete model is analogous as before and it is omitted here. The differential equations (5.14) change as follows

$$\frac{dV_T}{dt} = (\alpha - 1)q_p, \quad V_T(0) = V_0 - V_L, \quad (5.17a)$$

$$V_T \frac{dc_{T,1}}{dt} = c_{L,1}s(q_L - q_p + q_p R_1) - c_{T,1}s(q_L - q_p), \quad c_{T,1}(0) = c_{1,0}, \quad (5.17b)$$

$$V_T \frac{dc_{T,2}}{dt} = c_{L,2}s(q_L - q_p + q_p R_2) - c_{T,2}s(q_L - q_p), \quad c_{T,2}(0) = c_{2,0}, \quad (5.17c)$$

$$V_L \frac{dc_{L,1}}{dt} = c_{T,1}[sq_L + q_p(1 - s - \alpha)] \\ + c_{L,1}[-q_L s - q_p - q_p R_1 s + q_p s + q_p R_1], \quad c_{L,1}(0) = c_{1,0}, \quad (5.17d)$$

$$V_L \frac{dc_{L,2}}{dt} = c_{T,2}[sq_L + q_p(1 - s - \alpha)] \\ + c_{L,2}[-q_L s - q_p - q_p R_2 s + q_p s + q_p R_2], \quad c_{L,2}(0) = c_{2,0}. \quad (5.17e)$$

We can observe that the equation for V_T remains unchanged. As expected, there is an increase of concentrations in the tank $c_{T,i}$ by $c_{T,i}\alpha q_p/V_T$ and the solutes in the loop are diluted by $c_{T,i}\alpha q_p/V_L$, $i = 1, 2$.

Another difference between these processes concerns diluant rate addition α . If the diluant is introduced to the feed tank, it is practically unconstrained from above i.e. $\alpha \geq 0$. On the other hand, direct addition to the loop prevents the values of $\alpha > 1$ as it is not possible to insert more diluant than the withdrawn permeate.

Negligible differences were found when simulations of both models (5.14) and (5.17) with various values of process parameters were compared. Therefore, it seems that the diluant insertion point does not play any significant role and both process configurations can be used without loss of performance. Therefore, the model (5.14) will be used.

5.1.6 Effect of Loop Parameters

The influence of parameters q_L and V_L was studied by simulating the model (5.14) and comparison was made to open-loop batch configuration (5.15). The following points could be summarized, at constant pressure, temperature, and for all admissible values of s

- within the practical bounds, the constant loop flow rate q_L has a negligible effect over the model/concentrations,
- the closed-loop model is equivalent to the open-loop one if the loop volume V_L is within 1% of the initial feed volume V_0 ,

- as the ratio V_L/V_0 increases the concentrations reached after certain amount of time deviate from the open-loop equivalents.

5.2 Optimal Control

The process optimization of batch closed-loop DF as in batch open-loop DF, can aim at minimizing the processing time (4.18), and/or diluant consumption (4.19).

In addition, the batch closed-loop configuration has the potential to reduce the power requirements of the separation process. Therefore, a goal can be defined as minimization of the power required by the pumps.

The pumping power required for a batch membrane process with a single feed pump (open-loop) is given as (Zeman, 1996)

$$E_{\text{feed}} = q_1 P_f. \quad (5.18)$$

If a recirculation pump is used, the recycle stream only needs to be re-pressurized to P_f to compensate for the pressure loss due to flow through the membrane module, $\delta P = P_f - P_r$. The total power required by the process with recirculation (closed-loop) is given as

$$E_{\text{total}} = q_L \delta P + q_1 (P_f - \delta P), \quad (5.19)$$

where the first term represents the recirculation pump compensating for membrane pressure drop, and the second term represents the feed pump taking care of the rest of pressure requirements. Note that q_L will in general be much larger than q_1 . Thus, the pumping power is reduced roughly by a factor of $\delta P/P_f$. The actual value of this pressure ratio will be highly process dependent, but reductions in pumping power on the order of 50% for closed-loop configuration are possible (Zeman, 1996). However, the implementation of an extra pump (recirculation pump) adds up to the total costs.

The overall power required for separation can then be given as

$$\mathcal{J}_P = \int_0^{t_f} \left(q_L \delta P + q_1 (P_f - \delta P) \right) dt. \quad (5.20)$$

Note, however, that q_L is constant by the assumption while δP and P_f do not vary significantly due to operation at constant transmembrane pressure (4.1). Therefore, the power minimization problem can be simplified to

$$\mathcal{J}_P^* = \min_{\alpha(t), s(t)} \int_0^{t_f} q_1 dt. \quad (5.21)$$

5.2.1 Problem Formulation

We aim at minimization of a weighted sum of the total processing time, electric power, and the overall diluant consumption. The goals are to process the solution with initial volume V_0 , to increase the macro-solute concentration from $c_{1,0}$ to $c_{1,f}$, and simultaneously to decrease the micro-solute concentration from $c_{2,0}$ to $c_{2,f}$. The time-varying optimized variables are non-negative diluant ratio $\alpha(t)$, and recirculation ratio $s(t)$ constrained between 0 and 1. The optimal control problem can then

be defined as follows

$$\mathcal{J}^* = \min_{\alpha(t), s(t)} \int_0^{t_f} w_T + w_E q_1 + w_D \alpha q_p dt \quad (5.22a)$$

$$\text{s.t. (5.14),} \quad (5.22b)$$

$$V_T(0) = V_0 - V_L, \quad (5.22c)$$

$$c_{T,i}(0) = c_{i,0}, \quad i = 1, 2, \quad (5.22d)$$

$$c_{L,i}(0) = c_{i,0}, \quad i = 1, 2, \quad (5.22e)$$

$$c_{i,f} V_f = c_{T,i}(t_f) V_T(t_f) + c_{L,i}(t_f) V_L, \quad i = 1, 2, \quad (5.22f)$$

$$\alpha(t) \in [0, \infty), s(t) \in [0, 1]. \quad (5.22g)$$

The non-negative weighting coefficients w_T, w_E, w_D represent the weight (or price) for a unit of processing time, processing power, and diluant consumption, respectively.

5.2.2 Problem Solution

The optimization problem (5.22) can be solved using optimal control theory Hull (2003), Paulen and Fikar (2016). Two approaches are possible: analytical or numerical methods.

Optimal solutions for batch open-loop processes have been developed in Paulen and Fikar (2016), Paulen et al. (2015). These are based on Pontryagin's minimum principle (Pontryagin et al., 1962) and explicit analytical results can be found only for small systems with two differential equations.

The complexity of the model (5.14) implies the use of numerical methods to solve the problem (5.22).

For closed-loop DF optimization, we apply both CVP and OC approaches. The control variables $\alpha(t)$ and $s(t)$ are considered to be piece-wise constant (PWC) on time intervals of variable length.

Next, let us explore the power minimization in more detail. As it was derived in (5.21), the power consumption is closely related to overall volume treated by the feed pump P1. This can be minimized if two events are met: (i) return of the retentate to the feed tank should be as small as possible ($s = 0$) and (ii) minimization of the diluant consumption. Therefore, we can expect that the optimal power operation will be closely related to optimal diluant usage with total recirculation.

5.3 Optimal Control – Case Studies

We present three case studies differing in permeate flow models that are taken from literature. These demonstrate different aspects of optimization and optimal operation.

In all cases, we consider that the membrane is completely impermeable to the macro-solute. Therefore, its rejection coefficient as defined by (4.2) is $R_1 = 1$. The micro-solute completely passes the membrane, thus $R_2 = 0$.

5.3.1 Limiting Flux Model

In the first simulation, the aim is to process the solution of a volume 0.105 m^3 from the initial point $[c_{1,0}, c_{2,0}] = [10, 31.5] \text{ mol m}^{-3}$, to the final point $[c_{1,f}, c_{2,f}] = [100, 10] \text{ mol m}^{-3}$.

The limiting flux model as used in (4.15) for permeate flow is assumed

$$q_p = kA \ln \left(\frac{c_{\text{lim}}}{c_{L,1}} \right), \quad (5.23)$$

where the limiting concentration is $c_{\text{lim}} = 319 \text{ mol m}^{-3}$, mass transfer coefficient is $k = 0.0172 \text{ m h}^{-1}$, membrane area is $A = 1 \text{ m}^2$. The flow rate inside the loop taken from the ultrafiltration experimental data of Verasztó et al. (2013) is $q_L = 0.25 \text{ m}^3 \text{ h}^{-1}$ and the loop volume is $V_L = 0.005 \text{ m}^3$. The list of combinations of w_T , w_E and w_D used here is given as:

1. Minimum time scenario ($w_T = 1$, $w_E = 0$, and $w_D = 0$).
2. Almost minimum time scenario ($w_T = 1$, $w_E = 0.4$, and $w_D = 0$).
3. Multi-objective scenario ($w_T = 0.39$, $w_E = 1$, and $w_D = 0$).
4. Almost minimum power scenario ($w_T = 0.01$, $w_E = 1$, and $w_D = 0$).
5. Minimum power scenario ($w_T = 0$, $w_E = 1$, and $w_D = 0$).
6. Minimum diluant scenario ($w_T = 0$, $w_E = 0$, and $w_D = 1$).

The minimum time, minimum diluant, and minimum power scenarios can be considered as interesting extreme cases. The minimum time requirement is often imposed on membrane processing. As we will see, the minimum diluant/power represent limit cases only and are practically unattainable.

The weighting coefficients for the almost minimum time and almost minimum power scenarios are chosen such that the respective quantity increases within 10% of the theoretical minimal value.

To have both objectives minimized, multi-objective scenario was implemented. The weights were chosen to have minimization of both objectives (time and power) equally, as much as possible (Fig. 5.5).

The theoretical results for optimal operation of batch open-loop configuration predict (Paulen and Fikar, 2016, Paulen et al., 2013, 2015) that it will consist of three step strategy of time-varying α with modes: C, CVD, and dilution: $\alpha = (0, 1, \infty)$. The switching concentration from C to CVD of the macro-solute, for minimum time scenario is given by $c_1 = c_{\text{lim}}/e$ and increases towards c_{lim} for minimum diluant/power problem.

Optimal operation for batch closed-loop configuration was calculated numerically using the method of orthogonal collocations implemented in package Dynopt (Čižniar et al., 2005). Several values for number of optimized intervals (finite elements) were tried to reveal the structure of the optimal solution. It was found that three intervals were sufficient and the further increase of their number did not lead to any substantial improvement in optimal value of the cost function.

Fig. 5.2, 5.3, and 5.4 show optimal total concentration (c_1, c_2) trajectories and optimal profiles of manipulated variables, α and s , respectively, for different considered scenarios. Green circle and red cross in concentration trajectories denote the initial and final concentration points, respectively.

The results confirm an agreement of the trajectory of concentrations and diluant rate α with the batch open-loop configuration.

The trajectory of control input s is shown in Fig. 5.4. As the dilution (last) step is performed after the process has been stopped, the control s is not optimized during it. If the objective is to minimize

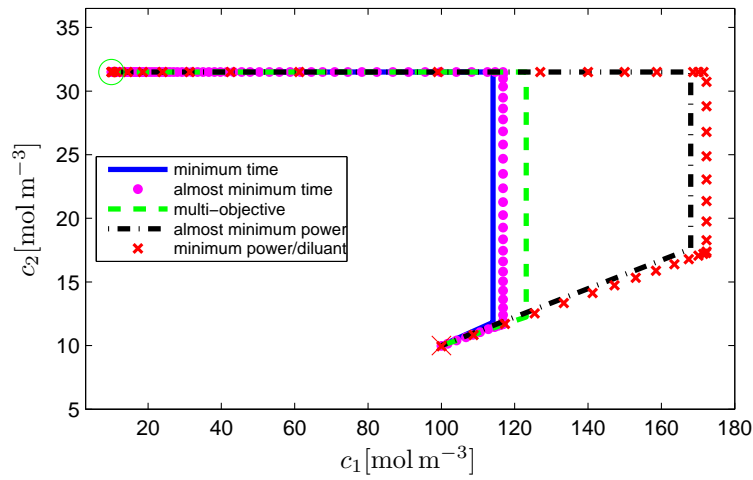
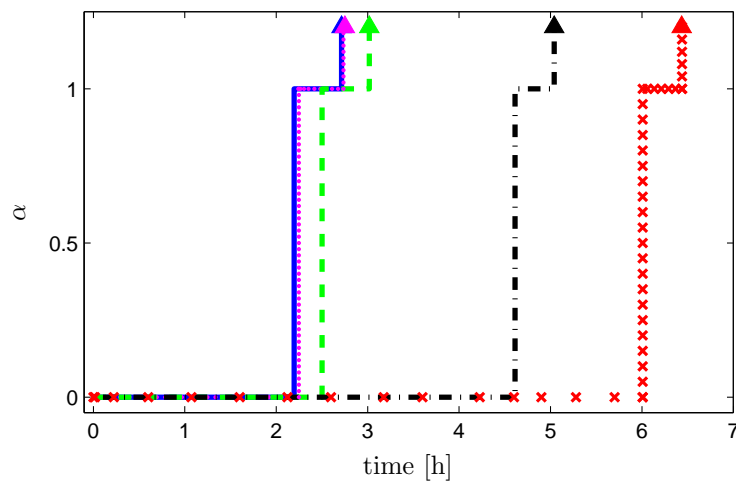
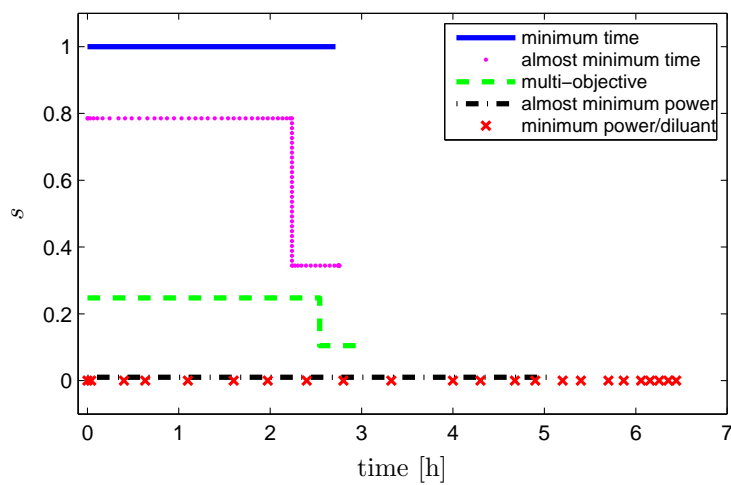
Figure 5.2: Evolution of component (c_1 and c_2) total concentrations for different scenarios.Figure 5.3: Optimal values of control α for different scenarios.Figure 5.4: Optimal values of control s for different scenarios.

Table 5.1: Comparison of total processing time, volume needed to be pumped, and diluant consumption for different scenarios.

| Scenario | w_T [€ h ⁻¹] | w_E [€h m ⁻³] | w_D [€h m ⁻³] | \mathcal{J}_T [h] | \mathcal{J}_P [m ³] | \mathcal{J}_D [m ³] |
|----------------------|-------------------------------|--------------------------------|--------------------------------|------------------------|--------------------------------------|--------------------------------------|
| Minimum time | 1 | 0 | 0 | 2.71 | 0.6797 | 0.0103 |
| Almost minimum time | 1 | 0.4 | 0 | 2.76 | 0.5108 | 0.0101 |
| Multi-objective | 0.39 | 1 | 0 | 3.02 | 0.2473 | 0.0095 |
| Almost minimum power | 0.01 | 1 | 0 | 5.05 | 0.1116 | 0.0077 |
| Minimum power | 0 | 1 | 0 | 6.46 | 0.1021 | 0.0076 |
| Minimum diluant | 0 | 0 | 1 | 6.46 | 0.1021 | 0.0076 |

the batch time, s is 1 and thus the process reduces to a pure batch process without recycle. Therefore, batch open-loop configuration is optimal for time minimization and recirculation only increases capital costs. On the other side, if the sole objective is to minimize energy, the recycle valve is fully open ($s = 0$) all the time.

The optimal values of recirculation ratio s for the first and second step decrease as the objective of minimization moves from time minimization to power minimization. Note also that the power and diluant consumption minimization scenarios coincide, as it was predicted above.

The results of optimal control obtained coincide with the logic of respective minimizations. As seen in concentration diagram, the switching towards CVD mode for power minimization occurs later than in time minimization case, so as to reduce the volume of diluant needed to be pumped. The switching concentration and duration of CVD/VVD mode (diluant pumped) have an inverse relation based on the condition $c_1/c_2 = c_{1,f}/c_{2,f}$. If C mode is longer, the CVD mode is shorter and vice versa. As C mode is longer, lower reduction in micro-solute is required to achieve $c_1/c_2 = c_{1,f}/c_{2,f}$ during CVD mode, and hence lower volume of diluant is consumed.

The recycle valve is completely open ($s = 0$) towards the loop and closed towards the tank for power minimization, in order for the feed pump to have the least volume to be pumped. Although this total recirculation saves pumping power, the duration of CVD step increases at the same time.

Table 5.1 shows a comparison of partial processing costs \mathcal{J}_T , \mathcal{J}_D , \mathcal{J}_P ((4.18)–(5.21)) using different scenarios. We can observe that the processing time and power are opposing objectives and cannot be minimized simultaneously. Minimum value of one of them results in maximum value of the other one.

The almost minimum time gave similar results to minimum time scenario as seen in Table 5.1, and almost minimum power also gave similar results to minimum power scenario. The volume needed to be pumped did not increase substantially (9%) but the process time is reduced by 1.41 hours (20% reduction).

The Pareto front representation of the relation between these opposing objectives, i.e. time and power is depicted in Fig. 5.5. It can be observed that reduction of the power required is achieved at the expense of processing time, and vice versa. The utopia point (marked as hexagon) would be the perfect result for both objectives, as power and processing time both are minimum at this point. Practically, however, it is not possible to have minimum of both objectives. Hence, a multi-objective

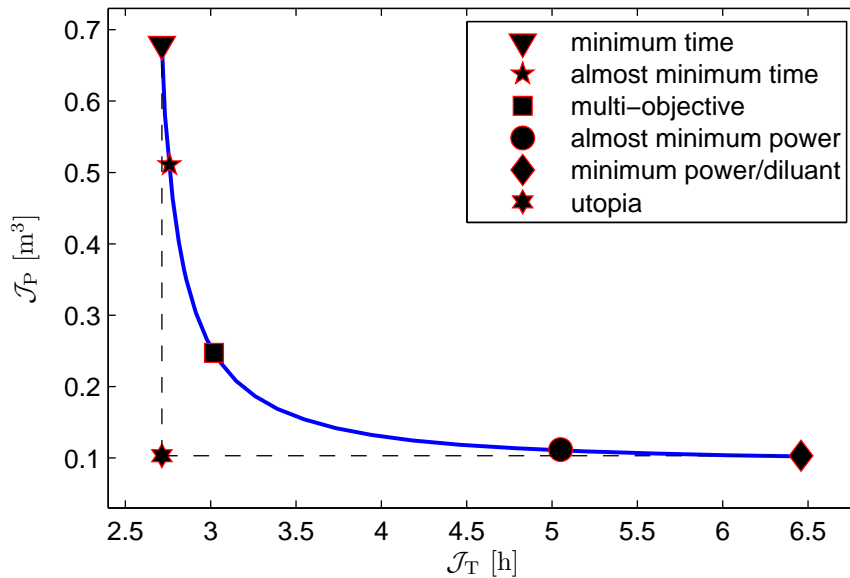


Figure 5.5: Pareto front diagram to depict the relation between optimized results, when moving from minimum time to minimum power.

optimal scenario located between both of them could be a good option.

With minimum power and time being extreme points, more realistic strategies are denoted by almost minimum scenarios. Thus, almost minimum time does not change the processing time much but greatly reduces the power (and diluant consumption). The same holds for the almost minimum power where the processing time is much reduced with only a slight increase of power needed. This is documented in both Table 5.1 and Fig. 5.5.

Let us now consider the situation when the final concentration of the macro-solute is increased to 170 mol m^{-3} . The theoretical results for time-optimal operation of batch open-loop configuration predict (Paulen and Fikar, 2016, Paulen et al., 2013, 2015) that it will consist of a three-step strategy of time-varying α with modes: C, CVD, and C: $\alpha = (0, 1, 0)$ with the same switching concentration as before.

Optimal operation for batch closed-loop configuration was calculated numerically using both the method of orthogonal collocations as well as control vector parametrization. The results confirm the observation from the first simulation part and are not repeated here.

We have also studied the effect of parametrization of the recirculation ratio s , and its effect on the final value of the cost function. We have found that the optimum is not particularly sensitive to s – if constant value is assumed over the whole processing time, the cost function increases by less than 1%. This is perfectly adequate in industrial conditions.

5.3.2 Separation of Lactose and Proteins

A case study taken from Rajagopalan and Cheryan (1991) is solved here where lactose is separated from proteins using ultrafiltration. The permeate flow rate model determined experimentally can be

described as follows:

$$q_p(c_{L,1}, c_{L,2}) = 63.42 - 12.439 \ln c_{L,1} - 7.836 \ln c_{L,2}, \quad (5.24)$$

where $c_{L,1}$ represents the concentration of proteins in the loop and $c_{L,2}$ represents the concentration of lactose in the loop. The aim is to process the solution of a volume 104 dL from the initial point $[c_{1,0}, c_{2,0}] = [3.3, 5.5] \text{ g dL}^{-1}$ to the final point $[c_{1,f}, c_{2,f}] = [9.04, 0.64] \text{ g dL}^{-1}$. The process parameters are the flow rate inside the loop $q_L = 400 \text{ dL h}^{-1}$ and the loop volume $V_L = 4 \text{ dL}$.

We study again different scenarios with the following weights:

1. Minimum time scenario ($w_T = 1$, $w_E = 0$, and $w_D = 0$).
2. Almost minimum power scenario ($w_T = 0.23$, $w_E = 0.77$, and $w_D = 0$).
3. Minimum power scenario ($w_T = 0$, $w_E = 1$, and $w_D = 0$).
4. Minimum diluant scenario ($w_T = 0$, $w_E = 0$, and $w_D = 1$).

The theoretical results for optimal operation of batch open-loop configuration suggest (Paulen and Fikar, 2016, Paulen et al., 2012, 2015) that it will consist of the three-step strategy of time-varying α with modes: C, VVD, and dilution: $\alpha = (0, 0.61, \infty)$.

Numerical optimization with the minimum power/diluant scenario gave the same and practically non-feasible solutions. The optimal operation occurs with $q_p \rightarrow 0$ and takes infinite time to reach the desired concentrations (Table 5.2). Hence, the reason to implement almost minimum power scenario is to minimize power but in a practically feasible fashion. Otherwise, the results in Table 5.2 are consistent with the previous case.

Numerical diluant strategy of α agrees with the theory and the results for scenarios 1 and 2 are shown in Figs. 5.6, 5.7, and 5.8. Green circle and red cross in concentration trajectories denote the initial and final concentration points, respectively. The recirculation ratio s for the minimum time scenario is equal to one and for the almost minimum power is almost zero.

As inferred in the previous case study, to minimize power/diluant, the C mode takes longer than the C mode of time minimization scenario (Fig. 5.7). Again, it follows from the inverse relation between the switching concentration and the end point of the CVD/VVD mode. The switching to VVD mode is at higher concentration resulting in reduction of diluant consumption (during VVD) to meet the condition $c_1/c_2 = c_{1,f}/c_{2,f}$.

This can also be comprehended in the sense of volume in the system. As C mode gets longer, the volume gets lower and macro-solute concentration increases while micro-solute concentration stays constant. Hence lower volume of diluant is needed to be pumped to reduce the same concentration of micro-solute, but for a lower volume of feed (solution remaining in the process after C mode).

Similar to previous case, due to $s \approx 0$ in almost minimum power scenario (5.8), the time taken by VVD mode is longer than the time taken by VVD mode of minimum time scenario. The other reason for the longer time duration of VVD step in minimum power scenario is the lower permeate flux due to higher concentration of macro-solute (c_1) reached during C mode.

It can be studied from Table 5.2 that the difference in power consumption is quite large when the minimum time and the almost minimum power scenarios are compared. To investigate the main source

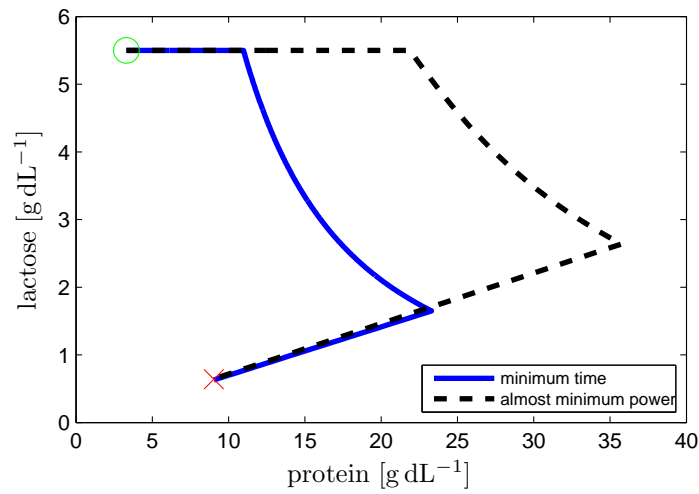
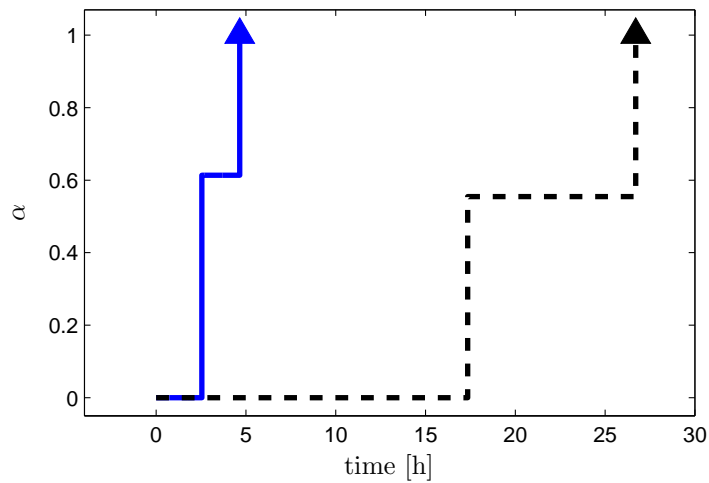
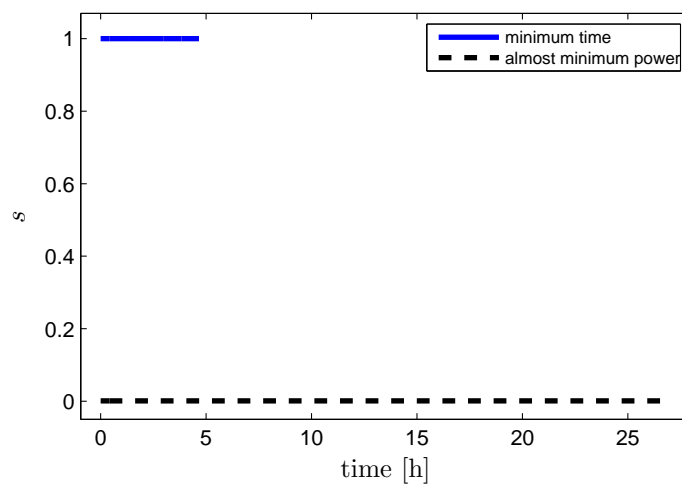


Figure 5.6: Separation of lactose from proteins: total concentration diagram.

Figure 5.7: Separation of lactose from proteins: optimal values of control α .Figure 5.8: Separation of lactose from proteins: optimal values of control s .

of power reduction, we have simulated the process with optimal α from the almost minimum power scenario but in open-loop strategy ($s = 1$) and assuming identical initial and final concentrations.

The processing time was close to the minimum time scenario but the power consumption was similar to the one for the minimum time case. Hence, optimization of solely α will not lead to significant power reduction. The recirculation ratio s is the decisive factor, and needs to be optimized when power minimization is a part of the objective.

5.3.3 Separation of Albumin and Ethanol

The last case study investigates separation of albumin and ethanol presented in Jaffrin and Charrier (1994). The permeate flow rate model determined experimentally as a function of both concentrations can be described as follows:

$$q_p(c_{L,1}, c_{L,2}) = \frac{1}{b_1 + b_2 c_{L,1} + b_3 c_{L,2} + b_4 c_{L,1} c_{L,2} + b_5 c_{L,1}^2 + b_6 c_{L,2}^2}, \quad (5.25)$$

where $c_{L,1}$ and $c_{L,2}$ represent the concentration of albumin and ethanol inside the loop, respectively. The experimental values of the permeate flow coefficients are given in Jaffrin and Charrier (1994).

The aim is to process the solution of a volume of 0.0699 m^3 from the initial point $[c_{1,0}, c_{2,0}] = [15, 193.4] \text{ kg m}^{-3}$, to the final point $[c_{1,f}, c_{2,f}] = [80, 0.1] \text{ kg m}^{-3}$. The process parameters are $V_L = 0.0033 \text{ m}^3$, $q_L = 0.18 \text{ m}^3 \text{ h}^{-1}$. The original study assumes upper limit on diluant ratio $\alpha_{\max} = 1$.

Theoretical analysis (Paulen and Fikar, 2016, Paulen et al., 2011, 2015) of the batch open-loop process for the given initial and final conditions states that the optimal diluant ratio strategy depends strongly on the type of the cost function to be minimized. For the minimum time problem it is a three step strategy of time-varying $\alpha = (1, \alpha(t), 1)$ with singular control being a complex function of time. For the minimum diluant it is a two step strategy $\alpha = (0, 1)$.

The four cases of multi-objective optimization were investigated: minimum time, minimum diluant, minimum power, and multi-objective with $w_E = 1$ and $w_T = 0.2$. The weights were chosen similarly to the multi-objective scenario of the limiting flux model, i.e. to get into the mid range of both minimum time and minimum power.

The total concentration of ethanol and albumin along with optimal control (α, s) evolution is depicted in Figs. 5.9, 5.10 and 5.11, respectively. The dots in Fig. 5.10 and 5.11 specify the final time points. The optimal strategy consists of two time intervals for all scenarios. It can be observed that

Table 5.2: Separation of lactose from proteins: comparison of individual cost functions for different scenarios.

| Operation | w_T [€ h ⁻¹] | w_E [€ h dL ⁻¹] | w_D [€ h dL ⁻¹] | \mathcal{J}_T [h] | \mathcal{J}_P [dL] | \mathcal{J}_D [dL] |
|----------------------|-------------------------------|----------------------------------|----------------------------------|------------------------|-------------------------|-------------------------|
| Minimum time | 1 | 0 | 0 | 4.65 | 1860 | 50 |
| Almost minimum power | 0.23 | 0.77 | 0 | 26.8 | 112 | 38 |
| Minimum power | 0 | 1 | 0 | 165.2 | 107.8 | 37 |
| Minimum diluant | 0 | 0 | 1 | 165.2 | 107.8 | 37 |

Table 5.3: Separation of albumin and ethanol: comparison of individual cost functions for different scenarios.

| Operation | w_T [€ h ⁻¹] | w_E [€ h m ⁻³] | w_D [€ h m ⁻³] | \mathcal{J}_T [h] | \mathcal{J}_P [m ⁻³] | \mathcal{J}_D [m ⁻³] |
|-----------------|-------------------------------|---------------------------------|---------------------------------|------------------------|---------------------------------------|---------------------------------------|
| Minimum time | 1 | 0 | 0 | 2.54 | 0.457 | 0.113 |
| Multi-objective | 0.2 | 1 | 0 | 3.08 | 0.262 | 0.085 |
| Minimum power | 0 | 1 | 0 | 5.47 | 0.132 | 0.075 |
| Minimum diluant | 0 | 0 | 1 | 5.47 | 0.132 | 0.075 |

except the minimum time scenario, the other two follow in accordance with the theory the traditional two step C-CVD operation with control α being 0 in the first step in order to concentrate (C) albumin and then constant volume diafiltration (CVD) with $\alpha = 1$ to reduce the concentration of ethanol.

The optimal minimum time scenario differs slightly from the theory: it starts with variable volume diafiltration (VVD) to increase albumin and simultaneously reduce ethanol and then continues with CVD until the final concentrations were met. This behavior is however in accordance with the numerical results found in (Paulen and Fikar, 2016, Paulen et al., 2011). The approximation of analytical three step diluant strategy for minimum time i.e. [CVD, VVD, CVD] was also tested and the optimal cost function value was practically the same as the numerical optimum of VVD followed by CVD strategy. This shows that the objective value is not very sensitive to the first CVD step of the analytical approach.

The control s too, according to the theory in this thesis and earlier case studies is on maximum ($s = 1$) in order to minimize time, and on minimum ($s = 0$) in order to minimize power. In other cases, it lies between the maximum and minimum.

Table 5.3 provides the values of different minimization objectives. The time as in other case studies is maximum for minimum power scenario and the converse applies for the power minimization problem. The diluant consumption was identical for minimum power and minimum diluant scenario, along with power consumption.

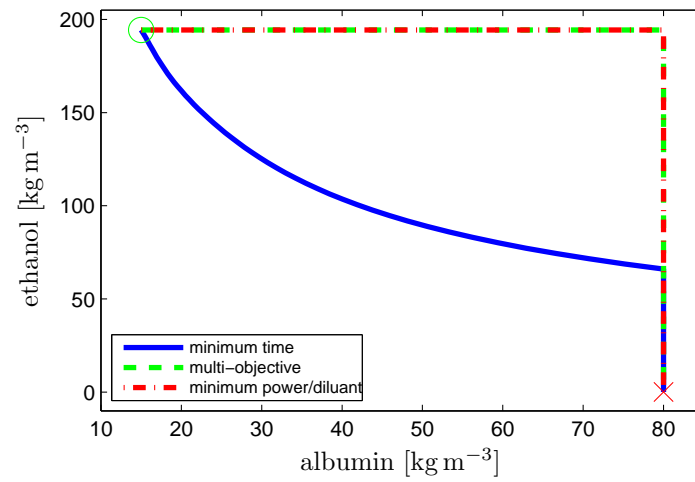


Figure 5.9: Separation of albumin and ethanol: total concentration diagram.

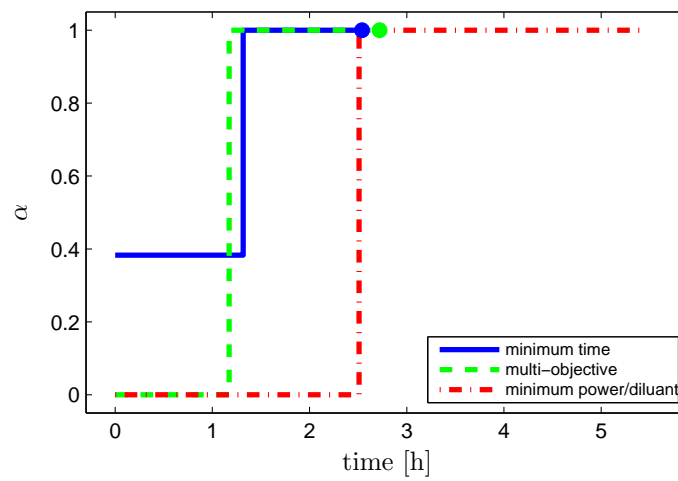


Figure 5.10: Separation of albumin and ethanol: optimal values of control α .

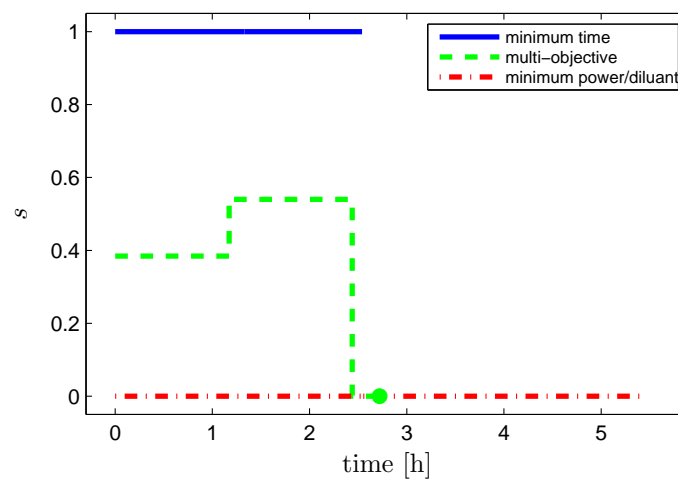


Figure 5.11: Separation of albumin and ethanol: optimal values of control s .

Chapter 6

Conclusions

In this doctoral thesis investigation of optimal operation of batch diafiltration membrane processes has been researched. The following highlights comprise the contributions of this thesis towards research on membrane process optimization:

1. Modeling of batch (open-loop) and batch with recirculation (closed-loop) types of membrane diafiltration processes.
2. Comparison of these two types of diafiltration configurations based on economical benefits they bring to separation.
3. Modeling of filtration rates using experimental data. The dynamic optimization problem was solved to find optimal parameters of filtration models.
4. Optimal operation of batch open-loop DF was proposed using Pontryagin's minimum principle to find the optimal diluant addition rate. It was experimentally verified using the experimental filtration models estimated. The numerical optimization was performed for batch closed-loop DF to find the optimal diluant addition rate and recirculation ratio. Case studies were performed to study the optimal operation for both batch configurations.

The results based on the previous findings, and on this research work showed that the optimal operation consists of a three step strategy for both open-loop and closed-loop batch configurations. To be precise, three piece-wise constant inputs were found to satisfy the optimization objectives. The first and the last step use either pure filtration or pure dilution and the middle step is characterized by staying on singular surface where singular control is applied.

In both open-loop and closed-loop batch processes, multi-objective NLP problem was formulated. The batch open-loop DF optimization problem aimed at minimizing processing time and diluant consumption, while batch closed-loop aimed at minimization of power consumption, processing time, and diluant consumption.

Experimental results of case studies for batch open-loop NDF to remove salt and concentrate lactose proved that optimal strategies improve the economics by reducing both processing time and diluant consumption, when compared to classical industrial strategies. In addition, the implementation of

these optimal strategies does not require any alteration in current hardware and software setup in industries.

Numerical optimization results of case studies for closed-loop batch DF showed that power and diluant minimizations are equivalent. The same set of optimal controls can be implemented to minimize diluant and power consumption. Time minimization on the other hand was achieved on the expense of higher diluant and power consumption.

The comparison of open-loop and closed-loop batch DF was done based on optimization results of case studies. It was concluded that for time minimization, recirculation is not required, only open-loop batch DF is enough. The configuration with possibility of partial recirculation (closed-loop) is useful when power minimization is a part of our optimal control problem.

Future work motivation can be summarized in the following items

- Online model estimation: Another part of the research that can be experimented with to get better results, is online estimation of filtering models. In this research the model was estimated parameters were optimally obtained from process data, offline. Then this model was used to find the optimal strategy offline, followed by its implementation on plant. The future work will be to estimate the model parameters online, calculate the optimal strategy and steer the experiment optimally based on these online calculations, i.e. real-time optimal strategy implementation.
- Membrane types: The optimal operation experimental verification done was based on nanodifiltration of lactose and salt solution. As this optimal operation theory is universal for all batch diafiltration processes, it would be interesting in future to verify it with other membranes, and for other solutes. These experiments will concrete the results of our optimal control strategy, and also help in scaling the level of improvements coming from optimal operation, based on a variety of experiments.
- Rejection coefficients: In current research the rejection of lactose and NaCl by the membrane was considered to be constant. In future, the optimal strategy could be designed and implemented considering these rejection coefficients as functions of concentrations. This will help in calculating more precise concentrations, leading to more exact optimization results.
- Experiments – partial recirculation: The experimental verification of the optimal control strategy designed and simulated in current work for batch closed-loop diafiltration.

Bibliography

- A. Abdel-Karim, S. Leaper, M. Alberto, A. Vijayaraghavan, X. Fan, S. M. Holmes, E. R. Souaya, M. I. Badawy, and P. Gorgojo. High flux and fouling resistant flat sheet polyethersulfone membranes incorporated with graphene oxide for ultrafiltration applications. *Chemical Engineering Journal*, 334:789 – 799, 2018.
- J. Andersson. *A General-Purpose Software Framework for Dynamic Optimization*. PhD thesis, Arenberg Doctoral School, KU Leuven, Department of Electrical Engineering (ESAT/SCD) and Optimization in Engineering Center, October 2013.
- AWWA. Microfiltration and ultrafiltration membranes for drinking water - manual of water supply practices. American Water Works Association (AWWA), edition-1, 2005.
- B. Balanec, M. Vourch, M. Rabiller-Baudry, and B. Chaufer. Comparative study of different nanofiltration and reverse osmosis membranes for dairy effluent treatment by dead-end filtration. *Separation and Purification Technology*, 42(2):195 – 200, 2005.
- E. Balsa-Canto, J. R. Banga, A. A. Alonso, and V. S. Vassiliadis. Dynamic optimization of chemical and biochemical processes using restricted second-order information. *Computers and Chemical Engineering*, 25(4–6):539–546, 2001.
- R. Bellman. *Mathematical Optimization Techniques*. RAND books. University of California Press, 1963.
- L. T. Biegler. An overview of simultaneous strategies for dynamic optimization. *Chemical Engineering and Processing*, 46:1043–1053, 2007.
- M.R. Bilad, V. Discart, D. Vandamme, I. Foubert, K. Muylaert, and Ivo F.J. Vankelecom. Coupled cultivation and pre-harvesting of microalgae in a membrane photobioreactor (MPBR). *Bioresource Technology*, 155:410 – 417, 2014.
- W. F. Blatt, A. Dravid, A. S. Michaels, and L. Nelsed. Solute polarization and cake formation in membrane ultrafiltration: Causes, consequences, and control techniques. *Membrane Science and Technology*, pages 47–91, 1970.

- R. Boerefijn, Z. Ning, and M. Ghadiri. Disintegration of weak lactose agglomerates for inhalation applications. *International Journal of Pharmaceutics*, 172(1-2):199 – 209, 1998.
- A. E. Bryson, Jr. and Y. C. Ho. *Applied Optimal Control*. Hemisphere Publishing Corporation, 1975.
- A. Cassano, C. Conidi, L. Giorno, and E. Drioli. Fractionation of olive mill wastewaters by membrane separation techniques. *Journal of Hazardous Materials*, 248-249:185 – 193, 2013.
- J. Chandrapala, M. C. Duke, S. R. Gray, M. Weeks, M. Palmer, and T. Vasiljevic. Nanofiltration and nanodiafiltration of acid whey as a function of ph and temperature. *Separation and Purification Technology*, 160:18 – 27, 2016.
- Z. Chen, J. Luo, Y. Wang, W. Cao, B. Qi, and Y. Wan. A novel membrane-based integrated process for fractionation and reclamation of dairy wastewater. *Chemical Engineering Journal*, 313:1061 – 1070, 2017.
- M. Cheryan. *Ultrafiltration and Microfiltration Handbook*. CRC Press, 1998.
- M. Čížniar, M. Fikar, and M. A. Latifi. Matlab dynamic optimisation code dynopt. User’s guide. Technical report, KIRP FCHPT STU Bratislava, Slovak Republic, 2005.
- J. L. Cohen, D. Barile, Y. Liu, and J. M.L.N. de Moura Bell. Role of ph in the recovery of bovine milk oligosaccharides from colostrum whey permeate by nanofiltration. *International Dairy Journal*, 66: 68 – 75, 2017.
- C. Conidi, A. Cassano, F. Caiazzo, and E. Drioli. Separation and purification of phenolic compounds from pomegranate juice by ultrafiltration and nanofiltration membranes. *Journal of Food Engineering*, 195:1 – 13, 2017.
- J. G. Crespo, K. W. Böddeker, and North Atlantic Treaty Organization. Scientific Affairs Division. *Membrane Processes in Separation and Purification*. Developments in Oncology. Springer, 1994.
- B. Cuartas-Uribe, M.C. Vincent-Vela, S. Álvarez-Blanco, M.I. Alcaina-Miranda, and E. Soriano-Costa. Nanofiltration of sweet whey and prediction of lactose retention as a function of permeate flux using the Kedem-Spiegler and Donnan-steric partitioning models. *Separation and Purification Technology*, 56(1):38 – 46, 2007.
- J. Cui, X. Zhang, H. Liu, S. Liu, and K. L. Yeung. Preparation and application of zeolite/ceramic microfiltration membranes for treatment of oil contaminated water. *Journal of Membrane Science*, 325:420 – 426, 2008.
- J. E. Cuthrell and L. T. Biegler. On the optimization of differential-algebraic process systems. *AIChE Journal*, 33(8):1257–1270, 1987.
- B. Das, S. Sarkar, A. Sarkar, S. Bhattacharjee, and C. Bhattacharjee. Recovery of whey proteins and lactose from dairy waste: A step towards green waste management. *Process Safety and Environmental Protection*, 101:27 – 33, 2016.

- W. Demmer and D. Nussbaumer. Large-scale membrane adsorbers. *Journal of Chromatography A*, 852(1):73 – 81, 1999.
- Dow Water & Process Solutions. Filmtec reverse osmosis membranes technical manual. <http://www.dow.com/scripts/litorder.asp?filepath=/609-00071.pdf>.
- eWON. *eWON Family – General Reference Guide*, 2014. Rev. 3.0.
- G. Foley. Water usage in variable volume diafiltration: comparison with ultrafiltration and constant volume diafiltration. *Desalination*, 196:160 – 163, 2006.
- G. Foley. Three classic ultrafiltration problems solved with the exponential integral. *Education for Chemical Engineers*, 6(3):e90 – e96, 2011.
- C. J. Goh and K. L. Teo. Control parameterization: a unified approach to optimal control problems with general constraints. *Automatica*, 24(1):3–18, 1988.
- L. Gutiérrez, S. Hamoudi, and K. Belkacemi. Lactobionic acid: A high value-added lactose derivative for food and pharmaceutical applications. *International Dairy Journal*, 26(2):103 – 111, 2012.
- T. Hirmajer and M. Fikar. Optimal control of a hybrid coupled tanks system. In *Cybernetics and Systems 2006*, pages 41–45, 2006.
- T. Hirmajer, M. Čížniar, M. Fikar, E. Balsa-Canto, and J. R. Banga. Brief introduction to DOTcvp – dynamic optimization toolbox. In *Proceedings of the 8th International Scientific - Technical Conference Process Control 2008*, 2008.
- B. Houska, H. J. Ferreau, and M. Diehl. ACADO Toolkit – An Open Source Framework for Automatic Control and Dynamic Optimization. *Optimal Control Applications and Methods*, 32(3):298–312, 2011.
- D. G. Hull. *Optimal Control Theory for Applications*. Mechanical Engineering Series. Springer, 2003.
- M. Y. Jaffrin and J. Ph. Charrier. Optimization of ultrafiltration and diafiltration processes for albumin production. *Journal of Membrane Science*, 97:71–81, 1994.
- M. Jelemenský. *Optimal Control of Membrane Processes in the Presence of Fouling*. PhD thesis, ÚIAM FCHPT STU v Bratislave, 2016.
- M. Jelemenský, A. Sharma, R. Paulen, and M. Fikar. Time-optimal operation of diafiltration processes in the presence of fouling. In *12th International Symposium on Process Systems Engineering And 25th European Symposium on Computer Aided Process Engineering*, pages 1577–1582, 2015a.
- M. Jelemenský, A. Sharma, R. Paulen, and M. Fikar. Multi-objective optimization of batch diafiltration processes in the presence of membrane fouling. In *Proceedings of the 20th International Conference on Process Control*, pages 84–89, 2015b.
- M. Jelemenský, A. Sharma, R. Paulen, and M. Fikar. Time-optimal control of diafiltration processes in the presence of membrane fouling. *Computers & Chemical Engineering*, 91:343–351, 2016.

- A. Jönsson and G. Trägårdh. Ultrafiltration applications. *Desalination*, 77:135 – 179, 1990.
- M. J. Jornitz and T. H. Meltzer. *Filtration and Purification in the Biopharmaceutical Industry, Second Edition*. Drugs and the Pharmaceutical Sciences. CRC Press (Taylor & Francis), 2007.
- A. E. Khalifa, S. M. Alawad, and M. A. Antar. Parallel and series multistage air gap membrane distillation. *Desalination*, 417:69 – 76, 2017.
- S. Khemakhem, A. Larbot, and R. Ben Amar. New ceramic microfiltration membranes from tunisian natural materials: Application for the cuttlefish effluents treatment. *Ceramics International*, 35:55 – 61, 2009.
- Z. Kovács, M. Discacciati, and W. Samhaber. Modeling of batch and semi-batch membrane filtration processes. *Journal of Membrane Science*, 327(1-2):164 – 173, 2009a.
- Z. Kovács, M. Fikar, and P. Czermak. Mathematical modeling of diafiltration. *Hungarian Journal of Industry and Chemistry*, 37, 2009b.
- T. Lauw-Bieng and L. T. Biegler. Simultaneous solution and optimization strategies for parameter estimation of differential-algebraic equation systems. *Industrial & Engineering Chemistry Research*, 30:376–385, 1991.
- K. P. Lee, T. C. Arnot, and D. Mattia. A review of reverse osmosis membrane materials for desalination—development to date and future potential. *Journal of Membrane Science*, 370(1–2):1 – 22, 2011.
- N.N. Li. *Recent Developments in Separation Science*. Number v. 1-2 in CRC uniscience series. CRC Press, 1972.
- X. Li and J. Li. Dead-end filtration. In E. Drioli and L. Giorno, editors, *Encyclopedia of Membranes*, pages 1 – 3. Springer Berlin Heidelberg, 2015.
- H. Lutz. *Ultrafiltration for Bioprocessing*. Woodhead Publishing, 2015.
- J. Mallevialle, P. E. Odendaal, AWWA Research Foundation, M.R. Wiesner, Lyonnaise des eaux Dumez (Firm), and South Africa. Water Research Commission. *Water Treatment Membrane Processes*. McGraw-Hill, 1996.
- A.W. Mohammad, Y.H. Teow, W.L. Ang, Y.T. Chung, D.L. Oatley-Radcliffe, and N. Hilal. Nanofiltration membranes review: Recent advances and future prospects. *Desalination*, 356:226 – 254, 2015.
- P. Ng, J. Lundblad, and G. Mitra. Optimization of solute separation by diafiltration. *Separation Science and Technology*, 11(5):499–502, 1976.
- R. Paulen. Global dynamic optimization of processes. *Minithesis*, 2010.
- R. Paulen and M. Fikar. *Optimal Operation of Batch Membrane Processes*. Springer, 2016.

- R. Paulen, M. Fikar, Z. Kovács, and P. Czermak. Process optimization of diafiltration with time-dependent water adding for albumin production. *Chemical Engineering and Processing: Process Intensification*, 50(8):815 – 821, 2011.
- R. Paulen, M. Fikar, G. Foley, Z. Kovács, and P. Czermak. Optimal feeding strategy of diafiltration buffer in batch membrane processes. *Journal of Membrane Science*, 411-412:160–172, 2012.
- R. Paulen, M. Jelemenský, M. Fikar, and Z. Kovács. Optimal balancing of temporal and buffer costs for ultrafiltration/diafiltration processes under limiting flux conditions. *Journal of Membrane Science*, 444(0):87 – 95, 2013.
- R. Paulen, M. Jelemenský, Z. Kovács, and M. Fikar. Economically optimal batch diafiltration via analytical multi-objective optimal control. *Journal of Process Control*, 28:73–82, 2015.
- L. S. Pontryagin, V. G. Boltyanskii, R. V. Gamkrelidze, and E. F. Mishchenko. *The Mathematical Theory of Optimal Processes*. John Wiley & Sons, Inc., New York, 1962.
- N. Rajagopalan and M. Cheryan. Process optimization in ultrafiltration: Flux-time considerations in the purification of macromolecules. *Chemical Engineering Communications*, 106(1):57–69, 1991.
- S. Ramaswamy, H. J. Huang, and B. V. Ramarao. *Separation and Purification Technologies in Biorefineries*. Wiley, 2013.
- D. Rapaport. A membrane for all seasons. *Environmental Protection*, issue-07/01/2006, 2006.
- O. Rosen and R. Luus. Evaluation of gradients for piecewise constant optimal control. *Computers & Chemical Engineering*, 15(4):273 – 281, 1991.
- P. E. Rutquist and M. M. Edvall. *PROPT - Matlab Optimal Control Software*, 2010.
- F. Salehi. Current and future applications for nanofiltration technology in the food processing. *Food and Bioproducts Processing*, 92(2):161 – 177, 2014.
- H. N. Sandefur, M. Asgharpour, J. Mariott, E. Gottberg, J. Vaden, M. Matlock, and J. Hestekin. Recovery of nutrients from swine wastewater using ultrafiltration: Applications for microalgae cultivation in photobioreactors. *Ecological Engineering*, 94:75 – 81, 2016.
- J. Schaep, C. Vandecasteele, A. W. Mohammad, and W. R. Bowen. Analysis of the salt retention of nanofiltration membranes using the Donnan-steric partitioning pore model. *Separation Science and Technology*, 34(15):3009–3030, 1999.
- A. Sharma, M. Jelemenský, R. Paulen, and M. Fikar. Modelling and optimal control of membrane process with partial recirculation. In *Proceedings of the 20th International Conference on Process Control*, pages 90–95, 2015.
- A. Sharma, M. Jelemenský, R. Paulen, and M. Fikar. Estimation of membrane fouling parameters for concentrating lactose using nanofiltration. In *26th European Symposium on Computer Aided Process Engineering*, pages 151–156, 2016a.

- A. Sharma, M. Jelemenský, R. Valo, M. Kalúz, and M. Fikar. Process control education using a laboratory separation process. In *Preprints of the 11th IFAC Symposium on Advances in Control Education*, pages 4–9, 2016b.
- A. Sharma, M. Jelemenský, R. Paulen, and M. Fikar. Optimal operation of nanofilter based diafiltration processes using experimental permeation models. In *Proceedings of the 21st International Conference on Process Control*, pages 185–190, 2017a.
- A. Sharma, M. Jelemenský, R. Paulen, and M. Fikar. Modeling and optimal operation of batch closed-loop diafiltration processes. *Chemical Engineering Research and Design*, 122:198–210, 2017b.
- A. Sharma, R. Valo, M. Kalúz, R. Paulen, and M. Fikar. Experimental validation and comparison of time-optimal and industrial strategy for membrane separation process. In *Preprints of the 9th Vienna International Conference on Mathematical Modelling, Vienna, Austria, February 21-23, 2018*, pages 869–874, 2018.
- A. Sharma, R. Valo, M. Kalúz, R. Paulen, and M. Fikar. Implementation of optimal strategy to economically improve batch membrane separation. *Journal of Process Control*, 76:155 – 164, 2019.
- K.S. Spiegler and O. Kedem. Thermodynamics of hyperfiltration (reverse osmosis): criteria for efficient membranes. *Desalination*, 1(4):311 – 326, 1966.
- Synder. Nanofiltration membrane elements. Synder Sanitary Catalog 2014 - Synder Filtration, 2014.
- A.Y. Tamime. *Membrane Processing: Dairy and Beverage Applications*. Wiley, 2012.
- C. Y. Tang and J. O. Leckie. Membrane independent limiting flux for RO and NF membranes fouled by humic acid. *Environmental Science & Technology*, 41(13):4767–4773, 2007.
- C. M. Todaro and H. C. Vogel. *Fermentation and Biochemical Engineering Handbook*. Elsevier Science, 2014.
- M. Čižniar. Dynamic optimisation of processes. Master’s thesis, Faculty of Chemical and Food Technology, Radlinskeho 9, 812 37 Bratislava, Slovak Republic, 2005.
- M. Čižniar, D. Salhi, M. Fikar, and M.A. Latifi. Dynopt – dynamic optimisation code for MATLAB. In *Technical Computing Prague 2005*, 2005.
- B. Verasztó, A. Sharma, Q. D. Nguyen, Gy. Vatai, P. Czermak, and Z. Kovács. Membrane filtration technology for processing whey and converting whey-based lactose into galactooligosaccharides. In *Conference Proceeding of the 6th Membrane Conference of Visegrad Countries*, page E5, 2013.
- S.H. Yalkowsky, Y. He, and P. Jain. *Handbook of Aqueous Solubility Data, Second Edition*. CRC Press, 2016.
- N. Yin, G. Yang, Z. Zhong, and W. Xing. Separation of ammonium salts from coking wastewater with nanofiltration combined with diafiltration. *Desalination*, 268(1-3):233 – 237, 2011.

- Z. Yu, T. Karkaria, M. Espina, M. Hunjun, A. Surendran, T. Luu, J. Telychko, and Y. P. Yang. Comparing multi-module connections in membrane chromatography scale-up. *Journal of Biotechnology*, 206:38 – 41, 2015.
- L. J. Zeman. *Microfiltration and Ultrafiltration: Principles and Applications*. CRC Press (Taylor & Francis), 1996.

Author's Publications

Thesis Related

Journals

1. A. Sharma, M. Jelemenský, R. Paulen, M. Fikar. Modeling and optimal operation of batch closed-loop diafiltration processes. *Chemical Engineering Research and Design*, vol. 122, pp. 198-210, 2017.
2. A. Sharma, R. Valo, M. Kalúz, R. Paulen, M. Fikar. Implementation of Optimal Strategy to Economically Improve Batch Membrane Separation. *Journal of Process Control*, vol. 76, pp. 155-164, 2019.

Conferences

1. A. Sharma, M. Jelemenský, R. Paulen, and M. Fikar. Modeling and Optimal Control of Membrane Process with Partial Recirculation. In *20th International Conference on Process Control*, Slovak Chemical Library, Štrbské Pleso, Slovakia, pp. 90–95, 2015.
2. A. Sharma, M. Jelemenský, R. Valo, M. Kalúz, M. Fikar. Process Control Education using a Laboratory Separation Process. In *11th IFAC Symposium on Advances in Control Education*, vol. 11, pp. 4–9, 2016.
3. A. Sharma, M. Jelemenský, R. Paulen, M. Fikar. Estimation of membrane fouling parameters for concentrating lactose using nanofiltration. In *26th European Symposium on Computer Aided Process Engineering*, Elsevier B.V, Slovenia, vol. 26, pp. 151–156, 2016.
4. A. Sharma, M. Jelemenský, R. Paulen, M. Fikar. Optimal Operation of Nanofilter Based Diafiltration Processes Using Experimental Permeation Models. In *21th International Conference on Process Control*, Slovak Chemical Library, Štrbské Pleso, Slovakia, pp. 185-190, 2017.
5. A. Sharma, R. Valo, M. Kalúz, R. Paulen, M. Fikar. Experimental validation and comparison of time-optimal and industrial strategy for membrane separation process. In *9th Vienna*

International Conference on Mathematical Modeling, Austria, 2018, pp. 869–874, 2018.

6. R. Paulen, A. Sharma, M. Fikar. Dynamic Real-time Optimization of Batch Membrane Processes using Pontryagin's Minimum Principle. In *28th European Symposium on Computer Aided Process Engineering*, Elsevier, vol. 28, pp. 1045–1050, 2018.

Other Publications

Journals

1. M. Jelemenský, A. Sharma, R. Paulen, M. Fikar. Time-optimal control of diafiltration processes in the presence of membrane fouling. *Computers & Chemical Engineering*, vol. 91, pp. 343–351, 2016.
2. A. Sharma, M. Fikar, M. Bakošová. Comparative study of Time Optimal Controller with PID Controller for a Continuous Stirred Tank Reactor. *Acta Chimica Slovaca*, no. 1, vol. 8, pp. 27–33, 2015.

Conferences

1. B. Verasztó, A. Sharma, Q. D. Nguyen, Gy. Vatai, P. Czermak, Z. Kovács: Membrane filtration technology for processing whey and converting whey-based lactose into galactooligosaccharides. In *Proceeding of the 6th Membrane Conference of Visegrad Countries*, E5 Warsaw, Poland: Polish Membrane Society, 2013.
2. M. Jelemenský, A. Sharma, R. Paulen, M. Fikar. Time-optimal Operation of Diafiltration Processes in the Presence of Fouling. In *12th International Symposium on Process Systems Engineering And 25th European Symposium on Computer Aided Process Engineering*, Elsevier B.V, Copenhagen, Denmark, pp. 1577–1582, 2015.
3. M. Jelemenský, A. Sharma, R. Paulen, M. Fikar. Multi-Objective Optimization of Batch Dialfiltration Processes in the Presence of Membrane Fouling. In *Proceedings of the 20th International Conference on Process Control*, Slovak Chemical Library, Štrbské Pleso, Slovakia, pp. 84–89, 2015.
4. A. Sharma, J. Drgoňa, D. Ingole, J. Holaza, R. Valo, S. Koniar, M. Kvasnica. Teaching Classical and Advanced Control of Binary Distillation Column. In *11th IFAC Symposium on Advances in Control Education*, vol. 11, pp. 348–353, 2016.

Curriculum Vitae

Ayush Sharma

Date of birth: 22.11.1990

Nationality: India

e-mail: ayushsharma999@yahoo.com

Education

- Doctoral Studies: from 2014
 - Faculty of Chemical and Food Technology, STU, Bratislava
 - Study program: Process Control
- Engineering Studies: 2011–2013
 - University of Salerno, Salerno, Italy
 - Study program: Masters in Food and Chemical Engineering
- Engineering Studies: 2012–2013
 - Corvinus University, Budapest, Hungary
 - Study program: Masters degree in Food Engineering – Major Food Process Engineering
- Bachelor Studies: 2007–2011
 - LP University, Phagwara, India
 - B.Tech in Biotechnology

Language Skills

- English – proficient
- Italian – basic
- Slovak – basic
- Hindi – proficient

Work Experience

- XSLT Developer/ Apttus Configurator: from 2017 – present,
Transformation and Operations, IBM International Services Center (IBM ISC), Bratislava, Slovakia
 - Developing XSLT code to transform data into printable formats (pdf, html, ods, wordml),
 - Developing print templates using X-Author,
 - Layout Configuration using JSON.
- Scientific Researcher: from 2014 – 2017, Department of Automation, Information and Mathematics, Faculty of Food and Chemical Technology. State Technical University of Bratislava, Slovakia.
 - Research
 - * Modelling and optimal control of membrane processes
 - * Automation and control theory
 - * Laboratory scale experiments with micro, nano, ultrafiltration and RO
 - Teaching
 - * Laboratory of Process Control
 - * Theory of Automatic Control I – Lab
 - * Industrial Control and Information Systems - II (XML, XSLT, DTD, XML Schema)

Computer/ IT Skills

- Windows, Linux
- MatLab, Simulink, WinCC
- Python
- XML, XSLT, XQUERY, DTD, XMLSCHEMA
- Microsoft Office
- Latex, xfig, winfig

- Superpro designer, Scilab
- Visual Basics
- SQL, DB2 Fundamentals

Interests

- Membrane technology for separation
- XML, XSLT transformations
- Plant and process automation
- Food manufacturing and engineering plant design
- Bioprocess engineering
- Mathematical modeling
- Membrane bioreactor and reactor designing
- Optimal control theory, and PID controller designing
- Food transformation and processing

Driving License type A and B

Resumé

V tejto dizertačnej práci sa zaoberáme optimálnym riadením vsádzkových diafiltračných membránových procesov. Membránové procesy majú široké uplatnenie v chemickom, potravinárskom a farmaceutickom priemysle a taktiež pri spracovaní odpadových vôd v prakticky všetkých druhoch priemyselnej výroby. Princíp membránovej separácie je založený na veľkosti molekúl rôznych zložiek roztokov. Diafiltrácia je frakčná metóda, ktorá využíva externé rozpúšťadlo spolu s rôznymi technikami membránovej separácie (napr. ultrafiltrácia, nanofiltrácia, mikrofiltrácia a reverzná osmóza) za účelom zníženia obsahu nečistôt (napr. solí) a na zvýšenie koncentrácie produktu (napr. proteínov enzýmov alebo farbív) v roztoku.

V rámci práce skúmame vsádzkové diafiltračné membránové procesy bez recirkulácie (open-loop) a s recirkuláciou (closed-loop). V oboch prípadoch predpokladáme, že celý proces pracuje pri konštantnom tlaku a konštantnej teplote. Počiatočný roztok sa pridá do nádrže a dodáva sa na membránu pomocou čerpadla. Membrána je navrhnutá tak, aby zadržala látky s veľkou molekulovou veľkosťou (makrozložka) a umožnila prechod menších častíc (mikrozložky) cez membránu. Časť roztoku, ktorá je zadržaná membránou (retentát), je privádzaná späť do nádrže. Časť, ktorá prechádza cez membránu a je vypustená zo systému, sa nazýva permeát.

Riadiacou premennou pre diafiltračné procesy je množstvo pridávaného rozpúšťadla (najčastejšie voda) a definovaného pomerom α medzi vstupným tokom rozpúšťadla a výstupným tokom permeátu. Existuje niekoľko tradičných módo, ktoré sú odlišné v hodnote α . Najznámejšie takéto módy sú

- koncentračný mód ($\alpha = 0$)
- diafiltračný mód s konštantným objemom $\alpha = 1$,
- diafiltrácia s klesajúcim objemom $\alpha = (0, 1)$,
- mód riedenia $\alpha = \infty$.

V prípade diafiltrácie s recirkuláciou je prítomná ďalšia riadiaca veličina, t.j. recirkulačný pomer (s). Môže sa pohybovať medzi $0 - 1$ a reprezentuje deliaci faktor medzi nádržou a obehom. $s = 0$ znamená, že žiadna látka sa nevracia do nádrže, zatiaľ čo $s = 1$ znamená úplný návrat do nádrže. $0 < s < 1$ znamená čiastočnú recirkuláciu.

Hlavným cieľom membránovej separácie je dosiahnuť požadovanú koncentráciu produktu a nečistôt. V tejto práci sa snažíme je dosiahnuť tento cieľ a zároveň minimalizovať produkčné náklady.

Pri membránových separačných procesoch existuje niekoľko druhov optimalizačných funkcií, ktoré poznáme, ako napríklad: minimalizácia času, minimalizácia spotreby rozpúšťadla a minimalizácia spotreby energie.

V prípade vsádzkovej diafiltrácie bez recirkulácie bola hlavným cieľom tejto práce implementácia stratégie optimálneho riadenia vyvinutého našou skupinou na laboratórnej membránovej separačnej stanici. Táto stratégia bola analyticky odvodená pomocou Pontrjaginovho princípu minima a je možné ju nájsť jej podrobný popis v Paulen and Fikar (2016). Základné parametre implementácie boli nasledovné:

1. Všetky koncentrácie sa môžu merať kedykoľvek bez toho, aby bolo potrebné vzorky uchovať.
2. Teplota a tlak môžu byť regulované na úrovni konštantnej žiadanej hodnoty.
3. Bezpečnostné opatrenia sú implementované tak, aby automaticky upravovali alebo dokonca zastavili proces pri dosiahnutí nebezpečných úrovní hodnôt.
4. Zariadenie môže byť ovládané na diaľku.
5. Všetky merania sa ukladajú a uchovávajú v pravidelných časových intervaloch.
6. Počas experimentov je možné implementovať analyticky nájdenú stratégiu riadenia.

Vyššie uvedené otázky boli riešené riadením zariadenia cez PLC pomocou Matlab a WinCC HMI.

Ďalším dosiahnutým cieľom bolo nájdenie vhodných prietokových modelov, ktoré sa hodia pre experimenty vykonané na tejto stanici. Tento cieľ bol dosiahnutý vykonaním dynamického prispôbenia modelov uvedených v odbornej literatúre experimentálnym údajom.

Po príprave zariadenia a získaní uspokojivých parametrizovaných prietokových modelov bolo ďalším cieľom vykonať a otestovať optimálnu stratégiu riadenia. Experimentálne sme uskutočnili niekoľko prípadových štúdií, ktoré sme následne porovnali s klasickými priemyselnými stratégiami na minimalizáciu času spracovania, minimalizáciu spotreby rozpúšťadla a vázenej kombinácie oboch prístupov.

V prípade vsádzkovej diafiltrácie s recirkuláciou sme v odborej literatúre nenašli žiadnu podrobnú štúdiu týkajúcu sa matematického modelovania a riadenia pre tento spôsob filtrácie. Prvým krokom bolo teda rozsiahle štúdium dostupnej literatúry. Potom sme uskutočnili matematické modelovanie na základe materiálovej bilancie vstupov a výstupov zo systému. Takto odvodený model sme potom zjednodušili a skúmali sa aj jeho ďalšie varianty. Potom sme na nájdenie optimálnej stratégie použili numerické dynamické optimalizačné techniky za účelom minimalizácie spotreby času, minimalizácie spotreby rozpúšťadla, spotreby energie, alebo ich vázenej kombinácie. Prípadové štúdie boli riešené pomocou simulácií za účelom štúdia výsledkov implementácie takejto optimálnej stratégie riadenia.

Závery boli vyvedené pre diafiltračné procesy. V prípade experimentálnej validácie optimálnej operácie pre diafiltráciu bez recirkulácie boli výsledky pozitívne. Optimálne stratégie boli lepšie ako klasické stratégie, ktoré sú v súčasnosti používané v priemysle. Úspešná bola aj optimalizácia riadenia diafiltrácie s recirkuláciou. Výsledky tiež naznačujú, že vsádzková diafiltrácia s recirkuláciou neprináša žiadne výhody (až na spotrebu energie) a môže byť nahradená klasickou vsádzkovou diafiltračnou konfiguráciou bez recirkulácie.